



THE HONG KONG  
POLYTECHNIC UNIVERSITY

香港理工大學

Pao Yue-kong Library

包玉剛圖書館

---

## Copyright Undertaking

This thesis is protected by copyright, with all rights reserved.

**By reading and using the thesis, the reader understands and agrees to the following terms:**

1. The reader will abide by the rules and legal ordinances governing copyright regarding the use of the thesis.
2. The reader will use the thesis for the purpose of research or private study only and not for distribution or further reproduction or any other purpose.
3. The reader agrees to indemnify and hold the University harmless from and against any loss, damage, cost, liability or expenses arising from copyright infringement or unauthorized usage.

### IMPORTANT

If you have reasons to believe that any materials in this thesis are deemed not suitable to be distributed in this form, or a copyright owner having difficulty with the material being included in our database, please contact [lbsys@polyu.edu.hk](mailto:lbsys@polyu.edu.hk) providing details. The Library will look into your claim and consider taking remedial action upon receipt of the written requests.

**HIGH PERFORMANCE ORGANIC  
ELECTROCHEMICAL  
TRANSISTORS FOR CHEMICAL  
AND BIOLOGICAL SENSING**

**WANG NAI XIANG**

**Ph.D**

**The Hong Kong Polytechnic University**

**2019**

**The Hong Kong Polytechnic University**

**Department of Applied Physics**

**High Performance Organic Electrochemical  
Transistors for Chemical and Biological Sensing**

**WANG Naixiang**

A thesis submitted in partial fulfillment of the requirements for  
the degree of Doctor of Philosophy

**August 2018**

# CERTIFICATE OF ORIGINALITY

I hereby declare that this thesis is my own work and that, to the best of my knowledge and belief, it reproduces no material previously published or written, nor material that has been accepted for the award of any other degree or diploma, except where due acknowledgement has been made in the text.

\_\_\_\_\_ (Signed)

\_\_\_\_\_ WANG Naixiang \_\_\_\_\_ (Name of student)



## Abstract

Organic electrochemical transistors (OECTs) have gained great attention in various chemical and biological sensing applications due to its intrinsic signal amplification function combined with highly efficient interfacing with ionic fluxes in biological environments. Besides, the freedom of synthesis, facile solution processing, superior biocompatibility and mechanical matching of organic materials offer OECTs a whole range of imaginative possibilities for investigation from fundamental device physics to biosensing related healthcare and wearable applications.

In this thesis, the microfabrication technique, electrical characterization, and sensing applications of rigid and flexible OECTs based on a series of semiconducting polymers were systematically investigated. These polymers included highly conductive poly(3,4-ethylenedioxythiophene):poly(styrene sulfonate) (PEDOT:PSS) for device operated in depletion mode, thiophene, thiadiazole or diketopyrrolo-pyrrole based p-type conjugated polymers for device operated in accumulation mode.

A simple and convenient photolithographic microfabrication process was established for miniaturization of OECTs into micrometre resolution, which was the fundamental technique for fabrication of the OECTs discussed over this whole thesis. Through miniaturization of channel area, the device response time could be dramatically reduced to  $10^{-5}$  s, which opened up the possibility to introduce AC measurements into electrochemical sensing applications. Then ion strength sensing, dopamine sensing and monitoring of cell activity were successfully demonstrated for PEDOT:PSS based OECTs. The precisely extracted transconductance signal indicated that the AC measurements could be a high reliable and anti-noise sensing method for investigation into multifunctional organic bioelectronic systems.



Then a series of high mobility p-type conjugated polymers were integrated into OECTs. Their electrical performance when operated in aqueous electrolyte was investigated. Process optimization, impedance analysis and ionic response behavior were carried out for better understanding of the working mechanism for OECTs employing these polymers. Through the analysis of the structure-property relationship, the mechanism of ionic penetration process and its interaction with polymer film would be promising to be clarified, and the results may shed light on further design and synthesis of novel conjugated polymers for the requirements of bioelectronic applications.

At last, OECT based on a recently reported semiconducting polymer, p(g2T-TT), was successfully exploited as flexible, label-free RNA sensor. The device showed stable performance in accumulation mode operation and high sensitivity to RNA biomarkers in physiological environment, with the detection limit down to  $10^{-12}$  M. The capacitance modulated sensing mechanism was investigated through variation of channel thickness and impedance analysis. The interaction of RNA molecules and polymer backbone was further investigated by characterization of electrolyte size effect on the p(g2T-TT) based OECTs. The successful demonstration of this sensor platform for detecting IL-8 mRNA, one biomarker for early detection of oral squamous cell carcinoma, indicates the possibility to employ this sensor in noninvasive cancer diagnosis applications.

In summary, the microfabrication technique by photolithography was established for design and fabrication of OECT in micrometer dimensions. The device physics and operation mechanism of OECT based on different types of organic materials were comprehensively investigated. Through carefully device optimization and functionalization strategies, the OECT could serve as a universal platform for various kinds of in vitro and in vivo sensing applications.



## List of Publications

- (1) **Wang, N.**; Liu, Y.; Fu, Y.; Yan, F. AC Measurements Using Organic Electrochemical Transistors for Accurate Sensing. *ACS Appl. Mater. Interfaces* **2018**, *10* (31), 25834–25840.
- (2) **Wang, N.**; Yang, A.; Fu, Y.; Li, Y.; Yan, F. Functionalized Organic Thin Film Transistors for Biosensing. submitted to *Accounts of Chemical Research*.
- (3) **Wang, N.**; Yan, F. Label-free RNA Sensing Based on Capacitance Modulated Organic Electrochemical Transistors. In preparation.
- (4) Fan, X.<sup>†</sup>; **Wang, N.**<sup>†</sup>; Yan, F.; Wang, J.; Song, W.; Ge, Z. A Transfer-Printed, Stretchable, and Reliable Strain Sensor Using PEDOT:PSS/Ag NW Hybrid Films Embedded into Elastomers. *Adv. Mater. Technol.* **2018**, *3* (6), 1800030.
- (5) Fan, X.; **Wang, N.**; Wang, J.; Xu, B.; Yan, F. Highly Sensitive, Durable and Stretchable Plastic Strain Sensors Using Sandwich Structures of PEDOT:PSS and an Elastomer. *Mater. Chem. Front.* **2018**, *2* (2), 355–361.
- (6) Yang, A.; Li, Y.; Yang, C.; Fu, Y.; **Wang, N.**; Li, L.; Yan, F. Fabric Organic Electrochemical Transistors for Biosensors. *Adv. Mater.* **2018**, *30* (23), 1800051.
- (7) Fu, Y.; **Wang, N.**; Yang, A.; Law, H. K.; Li, L.; Yan, F. Highly Sensitive Detection of Protein Biomarkers with Organic Electrochemical Transistors. *Adv. Mater.* **2017**, *29* (41), 1703787.
- (8) Fan, X.; Xu, B.; **Wang, N.**; Wang, J.; Liu, S.; Wang, H.; Yan, F. Highly Conductive Stretchable All-Plastic Electrodes Using a Novel Dipping-Embedded Transfer Method for High-Performance Wearable Sensors and Semitransparent Organic Solar Cells. *Adv. Electron. Mater.* **2017**, *3* (5), 1600471.



## Acknowledgements

This thesis describes the work I carried out as a PhD student in Department of Applied Physics of the Hong Kong Polytechnic University, in the Organic Electronics group between September 2015 and August 2018. I am thankful to the Research Grants Council of Hong Kong SAR government for funding support. As a research postgraduate student, I am also grateful for accommodation and financial support provided by the university and department of applied physics.

First of all, I would like to thank Prof. YAN Feng, my supervisor, for providing advices, support and encouragement throughout the period of my PhD study. I still remembered my first talk with Prof. Yan, during which he introduced me to the rich and colorful world of organic electrochemical transistors. Based on my previous research experience in organic electronic devices, I realized that this would be a promising direction which were beneficial for both fundamental study of device physics and real optoelectronic applications, especially chemical and biological sensing applications. With Prof. Yan's strong support, I was lucky to be awarded the Hong Kong PhD Fellowship by Research Grants Council, which made me focus on my research without worries behind. Most importantly, his way of generating scientific ideas, critical thinking, analyzing and solving problems came up from daily research, brought an undeniable benefit to me, especially for my research career life.

Furthermore, I would like to thank the technicians in Department of Applied Physics and clean room: Dr. CHAN Ngai Yui (Vincent) for instruments training; Dr. WONG Tai Lun (Terence) and Ms. LAU Joyce for guidance and maintenance of the facilities in clean room; Mr. CHAN Tsz Lam (Lam Two) and Ms. Ho Wing Man (Henrietta) for chemical ordering and lab safety management; Mr. LAM Kwan Ho (Vincent) for



information technology assistance. It would definitely spend me more time to carry out experiments without their patient and meticulous help.

Many thanks to Prof. SHI Peng for his advices and resources provided for the collaborative projects I participated in with Mr. XIE Kai. Moreover, I'm grateful to Prof. Sahika Inal, who led me to the interdisciplinary field of polymer science with optoelectronics nearly five years ago back in Potsdam, and now still focuses on the development of novel organic electrochemical transistors. She shared me the experiences and knowledges to help me handle these devices with less confusion. I would also like to thank Prof. Iain McCullough, and his student Alexander Giovannitti, who generously provided me the semiconducting polymers used in part of my work in this thesis.

My colleagues in department of applied physics, especially in our organic electronics group, who helped me in different aspects and made this workspace active and enjoyable, deserve a special thank: Dr. ZHANG Meng, Dr. FU Ying, Mr. Liao Caizhi, MAK Chun Hin, YANG Anneng, and LI Yuanzhe, with whom we always discussed the research topics and potential future directions; Dr. Fan Xi, who impressed me by his enthusiasm and passion into research and the capability to conduct experiment with delicate workmanship under primitive conditions; Dr. HUANG Xiaowen, Dr. CHEN Qingming and Dr. ZHAO Yuda, who shared their experiences with me on photolithographic process; Dr. XIE Chao, Dr. YOU Peng, Mr. TANG Guanqi, and many other students and postdoc researchers, who I spent much memorable time with in and outside our lab.

Cheers to my old friends and schoolmates, those who already earned a PhD degree or still struggling on the way, Prof. WEI Qiang, Dr. HU Yuandu, Dr. ZHANG Wang, Dr. GUO Jun, Dr. SHENG Yifeng, Ms. NIE Hao, Mr. HUANG Jianglou, Mr. LI



Yungui, and many more who are now striving in the industrial fields or already switched the direction of career beyond fundamental science. On the way to pursue own ideals, the thorny road of honor, it was your company, encouragement, information and resources sharing, that broke the geographic limits, brought me the confidence and courage through the hardships suffered.

Finally, I would like to send my sincerest gratitude to my mother and father, for their support, love and inspiration during my PhD study.



# Table of Contents

	<i><b>Page</b></i>
<b>Abstract</b>	<b>I</b>
<b>List of Publications</b>	<b>III</b>
<b>Acknowledgements</b>	<b>IV</b>
<b>Table of Contents</b>	<b>VII</b>
<b>List of Figures</b>	<b>X</b>
<b>Chapter 1 Introduction</b>	<b>1</b>
1.1 Background	1
1.2 Objectives of Research	5
1.3 Outline of Thesis	6
<b>Chapter 2 Literature Review</b>	<b>8</b>
2.1 Introduction	8
2.2 Working Mechanism of OECTs	9
2.3 Chemical Functionalization of OECTs for Bioelectronic Applications	12
2.3.1 Channel Functionalization	12
2.3.2 Electrolyte Functionalization	19
2.3.3 Gate Functionalization	22
<b>Chapter 3 AC Measurements for Accurate Sensing Applications of Organic     Electrochemical Transistors</b>	<b>32</b>
3.1 Introduction	32
3.2 Microfabrication of OECT	34
3.2.1 Materials	34
3.2.2 Device Fabrication	35



3.2.3 Device Characterization	38
3.2.4 Cell Cultivation	38
3.3 Electrical Measurements	39
3.3.1 Steady State Characteristics	39
3.3.2 Transient Characteristics and Ion Strength Sensing	41
3.4 Dopamine Sensors	45
3.5 Cell Activity Monitoring	50
3.6 Summary	53
<b>Chapter 4 High Mobility p-type Conjugated Polymers for Applications in</b>	
<b>Organic Electrochemical Transistors</b>	<b>54</b>
4.1 Introduction	54
4.2 Experimental Section	56
4.2.1 Materials	56
4.2.2 Device Fabrication	57
4.2.3 Device Characterization	58
4.3 Electrical Measurements	58
4.4 Effect of Thermal Annealing	63
4.5 Impedance Analysis	64
4.6 Effect of Electrolyte Size and Concentration	66
4.7 Summary	68
<b>Chapter 5 Label Free RNA Sensors Based on Capacitance Modulated Organic</b>	
<b>Electrochemical Transistors</b>	<b>69</b>
5.1 Introduction	69
5.2 Experimental Section	71
5.2.1 Materials	71
5.2.2 Device Fabrication	72
5.2.3 Device Characterization	72



5.3	Electrical Measurements	73
5.4	Label-free RNA Sensor Based on OECTs	74
5.4.1	Effect of Channel Thickness on RNA Sensitivity	74
5.4.2	Capacitance Modulated Sensing Mechanism	76
5.4.3	Impedance Analysis on RNA Sensing	78
5.4.4	Oral Cancer Biomarker Sensing	81
5.5	Size Effect on Polymer/Ion Interaction	82
5.5.1	Effect on Operation of OECTs	82
5.5.2	Impedance Analysis	84
5.6	Summary	86
<b>Chapter 6 Conclusions and Perspectives</b>		<b>87</b>
6.1	Conclusions	87
6.2	Perspectives	88
<b>References</b>		<b>91</b>

# List of Figures

<u>Figure</u>	<u>Captions</u>	<u>Page</u>
<b>Figure 1.1.</b>	Schematic diagram of working mechanism for (a) OFET, (b) Electrolyte-gated OFET and (c) OEET; (d) the typical OEET structure, with the symbol S, D, G represent source, drain and gate electrode respectively, d represents the thickness of channel layer. <sup>17</sup>	2
<b>Figure 1.2.</b>	Chemical structures of conjugated polymers employed in OEETs: (a) polypyrrole; (b) polyaniline; (c) PEDOT:PSS; (d) PEDOT-S; (e) PTHS; (f) p(g2T-TT); (g) p(NDI-g2T). <sup>38</sup>	4
<b>Figure 2.1.</b>	Electronic and ionic circuits illustrated in Bernards Model. The right graph shows the profile of potential drop in ionic circuit, under two different conditions, that whether channel capacitance ( $C_{CH}$ ) is larger than gate capacitance ( $C_G$ ) or not ( $C_{CH} > C_G$ or $C_{CH} < C_G$ ). <sup>17</sup>	9
<b>Figure 2.2.</b>	(a) Chemical structure of PEDOT:PSS, the holes generated on the conjugated backbone (red) is compensated by the sulfonate ions (blue) from PSS; <sup>77</sup> (b) Schematic diagram of the PEDOT:PSS morphology model for cation dedoping process; <sup>78</sup> (c) Typical transfer characterization and associated transconductance ( $g_m$ ) for PEDOT:PSS based OEET. <sup>77</sup>	10
<b>Figure 2.3.</b>	Chemical immobilization strategies for channel functionalization of OTFT sensors: (a) The device structure of an OEET sensor for capture of E. coli. bacteria; (b) the potential drops in the electric double layers in the OEET	



before and after capture of the bacteria on the PEDOT:PSS surface.<sup>82</sup> (c) OECT immunosensor for detection of prostate specific antigen/ $\alpha$ 1-antichymotrypsin complex, with the signal amplified by linked gold nanoparticles.<sup>85</sup> (d) The structure of biofunctional EGOFET with covalent bonded enzymes on the surface of  $\alpha$ -sexithiophene thin film.<sup>86</sup> (e) Schematic of the plasma assisted interfacial grafting of the tailored molecular antenna into the OTFT sensor, compared to a biological antenna of a butterfly.<sup>87</sup> ..... 14

**Figure 2.4.** Surface functionalization by membrane assembly. (a) Chemical structure of PEDOT:PSS with two other polyelectrolytes, and layer-by-layer assembly of these polyelectrolytes at the surface of channel material PEDOT:PSS, initially either by covalent attachment or physical adsorption.<sup>88</sup> (b) Scheme of phospholipid bilayers coating on the surface of EGOFET channel area.<sup>25</sup> (c) EGOFET immobilized with a bio-receptor layer with varying distances from the channel surface.<sup>89</sup> (d) Comparison of the transconductance-frequency curves of OECT alone (black squares), OECT coated with vesicles and PLs (filled circles), and the same device with addition of Alpha-hemolysin protein (open circles).<sup>90</sup> ..... 15

**Figure 2.5.** Biocompatibility modification for cell-based applications. (a) Optical images and transfer characterization of cancer cells cultured on channel area, before and after treatment of trypsin.<sup>95</sup> (b) Optical and scanning electron microscope images of the PEDOT:PSS films before and after autoclave



(AC).<sup>99</sup> (c) Optical images of cardiomyocytes cultured on OECT array, and the profile of a single action potential recorded by the OECT on day 5.<sup>100</sup> (d) Fluorescence imaging of live (green) and dead (red) PC12 neuron cells cultured on the functionalized PEDOT:PSS pattern for 5 days.<sup>101</sup> ..... 18

**Figure 2.6.** (a) Chemical structure of components of the ionic gel electrolyte and the schematic description of the mixture in the solid electrolyte layer of the OECT.<sup>108</sup> (b) Photograph of the screen printed all-solid-state OECT on flexible substrate.<sup>113</sup> (c) The breathing on the enzyme embedded paper based OECT, associated with the mechanism and the drain current response of the device towards exposure to ethanol.<sup>114</sup> (d) The schematic structure of the EGOFET integrated with an ion selective membrane.<sup>26</sup> ..... 21

**Figure 2.7.** (a) Schematic of the flexible OECT sensor integrated in the microfluidic system, with the modification of DNA on the surface of gate electrode; (b) potential drop across the whole OECT device with the effect of immobilization of DNA probe (red line,  $V_g'$ ) and targets (green line,  $V_g''$ ); (c) transfer characteristics of the OECT before and after the modification and hybridization of DNA on gold electrode.<sup>118</sup> (d) The scheme of a floating gate connected EGOFET for the detection of DNA; (e) transfer characteristics of the EGOFET before (red) and after (blue) the hybridization of complementary DNA. Inset shows the voltage shift of complementary and random DNA at various probe densities.<sup>119</sup> ..... 23



**Figure 2.8.** (a) Scheme and working mechanism of OECTs with gate electrode modified with certain functional proteins or cells; (b) current change of the OECT when exposed to the different cancer cell biomarker HER2 concentration.<sup>123</sup> (c) Device structure of OECT sensor modified with chitosan/nafion, graphene/rGO and the enzyme for glucose detection.<sup>124</sup> (d) Chiral discrimination of amino acid enantiomers by OECT modified with molecularly imprinted polymer film.<sup>125</sup> .....25

**Figure 2.9.** (a) Schematic diagram of OECT with an enzyme/polyaniline/nafion- graphene multilayer modified gate; (b) channel current response of the functionalized OECT to the addition of H<sub>2</sub>O<sub>2</sub> with various concentrations; (c) change of effective gate voltage versus concentration of H<sub>2</sub>O<sub>2</sub>, ascorbic acid (AA), and dopamine (DA).<sup>128</sup> (d) Schematic diagram of OECT modified with chitosan and graphene for dopamine sensing; (e) current response of OECT to the addition of dopamine with various concentrations; (f) change of effective gate voltage versus concentration of DA, uric acid (UA) and AA.<sup>129</sup> .....27

**Figure 2.10.** (a) Schematic structure of the electrolyte-gated OFET with procine odorant binding protein (pOBP) immobilized on the Au gate electrode; (b) the double layer capacitors formed in series at the corresponding interface of the device and the associated gate potential drop before (black) and after (red) the ligand capture.<sup>134</sup> (c) Detail procedures for gate surface modification used in detection of sialic acid by OECT; (d)



optical photography of the screen printed carbon electrode of OECT on flexible substrate; (e) drain current-time response to the addition of human cancer cells HeLa (black curve) and normal cells HUVEC (red curve) at the same concentration. Insert: normalized current response (NCR) of the devices to HeLa and HUVEC cells.<sup>135</sup> .....30

**Figure 3.1.** Device structure of the OECT. (a) Schematic diagram of an OECT cross-section and the wiring system for device operation. (b) Optical micrograph of an individual transistor and the whole OECT array. ....35

**Figure 3.2.** Fabrication process of OECT device by photolithography. (a)-(d), Au electrode deposition and patterning on the glass substrate. (e)-(g), patterning of PEDOT:PSS film between source and drain electrode. (h)-(i), final package of the device by SU-8 photoresist as an insulating layer. ....36

**Figure 3.3.** Height and phase AFM images of PEDOT:PSS films (a)-(b) before and (c)-(d) after all of the photolithography lift-off processes in device fabrication. ....37

**Figure 3.4.** (a) Output characteristics showing the drain current  $I_D$ , as a function of drain voltage  $V_D$ , with an applied gate voltage  $V_G$  varying from 0 V to 0.6 V. (b) Transfer curve and resulting transconductance at  $V_D = 0.05$  V. ....39

**Figure 3.5.** Leakage current of OECT (between channel and gate electrode) during the transfer characterization in Figure 3.4. ....40

**Figure 3.6.** (a) Time response to a  $V_G$  pulse of 0.2 V, with a drain voltage of 0.05 V, for OECT operated in a series of KCl solutions with increasing concentration from  $10^{-5}$  M to  $10^{-1}$



M. Inset: the time response of device operated in  $10^{-1}$  M KCl solution, with the time axis in millisecond range. (b) Extracted single exponential time constant as a function of KCl concentration. The line is a double-log linear fit.....42

**Figure 3.7.** Frequency dependence of (a) the transconductance value and (b) corresponding phase angle under various ionic concentration of KCl. The device is biased with  $V_D = 0.05$  V and  $V_G = 0.2$  V, and an additional 50 mV sinusoidal gate voltage oscillation is applied to measure the small-signal transconductance. ....43

**Figure 3.8.** (a) Channel transconductance ( $g_m$ ) response and (b) associated phase angle change of the OECT to additions of dopamine with different concentrations.  $V_D = 0.05$  V,  $V_G = 0.2$  V. ....47

**Figure 3.9.** (a)  $V_G$  dependence of transconductance ( $g_m$  vs.  $V_G$ ,  $V_D = 0.05$  V) of an OECT measured in PBS solution (pH = 7.4) before and after the addition of dopamine with the concentration of 10  $\mu$ M. (b) The change of effective gate voltage ( $\Delta V_G^{eff}$ ) as the function of the concentration of dopamine. ....48

**Figure 3.10.** DC channel current response of the OECT during the addition of dopamine with different concentrations.  $V_D = 0.05$  V,  $V_G = 0.4$  V. ....49

**Figure 3.11.** Monitoring the effect of living cells and drug treatment (5-FU) by (a) transconductance and (d) corresponding phase angle change. Inset, bright field images of cells seeded on the channel of device. Each image corresponds to one curve as



indicated. ....	51
<b>Figure 4.1.</b> Chemical Structures and abbreviations of the semiconducting polymers tested in this work. ....	57
<b>Figure 4.2.</b> (a) Output characteristics of PFT-100 based OEET for $-0.5 \text{ V} < V_G < 0 \text{ V}$ ; (b) transfer characteristics at $V_D = -0.5 \text{ V}$ , with $I_D$ shown in linear (red) and logarithmic (black) scale; (c) the gate leakage $I_G$ of the OEET during transfer measurement; (d) transient characteristics of $I_D$ (black) in response to a pulsed $V_G$ (blue) switched between $0.2 \text{ V}$ and $-0.4 \text{ V}$ . ....	59
<b>Figure 4.3.</b> Transfer characterization of (a) PCDTPT, (b) DPP-DTT, (c) PDPP2T-TT-OD and (d) $(\text{DPP-DTT})_{0.95}-(\text{TT-TOH})_{0.05}$ at $V_D = -0.5 \text{ V}$ , with $I_D$ shown in linear (red) and logarithmic (black) scale. ....	60
<b>Figure 4.4.</b> Comparison of transfer curves of PFT-100 based OEET prepared with different annealing temperature (a) $100 \text{ }^\circ\text{C}$ , (b) $150 \text{ }^\circ\text{C}$ , (c) $200 \text{ }^\circ\text{C}$ , and (d) $300 \text{ }^\circ\text{C}$ . ....	63
<b>Figure 4.5.</b> Impedance, phase and effective capacitance from EIS for (a-c) gold electrode and (d-f) PFT-100 film (coated on gold electrode) with the same area at a bias voltage ranging from $0.6 \text{ V}$ to $-0.8 \text{ V}$ , applied from working electrodes. ....	64
<b>Figure 4.6.</b> (a) Transfer characteristics of PFT-100 based OEET operated in sodium chloride aqueous electrolyte with various concentrations; (b) Drain current $I_D$ value extracted at $V_G = -0.8 \text{ V}$ versus the electrolyte concentration; (c) Transfer characteristics of PFT-100 based OEETs operated in aqueous solution with different electrolytes. ....	66
<b>Figure 5.1.</b> (a) Optical images of OEET pattern with the molecular	



structure of p(g2T-TT); (b) photographs of flexible OECT with different bending statuses; (c) output characteristics (drain current $I_D$ versus drain voltage $V_D$ ) under gate voltage $V_G$ varying from 0.2 to -0.6 V; (d) transfer curves ( $I_D \sim V_G$ ) with different bending radii.....	74
<b>Figure 5.2.</b> (a) Schematic of the OECT cross-section for RNA sensing; the change in transfer curves of the modified OECT with (b) thick p(g2T-TT) film and (c) thin p(g2T-TT) film upon addition of increasing concentration of mRNA; (d) Normalized current response of OECT with different channel thickness (thick, ~100 nm; medium, ~50 nm; thin, ~20 nm) to varying RNA concentrations.....	75
<b>Figure 5.3.</b> (a) Schematic of the sensing mechanism illustrating the interaction between RNA and polymer in the channel area of OECT; (b) Capacitance of p(g2T-TT) film corresponding to the film thickness $d$ .....	77
<b>Figure 5.4.</b> (a) Effective areal capacitance and (b) phase from EIS for p(g2T-TT) film coated on ITO substrate and modified with increasing RNA concentrations; (c) normalized capacitance response as a function of RNA concentration.....	79
<b>Figure 5.5.</b> Attenuated total reflection (ATR) Fourier transform infrared spectra of pure p(g2T-TT) film (black) and films with physical absorbed (red) or chemical bonded (green) RNA molecules.....	80
<b>Figure 5.6.</b> (a) The change of transfer curves of DNA probe modified OECT upon addition of increasing concentration of oral cancer biomarker IL-8 mRNA; (b) normalized current	



response of the device response to complementary RNA  
sequence and 4-base mismatched RNA sequence.....81

**Figure 5.7.** (a) The calculated radius of three monovalent anions versus  
the corresponding molar mass; (b) transfer characteristics of  
OECT with different electrolyte anions at the same  
concentrations of 1 M (with the same sodium counterion).....83

**Figure 5.8.** (a) Effective capacitance, (b) phase and (c) Nyquist plot  
from EIS for p(g2T-TT) film characterized in different  
electrolytes. (d) Comparison of the effective capacitance of  
p(g2T-TT) film and ITO electrode at varying bias voltage  
 $V_{\text{bias}}$  in different electrolytes. ....85

# Chapter 1 Introduction

## 1.1 Background

Organic electronics, as one of the most exciting and promising information technology nowadays, has drawn extensive research interests in the past decades.<sup>1,2</sup> One remarkable milestone is the discovery and synthesis of the first semiconducting polymer, polyacetylene, which led to the phenomenal growth of this field. It was back in 1970s, that Hideki Shirakawa, Alan Heeger, and Alan MacDiarmid first reported the high electrical conductivity of this polymer upon doping,<sup>3</sup> who were then awarded the Nobel Prize in Chemistry in 2000.<sup>4</sup> Ever since then, considering for the intrinsic advantages of organic materials, such as convenient solution processing, freedom of synthesis, mechanical flexibility and excellent biocompatibility,<sup>5</sup> a variety of organic semiconducting materials, including small molecules and conjugated polymers, have been developed to be integrated into numerous electronic devices, such as organic solar cells,<sup>6,7</sup> organic light emitting diode<sup>8,9</sup> and organic thin film transistors (OTFTs),<sup>10–12</sup> opening the door for this emerging field.

Typically, transistors are semiconducting devices widely used in integrated circuits for amplification or switch of electronic signals.<sup>13</sup> Small molecule organic materials and semiconducting polymers were successfully demonstrated to be integrated in transistors, demonstrating the concept of OTFTs, separately at 1964 and 1986.<sup>14,15</sup> From then on, OTFTs have been employed in various electrical applications, due to its desirable features in cost-efficiency and large area solution processability.<sup>16</sup> An OTFT consists of source and drain electrodes, which are connected by an organic semiconducting thin film. The current flow is modulated by the voltage applied from

an external gate electrode. Based on the difference in working mechanism, OTFTs generally fall into two categories, organic field effect transistors (OFETs) and organic electrochemical transistors (OECTs).

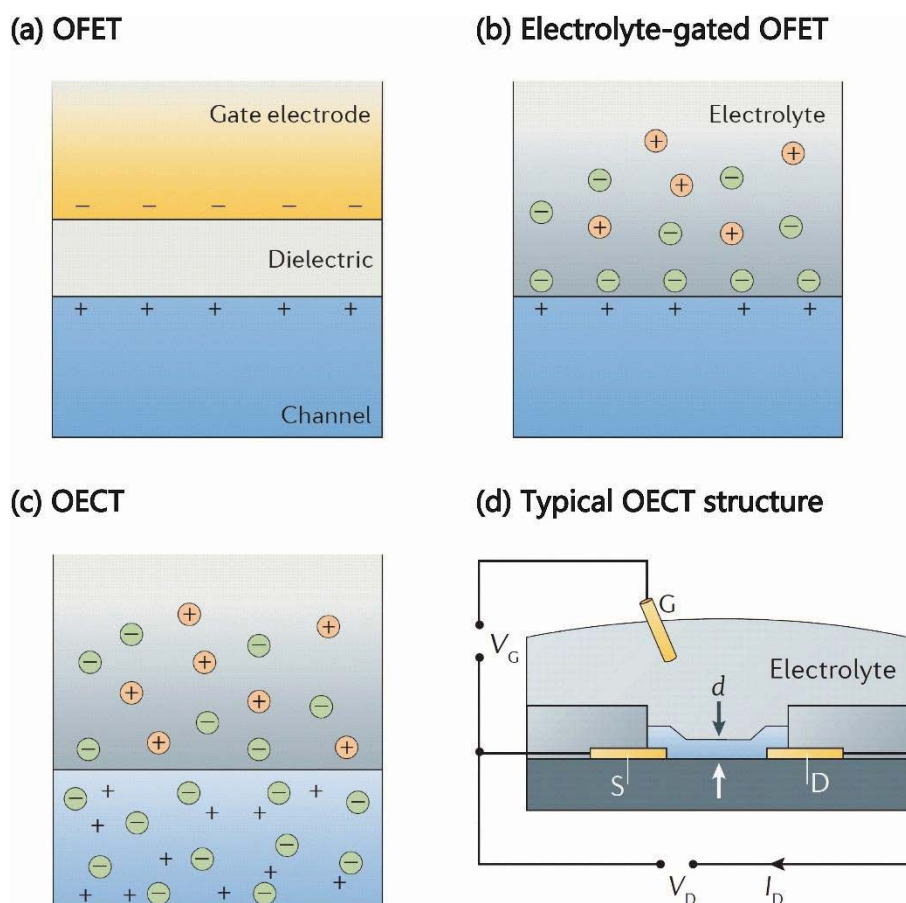


**Figure 1.1.** Schematic diagram of working mechanism for (a) OFET, (b) Electrolyte-gated OFET and (c) OECT; (d) the typical OECT structure, with the symbol S, D, G represent source, drain and gate electrode respectively, d represents the thickness of channel layer.<sup>17</sup>

In a classical OFET structure, a thin insulating layer is inserted between channel and gate electrode, forming a capacitor under gate voltage applied, therefore the electronic charges accumulated near the interface of channel/dielectric layer is modulated through field effect doping. (Figure 1.1(a)) For an extreme case of OFET, when the channel area directly exposed to aqueous electrolyte without separated by a dielectric layer, the so-called electrolyte-gated OFET (EGOFET), an electrical



double layer capacitor is formed near the interface, as illustrated in Figure 1.1(b). Since the electrical double layer is formed of ionic species in the aqueous electrolyte, the thickness is only a few angstroms, much thinner than the traditional dielectric layer, resulting in a much higher capacitance and lower operation voltage.<sup>18-22</sup> The remarkable features that electrolyte-gated OFET could present stable performance in aqueous electrolyte with extremely low gating voltage ( $< 1$  V) make it an ideal candidate for label-free, highly sensitive and selective sensing applications.<sup>23-26</sup> However, due to the intrinsic feature of the semiconducting channel material used here, the ions could not penetrate into the bulk of film, leading to a drawback that we could not take the advantage of ion/electron mixed conducting properties of semiconducting polymers for biosensing applications, as there will be no direct ion fluctuation between the biological tissues and the polymer backbone.

The other category of OTFTs is the organic electrochemical transistor, which is the major focus of this thesis. As can be seen from Figure 1.1(c), the channel current of an OECT is modulated by electrochemical doping of ions penetrating inside the bulk of the semiconducting layer. This volumetric capacitance could be several orders of magnitude larger than those parallel plate capacitors formed in OFETs, which could contribute to higher sensitivity and amplification capability for OECTs.<sup>27,28</sup> Therefore, since the first demonstration of the principle of OECT by Wrighton and coworkers in 1984,<sup>29</sup> the whole field started to take off. Beside the advantages in low operation voltage and stable performance in aqueous environment, which have been discussed in electrolyte-gated OFET, another significant strength of OECT comes from its electrochemical doping mechanism.<sup>30-33</sup> The need for high efficient electrochemical doping requires the semiconducting layer to be either loose and porous structured, or perform excellent swelling capability, both with the same objective, to enhance the efficiency of ionic/electronic exchange.<sup>34</sup> This unique

feature makes OEET especially suitable for direct “talk” with the complex biological molecules and activities, more accurate and convenient than employing the electrolyte-gated OFET, which is impermeable to ions.<sup>35</sup>

Seen from the typical OEET structure in Figure 1.1(d), the source (S) and drain (D) electrodes are normally made of metal or conductive polymers, simply for electron transport; the gate (G) electrodes could be metal, glassy carbon or Ag/AgCl, aiming to control the potential profile through the device or carry on catalytic sensing applications.<sup>36,37</sup> Therefore, what matters most to the device performance would be the channel layer, made up of the replaceable semiconducting materials.

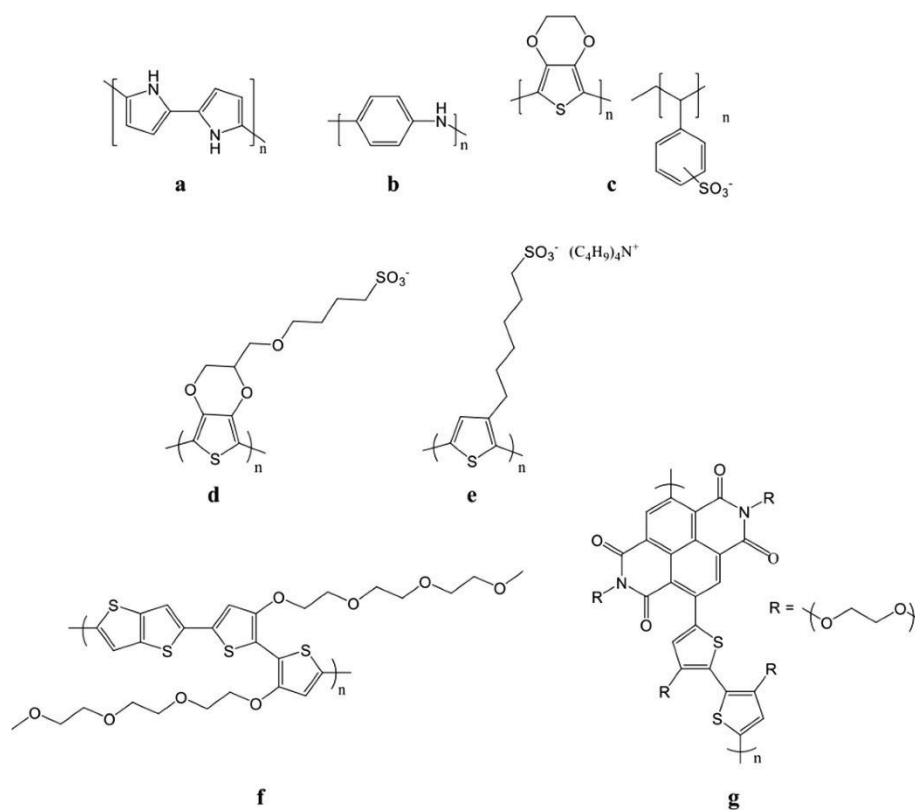


**Figure 1.2.** Chemical structures of conjugated polymers employed in OEETs: (a) polypyrrole; (b) polyaniline; (c) PEDOT:PSS; (d) PEDOT-S; (e) PTHS; (f) p(g2T-TT); (g) p(NDI-g2T).<sup>38</sup>

In the early stage of the development of OEET, the selection range for channel



materials was quite narrow. Conjugated polymers with simple repeating units, such as polypyrrole and polyaniline (Figure 1.2(a), (b)) were frequently employed, even though these materials were not stable during operation.<sup>39,40</sup> PEDOT:PSS, the predominately materials currently used in OECTs,<sup>41,42</sup> conjugated polyelectrolytes, such as PEDOT-S<sup>43</sup> and PTHS<sup>44</sup>, and some high mobility conjugated backbone with nonionic polar side chain functionalized, p(g2T-TT)<sup>45</sup> and p(NDI-g2T)<sup>46</sup>, (Figure 1.2(c)-(g)) were continuously developed by synthetic chemists, putting efforts in fabrication of high performance OECTs. For highly doped PEDOT:PSS, the intrinsic ON state might lead to high power consumption phenomenon due to the high current, which might not be suitable for logic circuits applications. Most of other materials are fabricated into OECT operated in accumulation mode, which means that at zero gate voltage, the channel has very few mobile holes and the transistor is in OFF state. After the gate voltage is applied, holes accumulate on the conjugated backbone of polymers to compensate the injected ions and the transistor is turned on, leading to a significant modulation of current output. Benefiting from the rapid growing of available semiconducting materials, OECTs have been demonstrated to be a promising and high efficient platform for various bioelectronic applications, such as high sensitive biomolecule detection,<sup>47-52</sup> tissue activity monitoring,<sup>53-59</sup> logic circuits for pixel drivers,<sup>60-65</sup> and memory/neuromorphic devices.<sup>66-69</sup>

## 1.2 Objectives of Research

The in-depth investigation into OECTs requires a cross disciplinary research covered several fields, such as electrical engineering, electro and synthetic chemistry, condensed matter physics and biological science. Though more than thirty years have passed since the first prototype of OECT was reported, better understanding of the working mechanism and device optimization are still in urgent need for various



application requirements. The major motivation of this thesis is to improve the performance of OECT and proceed device functionalization for fabricating novel chemical and biological sensors. The general objective here is to provide a comprehensive understanding of device operation, both for the accumulation and depletion mode OECTs, through varying processing technology, characterization methods, channel material design strategies and development of novel sensing mechanism for high sensitive biosensors.

Specifically, the first objective of this thesis is to decrease the response time for operation of OECT by device miniaturization through microfabrication technique. Then it is possible to employ transient (AC) characterization to enhance the sensing performance of OECT to ions and biomolecules. The second objective is to explore the possibility to employ conventional high mobility conjugated polymers in OECT operation. Through the analysis of the structure-property relationship, the results would shed light on the guideline for material design strategies of high performance OECTs. The last objective is to employ a novel accumulation mode OECT for RNA sensing applications. The in-depth investigation of sensing mechanism would lead to better understanding of interactions between conjugated polymers and biomolecules, and subsequently the ionic/electronic exchange in the operating mechanism of OECTs.

### 1.3 Outline of Thesis

The organization of this thesis is shown as follows:

**Chapter 1:** Introduction. In this part, the historical background and the evolution from organic electronics to the specific OECTs are introduced, followed by discussion of device classification and semiconducting materials. The objectives and outline of this

thesis are presented.

**Chapter 2:** Literature review. First the general working mechanism of OECTs is introduced, followed by an overview of recent efforts on functionalization of OECTs for bioelectronic applications. The design strategies are summarized majorly in three aspects, the channel, electrolyte, and gate functionalization.

**Chapter 3:** AC measurements for accurate sensing applications of OECTs. In this chapter, the microfabrication technique using photolithography is introduced for miniaturization of OECTs. Then a novel method for electrochemical sensing is developed, by recording both the transconductance and phase of the AC channel current in OECTs.

**Chapter 4:** High mobility p-type conjugated polymers for applications in OECTs. In this chapter, several thiadiazole and diketopyrrolo-pyrrole based conjugated polymer are characterized in OECT platform. Then for the PFT-100 based OECT, which demonstrated superior electrical performance compared to other polymers, further process optimization and ionic properties are investigated for comprehensive understanding of the doping/dedoping process and ionic penetration into the conjugated polymer film.

**Chapter 5:** Label free RNA sensors based on capacitance modulated OECTs. In this chapter, a flexible, label free RNA sensor based on a p-type accumulation mode OECT is developed, with the detection limit down to  $10^{-12}$  M in physiological environment. The sensing mechanism is further investigated through studying the interaction between semiconducting polymers and various ionic species in aqueous electrolytes.

**Chapter 6:** Conclusions and Perspectives. In this chapter, the summary of the work in this thesis is presented and further challenges and opportunities are proposed.

## Chapter 2 Literature Review

### 2.1 Introduction

The rising field of bioelectronics efficiently bridges semiconductor based electronic devices with biological environment. It solves the difficulty to soften the boundary between the mechanically hard, static microelectronic world with the soft, dynamic cell and tissue activities.<sup>70</sup> Therefore, bioelectronic devices have attracted much interests in the field of diagnosis and therapy.<sup>71–73</sup> Organic electrochemical transistors, owing to its intrinsic amplification capability of received signals, have emerged as one of the most advanced and modern sensing platforms for biosensors.<sup>74</sup> The advantages in synthetic freedom, low temperature solution processing and mechanical property matching, make OECTs easier to be integrated into wearable electronics, e-skin and implantable devices.

One of the major challenge in design and development of biosensors is the rapid, efficient signal capture and extraction of the biological recognition events. While OECTs are qualified to transduce the presence or change of target analytes into electrical signals, they are also possible to detect and amplify the interfering component in the complex biological systems. In order to enhance the sensitivity and specificity of these sensors, along with other analytical figure of merits, such as reproducibility, calibration range and linearity, accuracy and quantification, OECT sensors need to be proper functionalized through chemical or biological modifications.

In this chapter, we will first review the working mechanism of OECTs, both in depletion and accumulation modes. Then the functionalization strategies aiming to

fabricate high performance OECT sensors are presented, focusing on channel materials, electrolyte systems and gate electrodes in sequence. Various modification methods and sensing mechanisms are discussed in detail.

## 2.2 Working Mechanism of OECTs

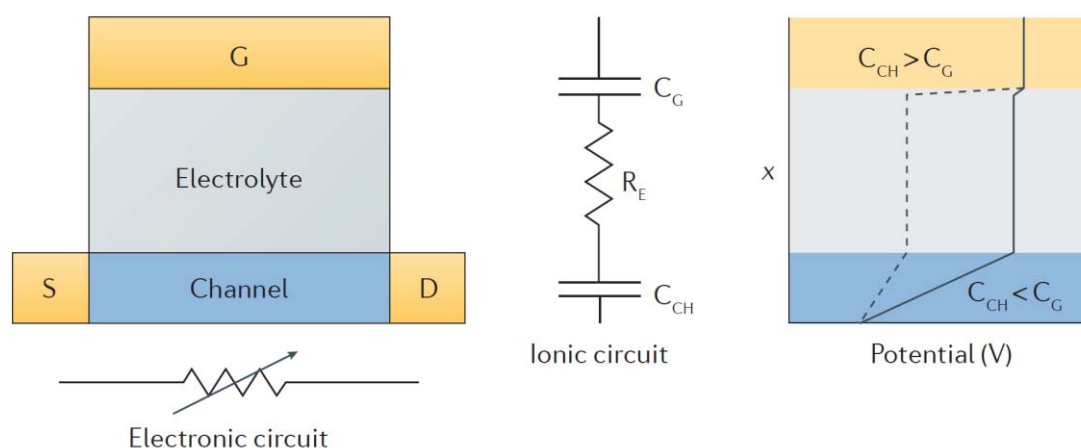


**Figure 2.1.** Electronic and ionic circuits illustrated in Bernards Model. The right graph shows the profile of potential drop in ionic circuit, under two different conditions, that whether channel capacitance ( $C_{CH}$ ) is larger than gate capacitance ( $C_G$ ) or not ( $C_{CH} > C_G$  or  $C_{CH} < C_G$ ).<sup>17</sup>

Typically, an OECT consists of source, drain and gate electrodes. A source drain voltage ( $V_D$ ) and source gate voltage ( $V_G$ ) are applied during operation, as shown in Figure 1.1(d). A most widely accepted operation mechanism is elaborated by the Bernards Model, which was proposed in 2007.<sup>75</sup> In this model, the OECT is regarded as a combination of two circuits, the ionic circuit and electronic circuit, as shown in Figure 2.1. In the electronic circuit, the semiconducting channel layer is regarded as a resistor, whose resistance is variable due to the gating effect. The ionic circuit includes three parts, capacitors corresponding to gate ( $C_G$ ), channel ( $C_{CH}$ ) and a resistor ( $R_E$ ) represents the resistance of aqueous electrolytes environment between channel and gate. As the capacitors are connected in series, the applied  $V_G$  drops

majorly on smaller capacitors, as illustrated in the right graph of Figure 2.1. This implies a notable guideline for device design, which is, for utilizing OECT as an ion to electron converter, the channel area should be much smaller than gate electrode, to confirm the necessary gating efficiency.<sup>36,76</sup> Other alternatives besides increasing gate electrode area are either using a thick conducting polymer film coated electrode (leading to larger  $C_G$ ) or employing nonpolarizable electrode, such as Ag/AgCl for gating. However, for OECT operated as electrochemical sensor (with the reaction occurs on gate electrode), the  $C_G$  should be decreased compared to  $C_{CH}$  to present higher sensitivity.

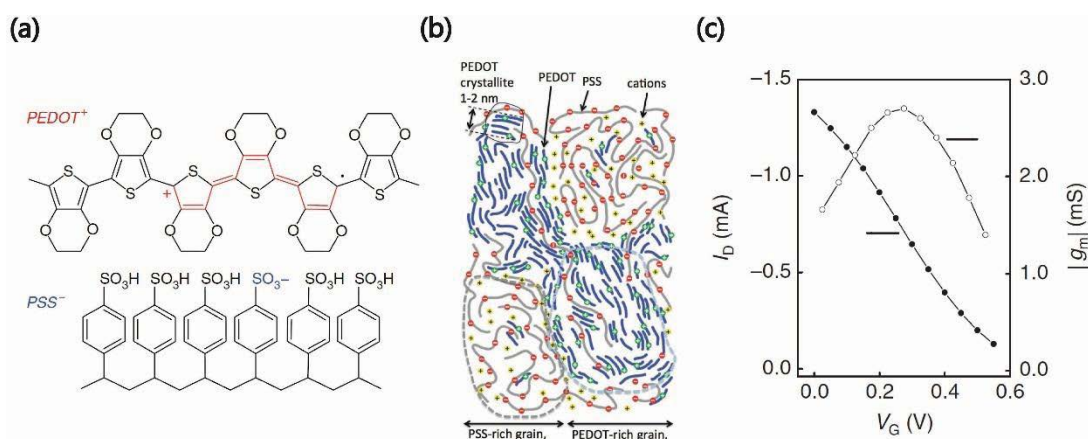


**Figure 2.2.** (a) Chemical structure of PEDOT:PSS, the holes generated on the conjugated backbone (red) is compensated by the sulfonate ions (blue) from PSS<sup>-</sup>;<sup>77</sup> (b) Schematic diagram of the PEDOT:PSS morphology model for cation dedoping process;<sup>78</sup> (c) Typical transfer characterization and associated transconductance ( $g_m$ ) for PEDOT:PSS based OECT.<sup>77</sup>

For OECT operated in depletion mode, the representative semiconducting polymer is the PEDOT:PSS, which is short for poly(3,4-ethyl-enedioxy thiophene):poly(styrene sulfonate). The PEDOT backbone is degenerately doped by PSS, resulting in high conductivities, which determine the initial ON state current of OECT. (Figure 2.2(a)) The morphology schematic shown in Figure 2.2(b) further indicates that crystalline PEDOT-rich grains dominate the hole conductivity, while the PSS-rich grains



contribute to ionic transport. When cations are driven into the PEDOT:PSS film under positive  $V_G$  applied, the dedoping process occurs, which could be described as the reversible redox reaction as follows,<sup>79</sup>



where  $M^{n+}$  represents the cations in the electrolyte,  $e^-$  is the electron provided from source electrode. The doping of cations results in the reduction of PEDOT and a decreasing hole concentration. Therefore, the channel current decreases with increasing  $V_G$ , as observed in the transfer characterization in Figure 2.2(c). According to Bernards model, the channel current at saturation region is given by,<sup>28</sup>

$$I_D = \frac{W}{2L} \cdot \mu \cdot d \cdot C^* \cdot (V_{th} - V_G)^2 \quad (2.2)$$

where  $L$  and  $W$  are the length and width of channel,  $\mu$  is the hole mobility,  $d$  is the channel thickness,  $C^*$  is the volumetric capacitance,  $V_{th}$  is the threshold voltage. This equation clearly indicates the contribution of device geometry and material property to the current modulation of OECTs. The product of mobility and volumetric capacitance,  $\mu C^*$  is extracted as the figure of merit of material to benchmark and evaluate the OECT performance.<sup>34</sup>

The transconductance ( $g_m$ ), another figure of merit, which was frequently cited to evaluate the amplification efficiency of OECT, could be simply derived from the first derivative of the above equation with respect to  $V_G$ ,

$$g_m = \frac{\partial I_D}{\partial V_G} = \frac{W}{L} \cdot \mu \cdot d \cdot C^* \cdot (V_{th} - V_G) \quad (2.3)$$

However, this equation could not well explain the non-monotonic dependence of  $g_m$  on gate voltage, as can be seen from the transconductance curve in Figure 2.2(c).



Lussem and coworkers claimed that the bell-shaped transconductance could be derived from the contact resistance (poor electrical contact between electrodes and channel materials),<sup>80</sup> especially for highly doped OECT. Friedlein and coworkers recently investigated the behavior of both depletion and accumulation mode OECT, concluding that this phenomenon arises from the disordered state of materials, which affects the electronic transport in channel.<sup>81</sup> This is an intrinsic property of device, that would exist even without contact resistance.

For OECTs operated in accumulation mode, the device is initially in the OFF state as the semiconducting polymer is undoped, which means the small amount of mobile holes is not sufficient for channel current flow. Upon anion injection under negative  $V_G$  bias (for p-type semiconducting polymer), the electrochemical doping of channel materials leads to accumulation of holes, switching the device to ON state. The equation 2.2 could also be applied to the accumulation mode OECT (with the voltage terms reversed), considering for the similar electrochemical doping mechanism.

## **2.3 Chemical Functionalization of OECTs for Bioelectronic Applications**

### **2.3.1 Channel Functionalization**

According to the working mechanism of device operation discussed above, the applied gate voltage modulates the channel current through the electrolyte (either from field effect or electrochemical doping), it is obvious that the functionalization on the surface of the channel area would provide a direct and efficient influence on the device response for the target analyte. Various strategies focused on the engineering of channel/electrolyte interface will be discussed as following.



### 2.3.1.1 Chemical immobilization

From a synthetic point of view, the introduction of bioactive groups or biorecognition sites onto the backbone of organic semiconductor materials, would definitely make the synthesis routes more complex and the processes more critical. Therefore, the chemical immobilization on the surface of the semiconducting layer, has been demonstrated as a facile strategy widely used for the channel functionalization of OTFTs. In 2012, our group first reported the capture and detection of *E. coli* O157:H7 bacteria by channel functionalized OECT (Figure 2.3(a)).<sup>82</sup> The active channel material PEDOT:PSS was chemically modified with amino end groups for further covalently bonded with anti-*E. coli* antibodies, a biorecognition element for specific capture of this bacteria. The electrostatic interaction between the negative charged bacteria and PEDOT:PSS leads to the sensitive changes in the gate potential drop near the electrolyte/channel interface (Figure 2.3(b)), resulting in the quantitative detection of the bacteria concentration down to  $10^3$  cfu·mL<sup>-1</sup>. Similar approaches employing the high affinity binding interactions between antibody and antigen were extensively investigated for OTFT based immunosensors, due to its high sensitivity and selectivity.<sup>83,84</sup> Nanomaterials such as gold nanoparticles were also integrated in the modification process, aiming to improve the sensitivity and dynamic range, considering for its important role in signal amplification (Figure 2.3(c)).<sup>85</sup>

Beside the antibody/antigen interaction, enzymes, the macromolecular biological catalyst, were frequently employed for the detection of biological molecules based on the specific acceleration of chemical reactions with analytes. As shown in Figure 2.3(d), the enzyme penicillinase was immobilized on the surface of  $\alpha$ -sexithiophene channel by chemical bonding and used for specific detection for penicillin.<sup>86</sup> Figure 2.3(e) illustrates the molecular antenna on the surface of the OTFT for the detection

of adenosine triphosphate (ATP).<sup>87</sup> The hydrolytic enzyme, apyrase, was linked to the channel surface by a plasma-assisted interfacial grafting method, which resulted in a low detection limit down to  $10^{-10}$  M for ATP. The influence of power and exposure time of the oxygen plasma treatment was carefully investigated for the mobility changes of the channel materials, demonstrating this is a micro-damage grafting approach.

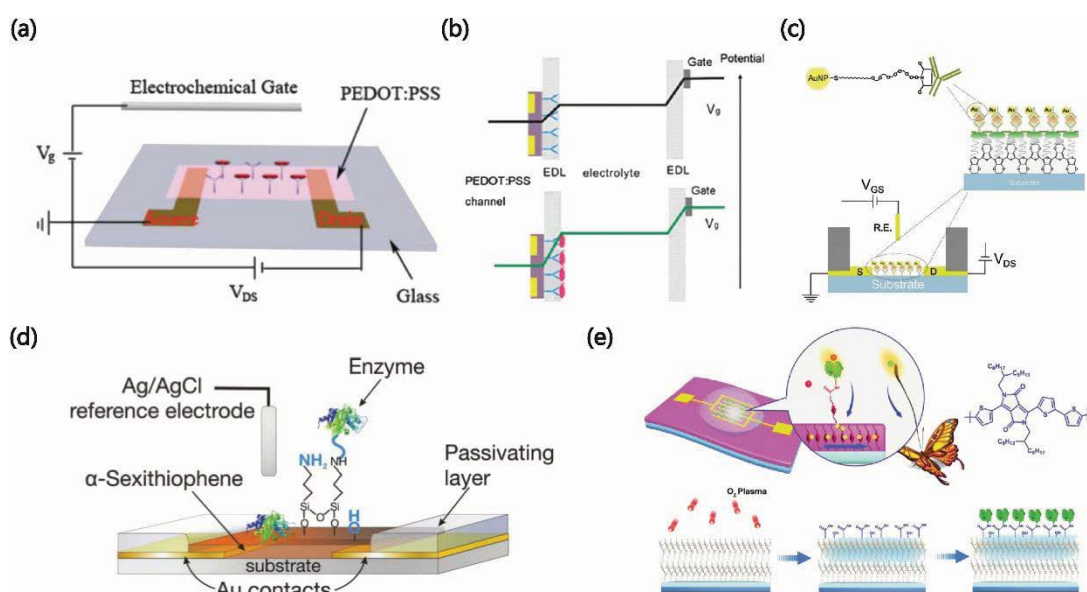


**Figure 2.3.** Chemical immobilization strategies for channel functionalization of OTFT sensors: (a) The device structure of an OEFT sensor for capture of *E. coli* bacteria; (b) the potential drops in the electric double layers in the OEFT before and after capture of the bacteria on the PEDOT:PSS surface.<sup>82</sup> (c) OEFT immunosensor for detection of prostate specific antigen/ $\alpha$ 1-antichymotrypsin complex, with the signal amplified by linked gold nanoparticles.<sup>85</sup> (d) The structure of biofunctional EGOFT with covalently bonded enzymes on the surface of  $\alpha$ -sexithiophene thin film.<sup>86</sup> (e) Schematic of the plasma assisted interfacial grafting of the tailored molecular antenna into the OTFT sensor, compared to a biological antenna of a butterfly.<sup>87</sup>

Above all, the chemical immobilization method efficiently functionalizes OTFT sensors with lower limit of detection and high specificity to certain analyte. However, cautions should be taken to evaluate whether and to what extent this kind of immobilization process may affect the intrinsic charge transport ability of

semiconducting channel layer. This is also one reason why enzymes and antibodies are more commonly employed in the gate functionalization processes, which will be discussed later. Therefore, more mild and high efficient routes still need to be explored for chemical immobilization of bioactive and biorecognition elements on the semiconducting layer.

### 2.3.1.2 Membrane Assembly

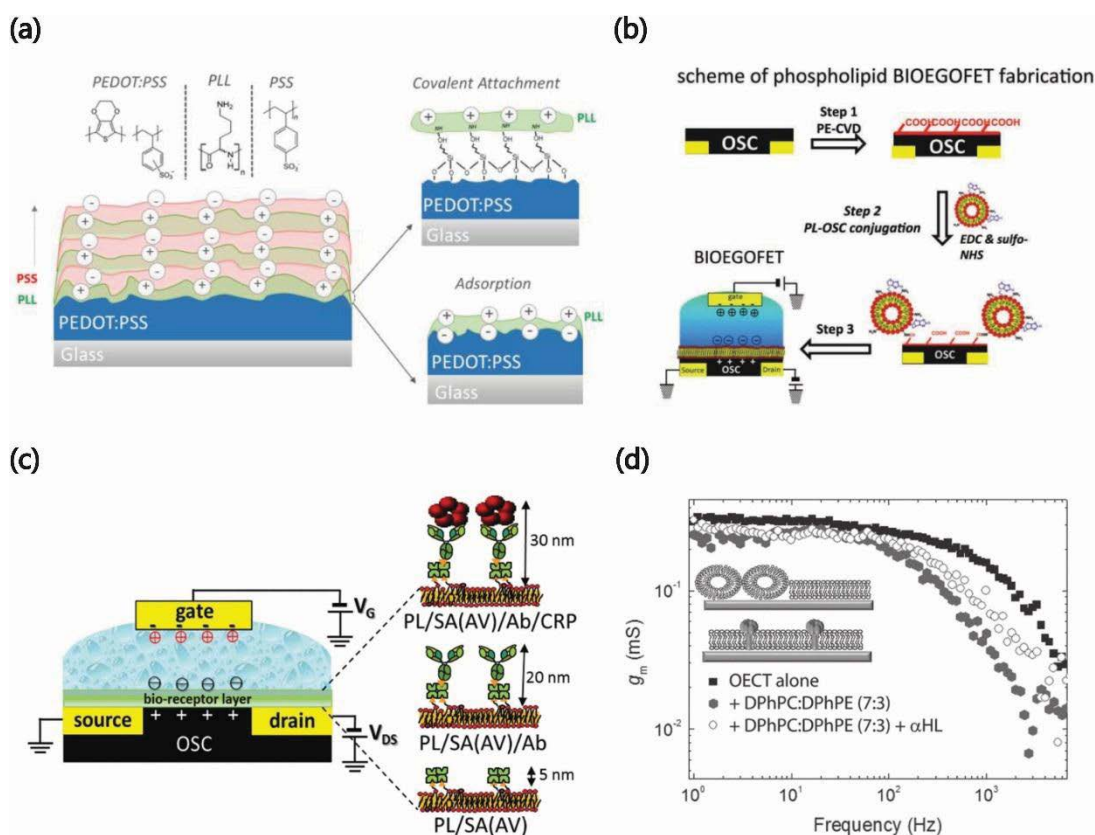


**Figure 2.4.** Surface functionalization by membrane assembly. (a) Chemical structure of PEDOT:PSS with two other polyelectrolytes, and layer-by-layer assembly of these polyelectrolytes at the surface of channel material PEDOT:PSS, initially either by covalent attachment or physical adsorption.<sup>88</sup> (b) Scheme of phospholipid bilayers coating on the surface of EGOFET channel area.<sup>25</sup> (c) EGOFET immobilized with a bio-receptor layer with varying distances from the channel surface.<sup>89</sup> (d) Comparison of the transconductance-frequency curves of OECT alone (black squares), OECT coated with vesicles and PLs (filled circles), and the same device with addition of Alpha-hemolysin protein (open circles).<sup>90</sup>



To avoid or reduce the potential damage induced by direct immobilization process on the channel layer, weak interactions, such as electrostatic force or amphiphilic self-assembly are introduced for surface membrane functionalization of channel area. As illustrated in Figure 2.4(a), a layer-by-layer assembly technique of polyelectrolytes was utilized for PEDOT:PSS based OECTs.<sup>88</sup> The initial layer could be deposited either by covalent bonded or via electrostatic adsorption, depending on the specific need of applications. After that the further addition of layers (poly-L-lysine and polystyrene sulfonate) were formed by the electrostatic interaction between the oppositely charged polyelectrolytes. This mild modification at the interface was expected to modulate the charge injection into the channel, which could provide an alternative efficient strategy for biosensing, such as RNA sensing in physiologically relevant electrolyte concentration. Phospholipid bilayers were also chosen to be modified on the surface of OTFT channel considering their advantages as versatile bio-systems. The basic procedures for functionalization of phospholipid bilayers (PLs) were drawn in Figure 2.4(b), using a conventional EDC/sulfo-NHS chemistry strategy.<sup>25</sup> The self-assembly of hydrophilic outer layers (the PL head) with a non-polar inner part (the PL tails) reduced the ion diffusion through the membrane, and therefore affect the device response. Another remarkable advantage is that the biotinylated PLs provided the binding sites for streptavidin or avidin labeled analytes, demonstrating the possibility for antibodies and proteins immobilized to fluid PLs coated at the channel area without altering the properties of the membranes. Based on this strategy, the bio-EGOFET sensor was successfully adopted for monitoring the protein binding event beyond Debye's length (Figure 2.4(c)).<sup>89</sup> This was mainly ascribed to the Donnan's equilibria within the protein acting as an additional capacitor to the electrolyte circuits. The capacitive tuning, instead of charges effect, could efficiently break through the Debye's screening and allow the sensors to be operated in high concentrated solutions like physiological



environment. From the perspective of bionics, the integration of functional transmembrane proteins into the supported PLs would open a wider border to set up new platforms for biosensing. Alpha-hemolysin was taken as an example to be inserted and detected by a PEDOT:PSS based OECT with surface coated PLs. Considering that this protein would form ion pores when inserted into the PLs, which opened an ionic channel for cations to pass through, the effect was clearly noticeable by the transconductance-frequency spectroscopy, where the cut-off shifted to higher frequencies with the existence of the protein, as more cations entered the channel (Figure 2.4(d)).<sup>90</sup> Further development of modeling on this system would allow extraction of more parameters for quantitative evaluation of the functions of these transmembrane proteins performed in the PLs, which would lead to a better understanding of trans-PL biological activities in actual organisms.

### 2.3.1.3 Biocompatibility Modification

Besides the improvements carried out for high sensitive and selective biological analytes detection, the applications of OTFTs in cell-based sensors are also emerging and attract great interests, as most of the semiconducting materials used in OTFTs are biocompatible and the cells or tissues could be in-situ cultivated and monitored on the devices.<sup>55,91–94</sup> Our group demonstrated the realization of cell-based biosensors by OECT with PEDOT:PSS as active layer, as shown in Figure 2.5(a).<sup>95</sup> The attach and detach processes of a human esophageal squamous epithelial cancer cell line were recorded by the transfer characterization, due to the effect of morphology change and surface charges redistribution of the attached cells on the channel area. As the culture condition for cancer cell lines is not very critical, only an ultraviolet radiation for 8 hours was presented for the sterilization of the OTFT sensing platform. More strategies should be taken into consideration for enhancing the biocompatibility, reducing the chances of infection and promoting the normal cell

culture on the OTFTs, while make minimum effects or degradation on the electrical performance of transistors.<sup>96–98</sup> The autoclave sterilization was systematically investigated on PEDOT:PSS microelectrodes and transistors, confirming that this frequently used clinical technique is efficient to get rid of the *E. coli* bacteria previously inoculated on the devices, while the morphology and the electrical characteristics did not alter or degrade significantly (Figure 2.5(b)).<sup>99</sup> Therefore, the autoclave was promising as a viable sterilization method for further introducing the OTFT sensors into clinical applications.

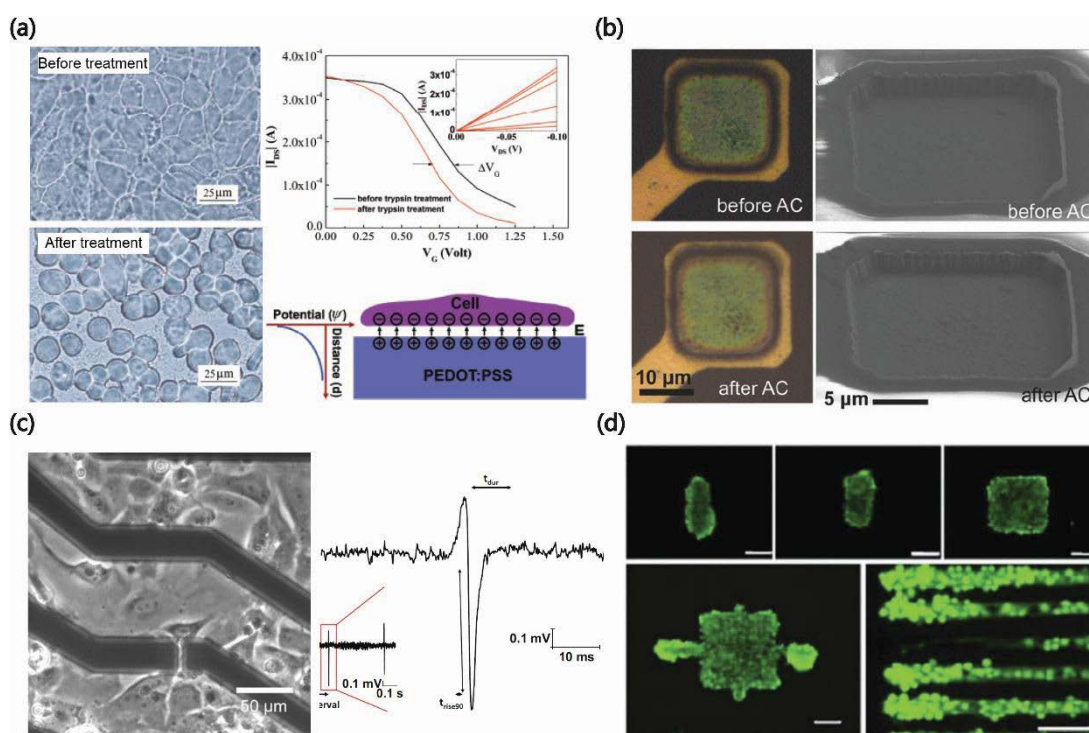


**Figure 2.5.** Biocompatibility modification for cell-based applications. (a) Optical images and transfer characterization of cancer cells cultured on channel area, before and after treatment of trypsin.<sup>95</sup> (b) Optical and scanning electron microscope images of the PEDOT:PSS films before and after autoclave (AC).<sup>99</sup> (c) Optical images of cardiomyocytes cultured on OECT array, and the profile of a single action potential recorded by the OECT on day 5.<sup>100</sup> (d) Fluorescence imaging of live (green) and dead (red) PC12 neuron cells cultured on the functionalized PEDOT:PSS pattern for 5 days.<sup>101</sup>

The culture for cells with specific functions needs more attention and the



pre-treatment process is more complicated. The recording and mapping of cardiac action potential generated from cardiomyocytes was demonstrated by a 16-channel OEET,<sup>100</sup> in which the cardiomyocytes were directly cultured on the surface of the PEDOT:PSS channel (Figure 2.5(c)). The devices were sterilized by the previously mentioned UV exposure and a subsequently immersion in 70% ethanol for a certain time. Then the fibronectin/phosphate-buffered solution was added to the device for surface coating, which played an important role in the adhesion of various types of cells onto the channel surface. The protein coating pretreatment is an effective technique to improve the biocompatibility of devices and guide the cell adhesion process. A facile biofunctionalization route was introduced by chemically coating a layer of extracellular matrix components on PEDOT:PSS.<sup>101</sup> The neuron cell line PC12 were seeded for observation of neuronal differentiation. As can be seen from Figure 2.5(d), the PC12 cells were perfectly confined to grow and differentiate only on top of the protein coated PEDOT:PSS pattern regions. The possibility to control cell adhesion and migration by simply carrying out surface coating of semiconducting polymer, indicates a great potential for tight integration of living cells with OTFT devices for further applications, such as stimulation and monitoring of specific cell functions, growth of designed neuron patterns for investigation of artificial neuronal networks.<sup>67,102,103</sup>

### 2.3.2 Electrolyte Functionalization

With continuously growing demand for disposable and wearable electronics,<sup>104–107</sup> planar structure design of OTFT combined with solid state electrolyte provides an alternative to get rid of the complex liquid handling in most of the non-laboratory detecting cases. In order to enhance the capability for specific detection, bioactive sites such as enzymes or mediators are incorporated into the electrolyte, for directly



facing the sensing interfaces. A fully solid state flexible OECT based lactate sensor was first reported by incorporating a lactate oxidase enzyme into the room temperature ionic liquid electrolyte (Figure 2.6(a)).<sup>108</sup> Several featured properties, such as wide electrochemical window, high stability and ionic conductivity, make this kind of solid electrolytes especially suitable for operation of electrochemical transistors.<sup>109–112</sup> The cross-linking technique to immobilize enzymes into the solid electrolyte could avoid considering for the poor solubilities of some catalytic mediators in aqueous solutions, and at the same time serves as a protective covering for the enzymes. The device was evaluated as a bandage-type sensor, which could detect the concentration of lactate in the sweat when it diffused into the solid electrolyte, demonstrating the possibility to be adopted in wearable electronics for health monitoring. Based on the same principle mentioned above, the screen printing technique was further introduced for the fabrication of the OECT sensor, as shown in Figure 2.6(b).<sup>113</sup> The metabolites such as glucose and lactate were detected on real human sweat samples, with the optimized detection limit suitable for the epidermal applications. Another possible way to take the advantage of the all-solid-state sensor is to employ it as a gas sensor. A disposal breathalyzer for alcohol sensing was realized on a paper based OECT, in which the electrolyte was made up of a collagen-based gel embeded with the enzyme alcohol dehydrogenase and its cofactor.<sup>114</sup> As illustrated in Figure 2.6(c), when simply breathing occurred on the surface of the breathalyzer, the ethanol contained in the breath caused a significant decrease in the drain current by the enzymatic catalyzed reaction in the electrolyte. It demonstrated that the inkjet-printed paper based OECT could serve as a reliable breathalyzer to evaluate the blood alcohol content in human subjects and its highly competitive features compared to the current commercialized products, such as low cost, disposable and environmental friendly nature of the devices.

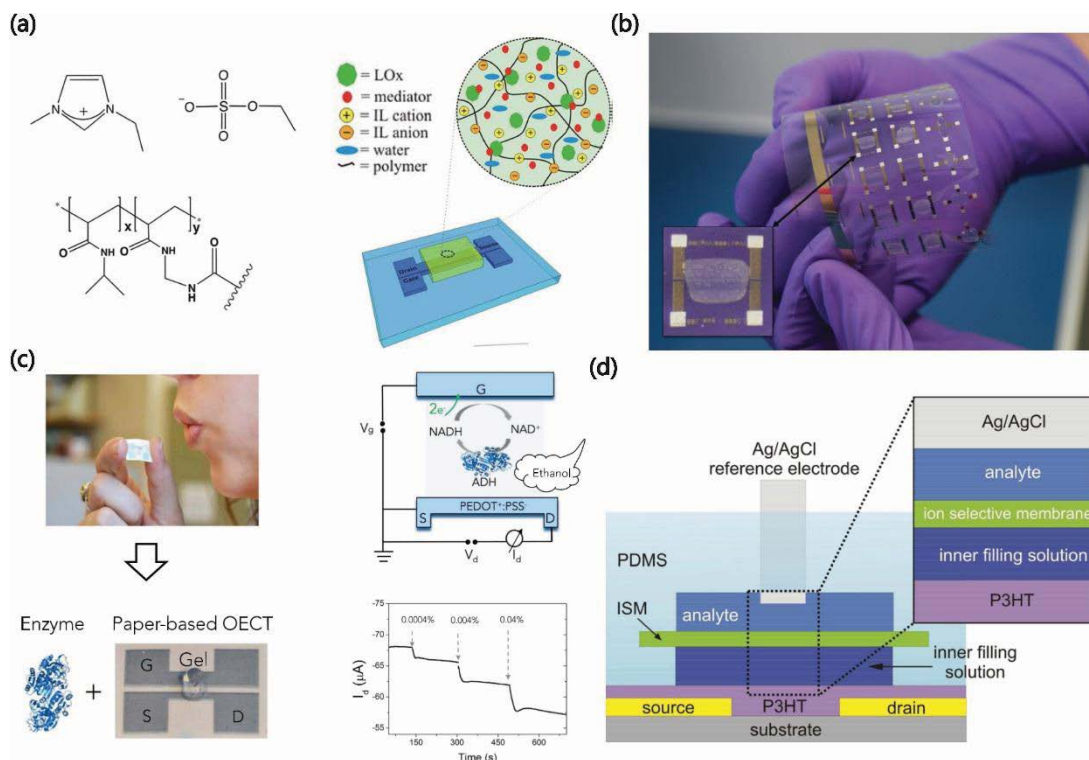


**Figure 2.6.** (a) Chemical structure of components of the ionic gel electrolyte and the schematic description of the mixture in the solid electrolyte layer of the OECT.<sup>108</sup> (b) Photograph of the screen printed all-solid-state OECT on flexible substrate.<sup>113</sup> (c) The breathing on the enzyme embedded paper based OECT, associated with the mechanism and the drain current response of the device towards exposure to ethanol.<sup>114</sup> (d) The schematic structure of the EGOFET integrated with an ion selective membrane.<sup>26</sup>

Besides the various attempts to employ solid electrolyte into the OTFT sensors, there are other efforts focusing on functionalization of the aqueous electrolytes, which is the typical solution discussed through this chapter. As seen from Figure 2.6(d), an ion selective membrane was inserted into the liquid electrolyte, separating it into two components, the analyte region and the inner filling solution.<sup>26</sup> The integration of this functional membrane provides the capability for the P3HT based electrolyte-gated OFET to carry out selective and reversible multiple ion detection. It is worth noting that since no direct modification or binding occurred on the semiconducting layer, the device performed higher stability and the reversible



detection could be much easier to realize by a simply flushing process. Furthermore, the detection of different ions by the same device could be achieved by replacing an appropriate ion selective membrane, which significantly expands the application fields.

### **2.3.3 Gate Functionalization**

Though versatile strategies have been employed targeting the semiconducting channel materials and the electrolytes for enhancing the sensing performance of both OECT and electrolyte-gated OFET biosensors, the major research interests and efforts, including from our group, are concentrated on the design of gate electrode functionalization. Considering that the gate electrodes, either made of metal or conducting organic materials, are isolated from the channel area, the surface modification or immobilization process will not affect normal operation and the device performance. More importantly, due to the basic mechanism of a transistor that the channel current (output) flowing between source/drain electrodes is controlled by the gate voltage (input), it has been demonstrated that a small change in the gate electrode can result in pronounced response of the channel current, which is beneficial for lower detection limit. Several strategies for gate functionalization, such as surface potential change, electrochemical reaction, nanomaterial modification and biorecognition element induced capacitive control are developed in recent years and the selected representative works will be discussed in this section.

#### **2.3.3.1 Surface Potential Modification**

The detection of intrinsic charges from biological molecules are of great interests to researchers as this is promising for constructing a direct, label-free, non-destructive sensing platform. Nucleic acid has been selected as a model molecule for OTFT

sensor applications not only because of its significant scientific importance in gene diagnostics, but also due to its low isoelectric point, which presents negative charges in physiological environment.<sup>115–117</sup>

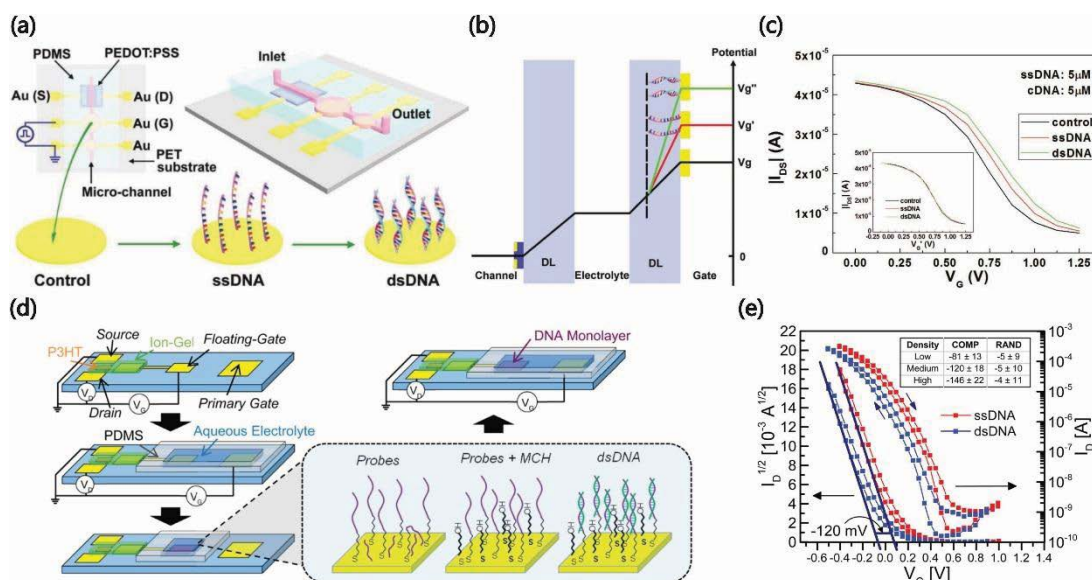


**Figure 2.7.** (a) Schematic of the flexible OECT sensor integrated in the microfluidic system, with the modification of DNA on the surface of gate electrode; (b) potential drop across the whole OECT device with the effect of immobilization of DNA probe (red line,  $V_{g'}$ ) and targets (green line,  $V_{g''}$ ); (c) transfer characteristics of the OECT before and after the modification and hybridization of DNA on gold electrode.<sup>118</sup> (d) The scheme of a floating gate connected EGOFET for the detection of DNA; (e) transfer characteristics of the EGOFET before (red) and after (blue) the hybridization of complementary DNA. Inset shows the voltage shift of complementary and random DNA at various probe densities.<sup>119</sup>

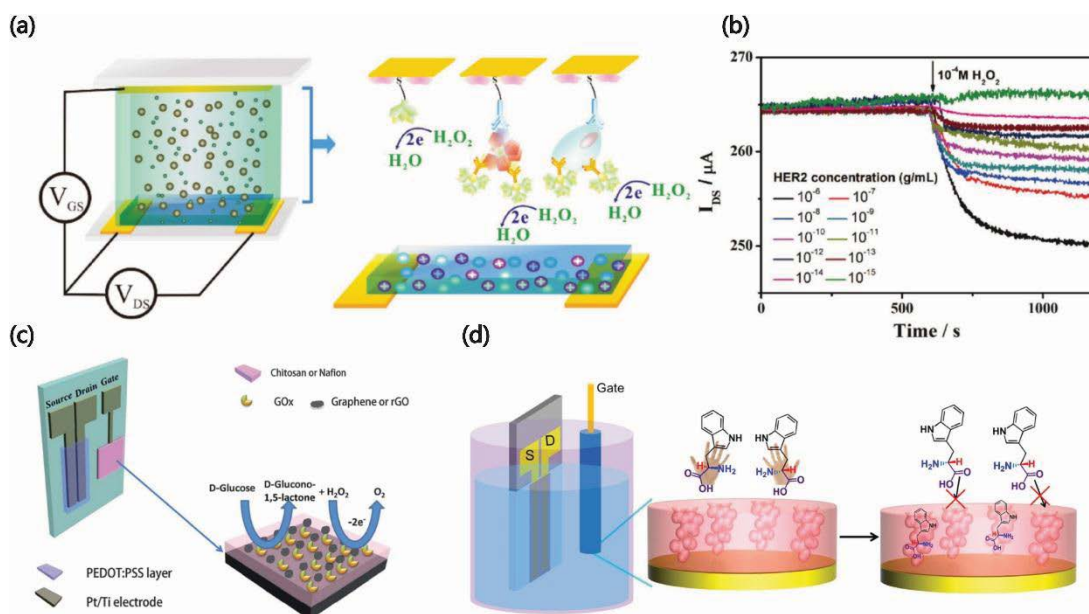
Our group reported an OECT based flexible microfluidic system employed for label-free sensing of DNA molecules, with a limit of detection down to  $10^{-11}$  M through a pulse-enhanced hybridization assistance.<sup>118</sup> As shown in Figure 2.7(a), the whole microfluidic device was deposited on PET substrate and the thiolated single stranded DNA probe was first immobilized on Au gate electrode. Then the complementary target DNA was detected by the modulation of surface potential on the gate electrode during hybridization process, as illustrated in the potential drop



diagram in Figure 2.7(b). A higher effective gate voltage was then required to offset the charge effect introduced by the hybridization of DNA, which resulted in a horizontal shift of transfer curves (Figure 2.7(c)). Therefore, the concentration of target DNA sequence could be clearly differentiated and recorded by the shift of gate voltage. A similar functionalization strategy was adopted by Frisbie's group for label-free DNA sensing by a P3HT based EGOFET.<sup>119</sup> The design of a floating gate physically separated the DNA detection reservoir with the operation of the transistor, effectively reducing the possibility of contamination or device degradation (Figure 2.7(d)). A horizontal shift to negative gate voltage was observed from the transfer characterization during the hybridization process, as shown in Figure 2.7(e). The opposite shift direction to the previously discussed OECT sensors was ascribed to the different operation mechanism (accumulation mode for EGOFET, compared to the depletion mode for PEDOT:PSS based OECT devices<sup>17</sup>). The sensing mechanism of floating gate design and origins of the DNA immobilization effect on the performance of OTFT sensors (surface charges, dipole orientations, potentials) were detailed discussed in a serial of references, which will not be analyzed here.<sup>22,120,121</sup>

### 2.3.3.2 Electrochemically Active (Enzyme) Modification

Electrochemical active modification of gate electrode could provide a promising method to further improve the sensitivity and selectivity of the OECT-based sensors. The type, amount and activity of the electrochemical active layer could greatly affect the analysis performance. Therefore, a substantial research effort has been undertaken to obtain an effective immobilization progress for highly active electrochemical layer modification on the gate electrode. Horseradish peroxidase (HRP) is one of the most frequently used electrochemical active enzyme in biosensors.<sup>122</sup> HRP can efficiently catalyze the electrochemical reaction of  $H_2O_2$ , which is often used in electrochemical signal generation processes for biosensing purposes.



**Figure 2.8.** (a) Scheme and working mechanism of OECTs with gate electrode modified with certain functional proteins or cells; (b) current change of the OECT when exposed to the different cancer cell biomarker HER2 concentration.<sup>123</sup> (c) Device structure of OECT sensor modified with chitosan/nafion, graphene/rGO and the enzyme for glucose detection.<sup>124</sup> (d) Chiral discrimination of amino acid enantiomers by OECT modified with molecularly imprinted polymer film.<sup>125</sup>

Recently, our group developed the OECT sensor to detect the specific protein biomarkers based on an HRP-labeled nanoprobe.<sup>123</sup> Figure 2.8(a) illustrates the device structure employing HRP-modified gate electrodes. In principle, the target cancer biomarker human epidermal growth factor receptor 2 (HER2) or the breast cancer cells were first selectively captured on top of gate electrode by the pre-modified antibody. Then HRP-labeled nanoprobe was specifically linked to the target protein or cells. Quantitative characterization of the HRP molecules by an electrochemical reaction of H<sub>2</sub>O<sub>2</sub> could be utilized to determine the concentration of target protein or cells captured on the gate electrodes. As shown in Figure 2.8(b), it could specifically detect the concentration of HER2 at 10<sup>-14</sup> g/mL (10<sup>-16</sup> M) level, several orders of magnitude lower than the value acquired from conventional cyclic voltammetry methods. This kind of functionalization strategy could serve as a versatile platform for



highly sensitive sensing and monitoring of different kinds of protein biomarkers in future applications.

Other kinds of enzymes were also integrated in organic transistors for electrochemically active sensing processes, such as glucose oxidase,<sup>124</sup> lactate oxidase,<sup>52</sup> cholesterol oxidase<sup>126</sup> and nitrate reductase<sup>127</sup>. Our group reported the realization of a high sensitive and selective glucose sensor by immobilizing glucose oxidase on platinum gate electrode, co-modified with biocompatible polymers (nafion and chitosan) and graphene-based materials (graphene or reduced graphene oxide flakes) (Figure 2.8(c)).<sup>124</sup> The interferents such as ascorbic acid and uric acid could be efficiently eliminated from the surface of gate by electrostatic interaction, and a linear response to glucose detection with the broad range from 10 nM to 1  $\mu$ M was established. Besides, molecularly imprinted polymer (MIP) film was introduced to OECT for the specific chiral recognition of D/L-tryptophan, and D/L-tyrosine (Figure 2.8(d)).<sup>125</sup> The electrocatalytic activity on the oxidation of these two amino acids could then be amplified by the transistor feature and a relative low detection limit of 2 nM could be reached.

As an extensive popular method used in chemical analysis and biological sensing, enzymic or other kinds of electrochemical active modifications play a very emerging and remarkable role when combined with organic transistors for sensing applications. Even a very weak electrochemical reaction generated at the gate area could induce a significant change of effective gate voltage and therefore, lead to a large current response for highly sensitive detection.

### 2.3.3.3 Enhancements from Nanomaterials

Nanomaterials modified gate electrodes could enhance the electrochemical activity

of the sensing sites and subsequently, the OECT sensitivity. As the “rising star” materials, graphene and other carbon-based materials are one of the most extensively investigated nanomaterials in sensing applications owing to their unique properties including high conductivity and stability.

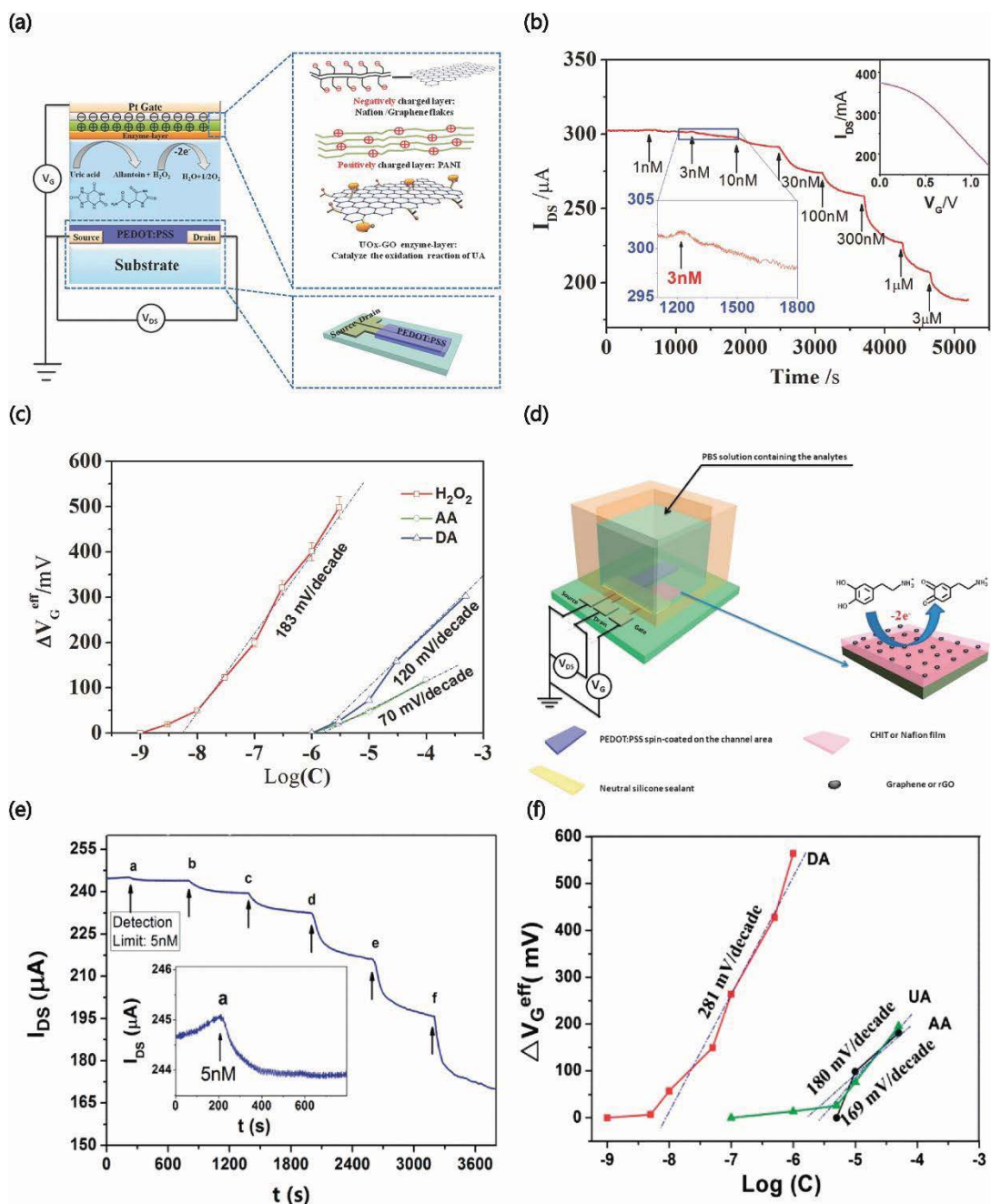


**Figure 2.9.** (a) Schematic diagram of OECT with an enzyme/polyaniline/nafion-graphene multilayer modified gate; (b) channel current response of the functionalized OECT to the addition of  $H_2O_2$  with various concentrations; (c) change of effective



gate voltage versus concentration of  $\text{H}_2\text{O}_2$ , ascorbic acid (AA), and dopamine (DA).<sup>128</sup> (d) Schematic diagram of OECT modified with chitosan and graphene for dopamine sensing; (e) current response of OECT to the addition of dopamine with various concentrations; (f) change of effective gate voltage versus concentration of DA, uric acid (UA) and AA.<sup>129</sup>

Our group introduced a universal sensing platform for highly selective detection of uric acid, cholesterol and glucose.<sup>128</sup> As shown in Figure 2.9(a), the polyaniline/nafion-graphene bilayer film was modified on gate electrode which only allowed  $\text{H}_2\text{O}_2$  to pass through. Other interferences such as ascorbic acid and dopamine were effectively blocked by the opposite charged layer structure due to electrostatic interaction. Therefore, the OECT performed both a high sensitivity to  $\text{H}_2\text{O}_2$  (Figure 2.9(b)) and a high selectivity to other interferences, indicated by the plot of changes in effective gate voltage versus the concentration (Figure 2.9(c)). Based on the good analytical performance, this sensor was further successfully applied in saliva analysis, which may shed light on non-invasive detection of biological molecules. Graphene modification on OECTs was also employed for dopamine sensing, as shown in Figure 2.9(d).<sup>129</sup> The sensitivity was improved to 5 nM (Figure 2.9(e)), much lower than conventional analytical methods, mainly contributed from the high conductivity of graphene flakes which could enhance the charge transfer during the electrochemical reaction. The selectivity was also improved by the co-modification of nafion or chitosan, similar as previous work. (Figure 2.9(f)) Besides graphene, other kinds of carbon-based nanomaterials such as single wall or multiwall carbon nanotubes were also considered for enhancing the sensing performance for epinephrine<sup>130</sup> and gallic acid,<sup>131</sup> which indicates the potential for fabricating low-cost, disposable sensing platforms.

Platinum nanoparticles, due to its outstanding electrocatalytic activity, and large specific surface area for enzyme immobilization, were also widely used in the



functionalization of OECT biosensors, aiming for high sensitive detection of glucose<sup>132</sup> and other metabolites.<sup>133</sup> In general, various nanomaterials have been applied in OECT-based gate electrode modifications. They greatly improve the detection performance, which holds great potential for noninvasive detection in body fluids that have a high requirement of sensitivity.

#### 2.3.3.4 Biorecognition Element Modification

Different types of biorecognition elements have been widely introduced into conventional sensing electrodes in the field of analytical chemistry, due to their high coupling affinity and specificity. Recently the importance of biorecognition elements attracted great attention to be integrated into the OECT and EGOFET based sensors, especially immobilized on the gate electrode. The ultra-sensitive detection of chiral differential interaction in odorant binding proteins (OBP) was demonstrated by Torsi's group, employing a EGOFET modulated by the ligand induced capacitance change.<sup>134</sup> The typical EGOFET structure was illustrated in Figure 2.10(a), while the gold electrode was immobilized with a monolayer of thiolated porcine OBP. The ligand S-(+)-carvone and R-(-)-carvone were differentially captured by this OBP, and therefore, caused a minor change in the series capacitance of this protein layer, which could effectively modulate the potential drop and the current response of the EGOFET (Figure 2.10(b)). The detection limit could reach 50 pM for the neutral ligand detection, which is a remarkable progress especially for the enantiomeric discrimination. Another example to integrate biorecognition element into OECT is the label-free detection of sialic acid, by means of the specific interaction between the sialic acid and phenylboronic acid, as shown in Figure 2.10(c).<sup>135</sup> The device was fabricated with screen-printed carbon electrodes on flexible plastic substrates (Figure 2.10(d)), demonstrated the potential for low-cost, disposable assay applications. Not only the free molecules, but also the cells with glycan terminal sialic acid presented

on the membrane surface could be directly captured by the modified gate electrode. The biosensor developed by this method presented the capacity to distinguish cancer cells from normal ones (Figure 2.10(e)), without the need of labeling or enzyme modification, indicating the advantages in simplifying the analysis, reducing the cost and enhancing the device stability. There are also other strategies to utilize the biomolecule recognition system, such as streptavidin immobilization for detection of biotinylated immunoglobulin G,<sup>136</sup> which shines light on the improvement of high sensitive and specific assay methods for nonspecific binding biomolecules, such as proteins, lipids, and some metabolites.<sup>137</sup>

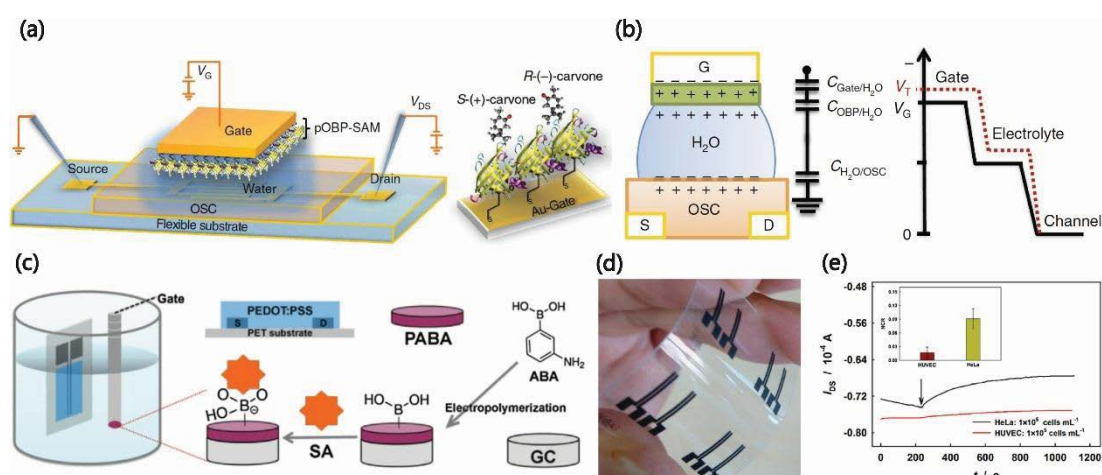


**Figure 2.10.** (a) Schematic structure of the electrolyte-gated OFET with porcine odorant binding protein (pOBP) immobilized on the Au gate electrode; (b) the double layer capacitors formed in series at the corresponding interface of the device and the associated gate potential drop before (black) and after (red) the ligand capture.<sup>134</sup> (c) Detail procedures for gate surface modification used in detection of sialic acid by OECT; (d) optical photography of the screen printed carbon electrode of OECT on flexible substrate; (e) drain current-time response to the addition of human cancer cells HeLa (black curve) and normal cells HUVEC (red curve) at the same concentration. Insert: normalized current response (NCR) of the devices to HeLa and HUVEC cells.<sup>135</sup>

With the various strategies for channel, electrolyte and gate functionalization discussed above, it is clearly indicated that the careful design of modifications at the channel/electrolyte, gate/electrolyte interfaces and bulk of the electrolyte play an



important role in enhancing the selectivity, detection limit while at the same time maintaining the stability (reproducibility) of the device. For most of the OTFT sensors, the sensing mechanism is frequently related to the change of the potential drop profile from the gate to channel by different methods, which is, the intrinsic advantage of OTFT as a signal amplifier. By efficiently combine this amplification and transducer function with the convenience in interfacing with ions and biological environment, both the EGOFET and OECT would be inspiring for further promoting biological applications with proper functionalization.



# Chapter 3 AC Measurements for Accurate Sensing Applications of Organic Electrochemical Transistors

In this chapter, a novel, convenient approach for microfabrication of OECT through photolithography technique is presented. Then, AC measurement (by recording both the transconductance and phase angle of AC channel current) is employed for electrochemical sensing of OECT, for example for the dopamine sensing (with the detection limit down to 1 nM). Furthermore, the AC driven devices employed for cell activity monitoring is demonstrated. By combing the miniaturization of OECT and signal extraction by lock-in amplifier, the precisely extracted transconductance and associated phase shift data could be a high reliable and anti-noise characterization method for further investigation into multifunctional organic bioelectronics systems.

## 3.1 Introduction

Organic electrochemical transistor (OECT) is one kind of organic thin film transistor which integrates electrolytes in their device structure. The possibility for OECT to interface with aqueous electrolytes provides great potential to improve the biological compatibility with metabolites, living cells and tissues, which mainly exists in aqueous environments.<sup>138</sup> Therefore, since the demonstration of the first OECT in 1984,<sup>29</sup> it has been extensively investigated as a promising platform for a wide range of chemical and biological sensing applications, including ions,<sup>48,139</sup> pH,<sup>140</sup> glucose,<sup>132,141</sup> dopamine,<sup>142,143</sup> bacteria,<sup>82</sup> cells,<sup>59,95,100</sup> and tissues<sup>53,144</sup>, etc.

The typical operation of OECT for sensing applications is to apply a source-drain



voltage, and then measure the source-drain current with the application of a gate voltage, which makes the device working under steady state mode. This raises the requirement that the channel current needs to be high enough to be distinguishable from environmental noise or current leakage from the device. At the same time the device needs to be operated at low voltages, to be compatible with biological species in aqueous environment. Therefore, DC driven operation might not be favorable for high precise sensing applications. In 2013, Khodagholy *et al.*<sup>77</sup> reported an effective process to fabricate high speed OECT array, and performed a detailed investigation into the steady-state and transient-state characteristics of the OECT device, indicating the possibility to operate the device in transient state for sensing applications. Then in 2015 Rivnay *et al.*<sup>145</sup> developed a new technique to combine OECT drain current measurement with simultaneous conventional impedance characterization, for in vitro cell based sensing. Ramuz *et al.*<sup>55</sup> also showed the possibility to use transconductance frequency spectrum for monitoring of coverage and differentiation of cells, which indicating the advantage of AC characterization in non-invasive dynamic assessment of the integrity of cells. More recently, a potential dynamic approach was introduced into an all-PEDOT OECT sensor used for dopamine detection by Gualandi *et al.*,<sup>27</sup> which demonstrated high selectivity to interferences by separating the redox waves of the transconductance curves for each compound. However, the possibility to employ transient state operation of OECT devices in electrochemical sensing applications has not yet been systematically investigated and developed.

In this chapter, we describe a simple and reproducible approach to miniaturize OECT device geometry by multilayer photolithography. By miniaturization of the channel area of OECT to cellular dimensions (5 to 22  $\mu\text{m}$ ), the speed of the device response could be raised up to the order of  $10^{-5}$  s, confirmed by the transient behavior



characterization with various ionic concentration. Therefore, the newly fabricated OECT could be operated over a broad range of frequencies in AC mode. The transconductance, defined as the ratio between modulation in the drain current  $\Delta I_D$  and the change in the gate voltage  $\Delta V_G$  ( $g_m = \Delta I_D / \Delta V_G$ ), could be adopted on chemical and biological sensing applications. Compared with conventional sensing methods which only monitoring the drain current, the transconductance sensing shows several advantages, such as more information available ( $g_m$  value in complex number with associated phase shift), frequency dependent, and high reliable detection from noisy environment (signal extraction and filtering by lock-in amplifier). Therefore, we apply this transconductance sensing technique to detect one major kind of neurotransmitter, dopamine (to the detection limit down to 1 nM, lower than the sensing under DC mode) and monitor the cell activity under various conditions, showing that the characterization in transconductance would be promising for further bioelectronic applications.

## 3.2 Microfabrication of OECT

### 3.2.1 Materials

Poly(3,4-ethylenedioxythiophene)–poly(styrene sulfonate) (PEDOT:PSS) (Clevios PH-500) was received from Heraeus as an aqueous solution. Phosphate buffered saline (PBS) solution (pH 7.4), dimethyl sulfoxide (DMSO), glycerin, dopamine and fluorouracil were all purchased from Sigma-Aldrich Co. and stored at 4 °C for further uses. (3-Glycidyloxypropyl) trimethoxysilane (GOPS) was purchased from International Laboratory, USA. AZ5214 and SU-8 2002 photoresist was purchased from Microchemicals GmbH.

### 3.2.2 Device Fabrication

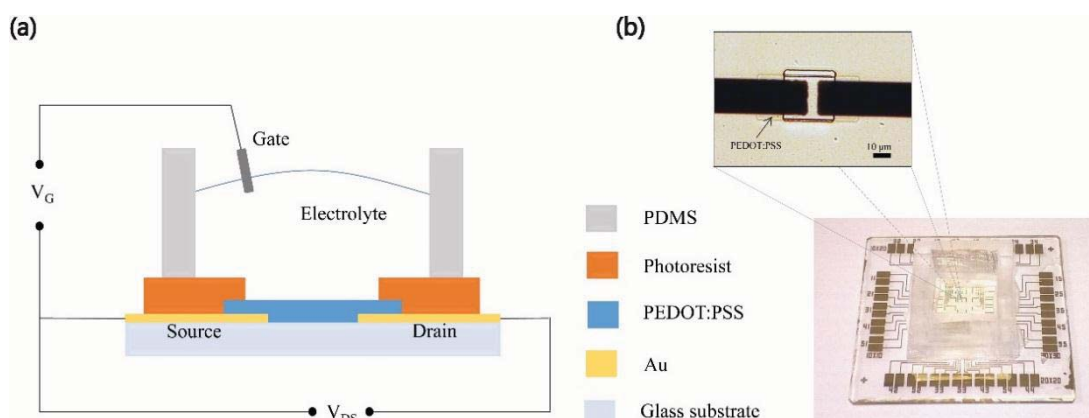


**Figure 3.1.** Device structure of the OEET. (a) Schematic diagram of an OEET cross-section and the wiring system for device operation. (b) Optical micrograph of an individual transistor and the whole OEET array.

The device architecture of the OEET is shown in Figure 3.1(a). A source drain voltage ( $V_D$ ) is applied on the PEDOT:PSS channel, while a gate voltage ( $V_G$ ) is applied through the electrolyte to modulate the channel current. As seen from the Figure 3.1(b), the final device was encapsulated with a PDMS well, for the convenience of aqueous operation. From the inset photo in Figure 3.1(b), a thin patterned layer of PEDOT:PSS could be observed, which is nearly transparent.

The fabrication process of OEET included the deposition and patterning of metal electrode, PEDOT:PSS semiconducting layer and photoresist insulating layer in sequence, as illustrated in Figure 3.2. Glass substrates were surface polished and cleaned by organic solvents and oxygen plasma methods. AZ5214 photoresist was spin coated and exposed to UV light using OAI 800 contact aligner and then developed by AZ400K developer. Then patterned Au ( $\sim 100$  nm)/Cr ( $\sim 10$  nm) source drain electrodes were deposited on the glass substrate by magnetron sputtering through a standard lift-off process. The channel length ( $L$ ) and width ( $W$ ) of the devices were  $5 \mu\text{m}$  and  $22 \mu\text{m}$  respectively. For the preparation of PEDOT:PSS film,

the aqueous dispersion was mixed with DMSO and glycerin (each with a volume ratio of 5 %) to improve the device stability and film conductivity. In addition, the cross-linker GOPS was added to the above dispersion with a volume ratio of 1% to prohibit PEDOT:PSS dissolution. The film was then annealed at 150 °C for 1 hour before the second lift-off process for patterning PEDOT:PSS film at the channel area. At last another layer of SU-8 2002 photoresist was spin coated and patterned on the surface of the PEDOT:PSS film, acting as an insulating layer to protect the Au electrodes from the aqueous electrolyte. Devices were subsequently immersed in PBS buffer solution to remove any excess of low molecular weight compounds. At last a reservoir made of poly(dimethylsiloxane) (PDMS) wall was attached to the substrate to form the aqueous electrolyte containing cell for characterization and sensing application of the devices.

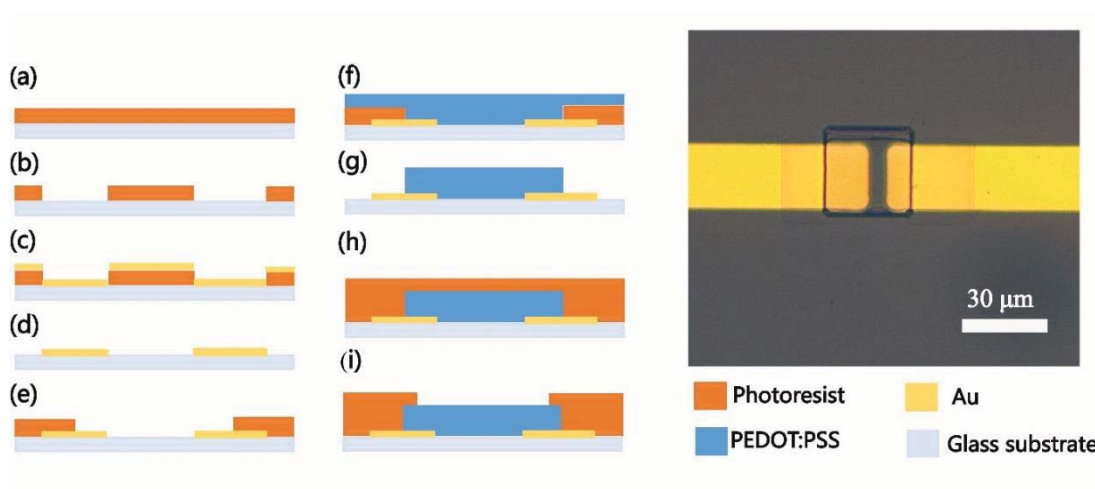


**Figure 3.2.** Fabrication process of OECT device by photolithography. (a)-(d), Au electrode deposition and patterning on the glass substrate. (e)-(g), patterning of PEDOT:PSS film between source and drain electrode. (h)-(i), final package of the device by SU-8 photoresist as an insulating layer.

Gate electrode of OECT was deposited separately by magnetron sputtering through a shadow mask, resulting in a 3 mm × 3 mm patterned Ti (~10 nm) / Pt (~100 nm) electrode. Then the electrode was immersed into the PBS solution in the PDMS well

for electrical characterization.

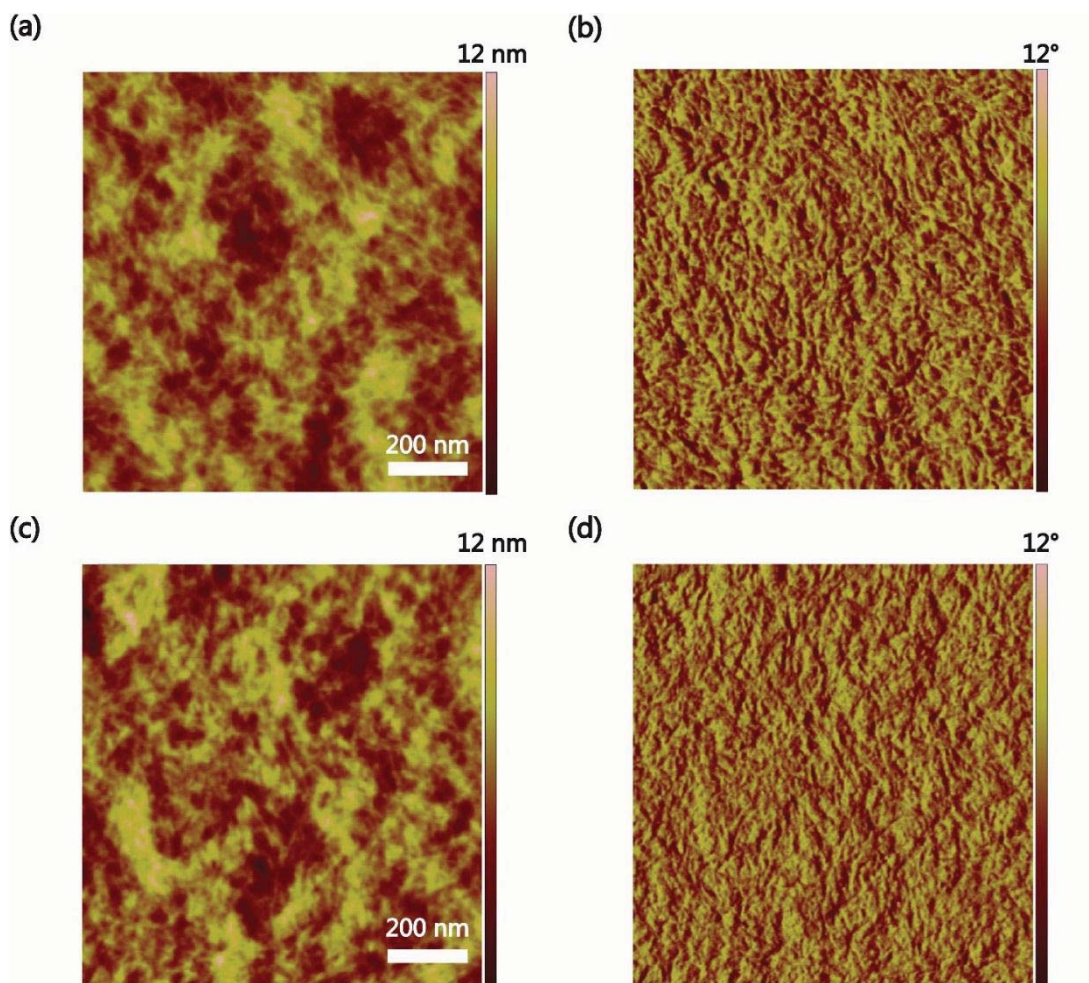


**Figure 3.3.** Height and phase AFM images of PEDOT:PSS films (a)-(b) before and (c)-(d) after all of the photolithography lift-off processes in device fabrication.

The atomic force microscopy characterization was carried out for investigation of the surface morphology of PEDOT:PSS during the photolithography process. As seen from Figure 3.3, the height and phase graphs of PEDOT:PSS before and after patterned and washed with acetone showed nearly no differences, with the surface roughness of both films (RMS value) around 1.7 nm. This indicates that this polymer film is very stable during the device fabrication, which could tolerate both the organic solvent erosion and the mechanical lift-off process by ultrasonication.

### 3.2.3 Device Characterization

The OECT device was immersed in PBS buffer solution, as shown in Figure 3.1(a). The optical images of the device and cells were observed by Olympus IX71 inverted microscope. The output and transfer characteristics of the devices were measured by two Keithley source meters (Keithley 2400). For the transient behavior measurement, an Agilent 33220A waveform generator was used to provide the gate voltage pulse, and the channel current response was recorded by the Tektronix TDS2000C Digital Storage Oscilloscope. For the small signal transconductance measurement, the sinusoids gate input (with the amplitude of 50 mV and a certain bias) was applied by the waveform generator and the drain current was converted by SR570 Low Noise Current Preamplifier into voltage signal and then collected by the SR830 DSP Lock-in Amplifier, to get the transconductance,  $\Delta I_D/\Delta V_G$  and the corresponding phase angle shift. The instruments above were connected and controlled by a customized LabVIEW program. The dopamine aqueous solution (diluted with PBS) with designed concentration were added into the PBS solution to measure the sensor response reflected in transconductance.

### 3.2.4 Cell Cultivation

Human breast adenocarcinoma cancer cell line (MDA-MB-231) was obtained from American Type of Culture Collection (ATCC). The cells were maintained routinely in Dulbecco's modified eagle medium (DMEM) with 4500 mg/l glucose (Invitrogen) as basic medium supplemented with 5% Fetal Bovine Serum (FBS, Invitrogen) together with penicillin and streptomycin (Invitrogen). The cells were seeded in the PDMS well of the OECT device and cultured in a humidified incubator at 37 °C with 5% CO<sub>2</sub>/95% air for a certain time, before taken out for further optical or electrical

characterization.

### 3.3 Electrical Measurements

#### 3.3.1 Steady State Characteristics

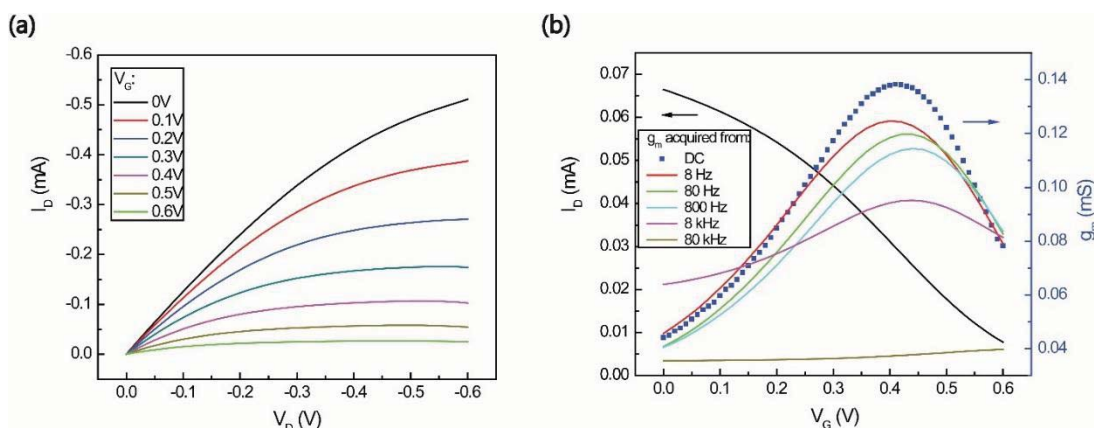


**Figure 3.4.** (a) Output characteristics showing the drain current  $I_D$ , as a function of drain voltage  $V_D$ , with an applied gate voltage  $V_G$  varying from 0 V to 0.6 V. (b) Transfer curve and resulting transconductance at  $V_D = 0.05$  V.

Figure 3.4(a) shows the output characteristics of a typical OECT with negative sweep bias (0 to -0.6 V) at the drain, under the stepped gate voltage varied from 0 V to 0.6 V, applied from the Pt gate electrode immersed into PBS solution. The corresponding transfer curve for  $V_D = 0.05$  V is shown in Figure 3.4(b). The drain current decreases with the increasing gate voltage, showing the typical low voltage operation of OECT in the depletion regime. This behavior is consistent with the model developed by Bernardis in 2007<sup>75</sup>: the cations from the electrolyte could be injected into the PEDOT:PSS film to compensate the acceptors ( $SO_3^-$ ) on the PSS upon the application of a positive gate voltage. Consequently, the hole mobility and the channel conductance could be modulated. The transconductance extracted from the transfer curve reaches a peak value of  $g_m = 0.138$  mS at  $V_G = 0.41$  V.

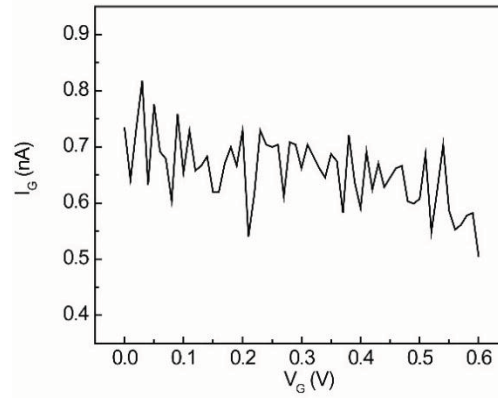


**Figure 3.5.** Leakage current of OECT (between channel and gate electrode) during the transfer characterization in Figure 3.4.

It is also worth noted that the simultaneously measured gate current (leakage) of the devices is less than 30 nA throughout the output and transfer characterization. Especially for the transfer test, the gate current is below 1nA, (Figure 3.5) demonstrating the superior insulation performance of the SU-8 photoresist layer.

Then AC method was introduced for device characterization. A small sinusoidal oscillation signal ( $v_g$ , 50 mV in amplitude) with the frequency of  $f$  is superimposed on the constant gate voltage bias  $V_G$ , forming the AC channel current of OECT. The complex AC gate voltage  $v_G$  and the corresponding channel current  $i_D$  (consists of DC component  $I_D$  and AC component  $i_d$ ) are given by,

$$\begin{aligned} v_G &= V_G + v_g = V_G + |v_g|e^{j2\pi ft} \\ i_D &= I_D + i_d = I_D + |i_d|e^{j(2\pi ft + \theta)} \end{aligned} \quad (3.1)$$

Then the transconductance is defined as,

$$g_m = \left. \frac{\Delta i_D}{\Delta v_G} \right|_{V_D} = \frac{|i_d|}{|v_g|} e^{j\theta} \quad (3.2)$$

Therefore, by superimposing a small sinusoidal signal (with fixed amplitude  $|v_g|$ ) to the gate voltage, the transconductance  $g_m$  with corresponding phase shift angle  $\theta$



could be collected simultaneously by the lock-in amplifier.

By simply sweeping the gate bias  $V_G$  from 0 V to 0.6 V, the  $g_m - V_G$  relations under different operation frequencies were obtained, as shown in Figure 3.4(b). It is reasonable that when operated at relative low frequencies (red line in Figure 3.4(b)), the transconductance curves are quite similar to the one derived from the transfer characterization at steady state, approaching a peak value at around  $V_G = 0.41$  V. With the increase of the operation frequency from 8 Hz to 80 kHz, the peak value decreases due to the limited rate of ions moving between the aqueous electrolyte and PEDOT:PSS channel.

### 3.3.2 Transient Characteristics and Ion Strength Sensing

Though the large scale OECTs (with the length and the width of the channel in the range of millimeter) have been successfully developed in various kinds of sensing applications, a major drawback always persists, which is the slow device operation. According to previous investigations<sup>77,145</sup>, it is confirmed that the drain current depends on the number of ions that could be injected into the channel, which in turn determines the time needed for the device to reach steady state. Here a gate voltage pulse ( $V_G = 0.2$  V) is applied through the electrolyte with various KCl concentrations, to investigate the effect of ionic concentration on the transient response time, as shown in Figure 3.6(a). The  $I_{DS}$  channel current is monitored simultaneously with the applied pulsed  $V_G$ . When the  $V_G$  switched from 0 V to 0.2 V, a rapid decrease of  $I_{DS}$  was followed by nearly steady state behavior after a certain time interval. According to the Bernards' model<sup>75</sup> and further investigation by Friedlein et al<sup>31</sup>,

$$I_D(t) = I_D(0) + \Delta I_D \left[ 1 - e^{-\frac{t}{\tau_{RC}}} \right] \quad (3.3)$$

The ionic RC time constant  $\tau_{RC}$  is the key factor limiting the response speed of the device. Then a first order exponential decay ( $I_{DS} \sim \exp(-t/\tau_{RC})$ ) is applied on the fitting of the responding drain current curve, to extract the transient response time  $\tau$ . The relationship between response time and the KCl concentration is fitted on the double log axis in Figure 3.6(b). The result indicates that the response time has a good linear relation with the ion concentration in the electrolyte, under a log-log plot, thus signifies that the response time of OECT is dominated by the rate of ion transport between the channel and the electrolyte. As can be seen from Figure 3.6(b), the response time is shortened from 0.32 s to  $5.58 \times 10^{-5}$  s, over four orders of magnitude, as the result of increasing KCl concentration from  $10^{-5}$  M to  $10^{-1}$  M.

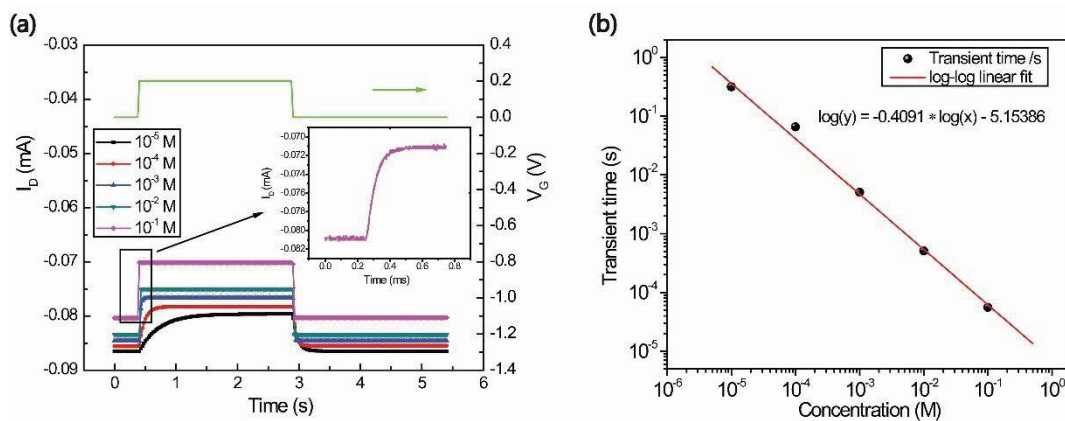


**Figure 3.6.** (a) Time response to a  $V_G$  pulse of 0.2 V, with a drain voltage of 0.05 V, for OECT operated in a series of KCl solutions with increasing concentration from  $10^{-5}$  M to  $10^{-1}$  M. Inset: the time response of device operated in  $10^{-1}$  M KCl solution, with the time axis in millisecond range. (b) Extracted single exponential time constant as a function of KCl concentration. The line is a double-log linear fit.

Another analytical method to investigate the ion transport behavior at the interface between channel and electrolyte is the frequency dependence of the transconductance. A 50 mV sinusoidal oscillation is then superimposed on the gate bias, and the transconductance is determined by the amplitude ratio between the drain current oscillation and the input sinusoidal signal. Figure 3.7(a) indicates the tendency that the  $g_m$  increases with rising KCl concentration, throughout the whole

frequency range. The range of plateau region for  $g_m$  also shows a dependence on the ionic concentration, which is, in consistent with the transient time response as described in Figure 3.7(a). The corresponding phase angle shift in Figure 3.7(b) also shows the same trend, while it is worth noted that when the ion concentration is higher than  $10^{-3}$  M, the phase angle keeps at a constant value at low frequency region, and only the shift of the curves along x-axis could be observed for varying concentrations.

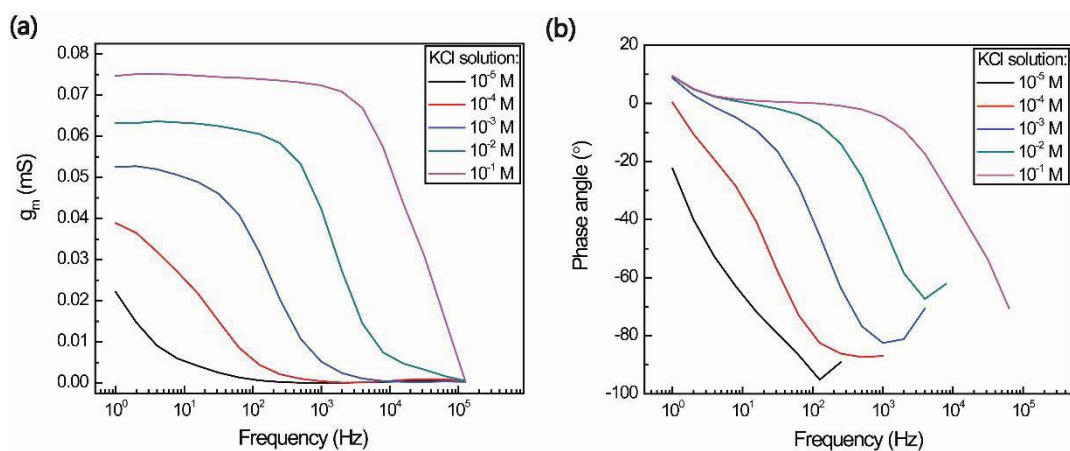


**Figure 3.7.** Frequency dependence of (a) the transconductance value and (b) corresponding phase angle under various ionic concentration of KCl. The device is biased with  $V_D = 0.05$  V and  $V_G = 0.2$  V, and an additional 50 mV sinusoidal gate voltage oscillation is applied to measure the small-signal transconductance.

The decrease of  $g_m$  with increasing frequency here provides another method to extract the response time of OEET device. The cut-off frequency is defined at the point when the  $g_m$  value decreases to 0.707 of the maximum value (-3 dB).<sup>58,88</sup> So the response time is the reciprocal of the cut-off frequency, and again the relationship between the response time and the concentration could be fitted into a power function relationship, which is similar to that obtained from the transient measurements. Therefore, both the transient and the AC methods can be used to characterize the response time of an OEET and used to decide the ion concentrations in electrolytes.



According to previous investigations by Khodagholy *et al.*<sup>77</sup>, the response time of OECT is majorly limited by the ion transport in the ionic circuit (between the aqueous electrolyte and PEDOT:PSS film), considering that the hole transport in the PEDOT:PSS channel is a much faster step. Therefore, this relationship between the response time and the ionic concentration could be explained by simplifying the ionic circuit as a resistor (with the resistance  $R$ ) and capacitor (with the capacitance  $C$ ) in series. According to the definition, the conductance  $G$  of the electrolyte solution is given by:

$$G = \frac{1}{R} = \kappa \frac{A}{l} = \Lambda_m C_{ion} \frac{A}{l} \quad (3.4)$$

where  $\kappa$  is the electrolyte conductivity,  $l$  and  $A$  are the length and the cross-section area of the ionic circuit, and  $\Lambda_m$  represents the molar conductivity. Therefore, the resistance is given by:

$$R = \frac{l}{\Lambda_m C_{ion} A} \quad (3.5)$$

For the analysis of capacitance in PEDOT:PSS film, recently Proctor *et al.*<sup>27</sup> built up a simple model by describing the capacitance in terms of the sites where holes are replaced by the ions injected from the electrolyte. Hence the volumetric capacitance  $C^*$ , which is the capacitance per unit volume, is given by:

$$C^* = \frac{C'_{DL}}{\alpha} \quad (3.6)$$

where  $C'_{DL}$  is the conventional double layer capacitance from Helmholtz model and  $\alpha$  is the average distance between sites. The volumetric capacitance could then be further derived,



$$C^* = \frac{C'_{DL}}{\alpha} = \frac{\varepsilon_0 \varepsilon_r}{d} \cdot \frac{1}{\alpha} = \frac{\varepsilon_0 \varepsilon_r}{\frac{1}{F} \sqrt{\frac{RT \varepsilon_0 \varepsilon_r}{2c_{ion}}}} \cdot \frac{1}{\alpha} = \frac{F}{\alpha} \sqrt{\frac{2c_{ion}}{RT \varepsilon_0 \varepsilon_r}} \quad (3.7)$$

where  $\varepsilon_0$  and  $\varepsilon_r$  are the vacuum and relative permittivity,  $d$  is the thickness of the electric double layer,  $F$  the Faradic constant,  $R$  the gas constant and  $T$  the absolute temperature. Then the response time is given by the RC time of the circuit:<sup>28</sup>

$$\tau_{RC} = RC^* = \frac{l}{\Lambda_m c_{ion} A} \cdot \frac{F}{\alpha} \sqrt{\frac{2c_{ion}}{RT \varepsilon_0 \varepsilon_r}} = \frac{lF}{\alpha \Lambda_m A} \sqrt{\frac{2}{RT \varepsilon_0 \varepsilon_r}} \cdot c_{ion}^{-1/2} \quad (3.8)$$

This equation indicates that, under an optimum condition, the time constant  $\tau_{RC}$  is proportional to  $c_{ion}^{-1/2}$ . The experimental results from both the transient and the AC measurements show the same power function relationship between  $\tau_{RC}$  and  $c_{ion}$  with the exponent of around -0.41. This can be ascribed to the fact that the molar conductivity  $\Lambda_m$  is also concentration dependent (in diluted solution,  $\Lambda_m$  decreases with increasing ionic concentration). For the concentration varying in such a wide range, deviation from the idealized model may present.

### 3.4 Dopamine Sensors

When the OECT is operated at steady state, the channel current  $I_D$  can be modulated by  $V_G$  according to the electrochemical doping of cations from the aqueous electrolytes.<sup>29</sup> A simple device model has been presented and an analytical expression has been derived by Bernards et al., pointing out that channel current  $I_D$  should be given by the following equation,<sup>75,146</sup>

$$I_D = \frac{q\mu p_0 t W}{LV_p} \left( V_p - V_G^{eff} + \frac{V_D}{2} \right) V_D, \quad (\text{when } |V_D| \ll |V_p - V_G^{eff}|)$$

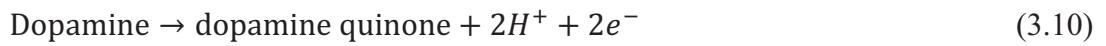
$$V_p = qp_0 t / c_i$$



$$V_G^{eff} = V_G + V_{offset} \quad (3.9)$$

where  $q$  is the electron charge,  $\mu$  is the hole mobility,  $p_0$  is the initial hole density (when  $V_G = 0$  V) in the PEDOT:PSS layer with the thickness of  $t$ ,  $V_p$  and  $V_G^{eff}$  are the pinch-off voltage and the effective gate voltage, respectively, and  $V_{offset}$  is the offset voltage at the interface of the gate or electrolyte;  $c_i$  is the capacitance per unit area.

The OECT with a Pt gate electrode was then used for dopamine sensing, due to the electro-oxidation reaction on the surface of the gate electrode, shown as following,



The electro-oxidation of dopamine releases two electrons per dopamine molecule and generates faradic current when the electrons are withdrawn from the gate electrode, which could further change the localized potential drop, and hence change the effective gate voltage  $V_G^{eff}$  given by,<sup>142</sup>

$$V_G^{eff} = V_G + 2.30(1 + \gamma) \frac{kT}{2q} \log[C_{dopamine}] + A \quad (3.11)$$

Where  $\gamma$  is the capacitance ratio, defined as  $C_C/C_G$ , in which  $C_C$  and  $C_G$  are the channel /electrolyte capacitance and gate/electrolyte capacitance, respectively;  $k$  is the Boltzmann's constant and  $T$  is the temperature;  $[C_{dopamine}]$  is the concentration of dopamine, and  $A$  is a constant.

Therefore, by combining equation (3.9) and (3.11), the modulation of channel current  $I_D$  is induced by the change of effective gate voltage  $V_G^{eff}$ , which is dependent on the concentration of dopamine. Therefore, the increase of dopamine concentration in the electrolyte will increase the  $V_G^{eff}$ , which in turn decrease the channel current. This is the typical sensing mechanism of the device to dopamine,

which is similar to those of the OECT based hydrogen peroxide and glucose sensors reported before.<sup>128,132,147</sup>

Then a small sinusoidal oscillation signal ( $v_g$ , 50 mV peak-to-peak) is superimposed on the gate bias  $V_G$ , changing the operation of OECT from steady state to transient state. The transconductance  $g_m$  with corresponding phase shift angle ( $\theta = \theta_{ds} - \theta_{ref}$ ) could be collected simultaneously by the lock-in amplifier. Based on above discussions, the  $g_m$  response could also be modulated by the change of effective gate voltage  $V_G^{eff}$ , which is further dependent on the concentration of dopamine in the electrolyte.

For AC characterization, lock-in amplifier is involved to introduce one notable advantage that the extracted  $g_m$  signal and phase angle  $\theta$  are collected only at the specific reference frequency settled by the small sinusoidal signal from gate voltage, which means that the background and noise signals at frequencies other than the reference frequency are filtered by the phase sensitive detection and subsequently a low pass filter and do not affect the recorded measurement results.

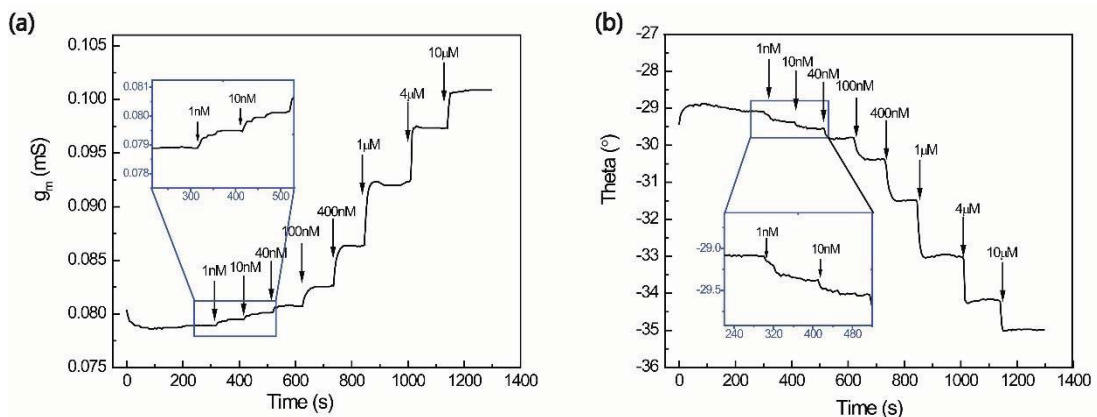


**Figure 3.8.** (a) Channel transconductance ( $g_m$ ) response and (b) associated phase angle change of the OECT to additions of dopamine with different concentrations.  $V_D = 0.05$  V,  $V_G = 0.2$  V.

In sensing applications, the  $V_{DS} = 0.05$  V and  $V_G = 0.2$  V with the 50 mV sinusoidal

oscillation are fixed, the response of the OECT to continuous addition of dopamine is monitored by measuring the real-time  $g_m$  response. Figure 3.8(a) and (b) shows the real-time collection of  $g_m$  and corresponding  $\theta$  data during the additions of various concentrations of dopamine in PBS solution. It is notable that the device starts to exhibit a signal response to the addition of 1 nM dopamine, and the relative change of  $g_m$  and  $\theta$  also increase with the increasing of dopamine concentration.

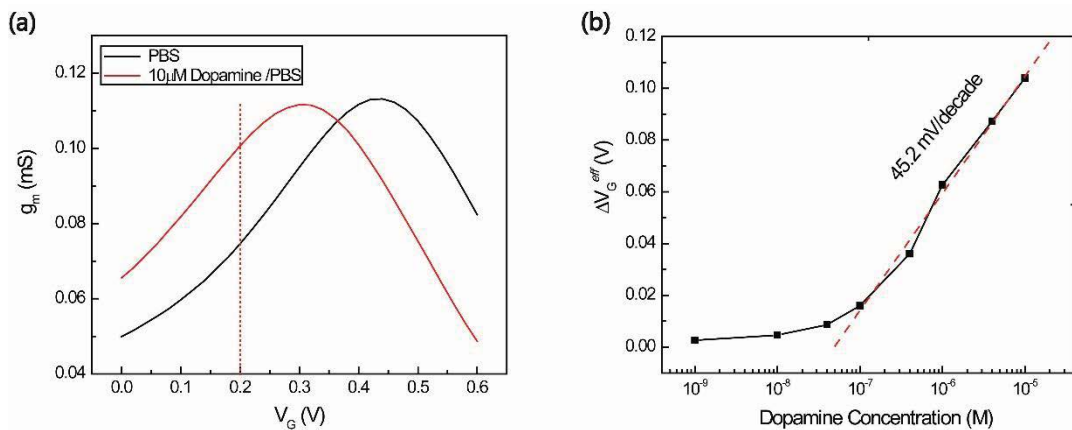


**Figure 3.9.** (a)  $V_G$  dependence of transconductance ( $g_m$  vs.  $V_G$ ,  $V_D = 0.05$  V) of an OECT measured in PBS solution (pH = 7.4) before and after the addition of dopamine with the concentration of 10  $\mu$ M. (b) The change of effective gate voltage ( $\Delta V_G^{eff}$ ) as the function of the concentration of dopamine.

The change of  $g_m$  and  $\theta$  can be clarified by the change of  $\Delta V_G^{eff}$  due to the oxidation reaction of dopamine at the surface of gate electrode. This will further result in the horizontal shift of the  $g_m - V_G$  curve. As indicated in Figure 3.9(a), the curve shows roughly 150 mV shift to lower  $V_G$  region when characterized in 10  $\mu$ M dopamine PBS solution compared to the blank PBS solution. The effective gate voltage corresponding to the transconductance at different dopamine concentrations could also be read out from the  $g_m - V_G$  curve of the device characterized in blank PBS solution. Figure 3.9(b) shows the relationship between the variation of  $\Delta V_G^{eff}$  and the concentration of dopamine [ $C_{dopamine}$ ]. We can find that  $\Delta V_G^{eff}$  is proportional to  $\log[C_{dopamine}]$  in the range of  $1 \times 10^{-7}$  M to  $1 \times 10^{-5}$  M, across two orders of magnitude,

which is consistent with equation (3.11). The slope value (45.2 mV/decade) of the fitting curve (dashed line in Figure 3.9(b)) can indicate the response of the device towards the target analyt, which could also be used to derive the capacitance ratio  $\gamma = 0.53$  in equation (3.11). The relatively small value of  $\gamma$  can be explained by the influence of device geometry, according to the definition,

$$\gamma = \frac{C_{channel}}{C_{gate}} = \frac{c_{ch} \times A_{ch}}{c_g \times A_g} \quad (3.12)$$

where  $c_{ch}$  and  $c_g$  are the channel and gate capacitance per unit area, and  $A_{ch}$  and  $A_g$  are the area of channel and gate electrode, respectively. The capacitance ratio is tunable and proportional to  $A_{ch}/A_g$ . As we patterned the channel area into the micrometer region by photolithography, the area ratio  $A_{ch}/A_g$  is significantly reduced, which then decreases the value of  $\gamma$ , and subsequently the slope of the fitting curve in Figure 3.9(b).

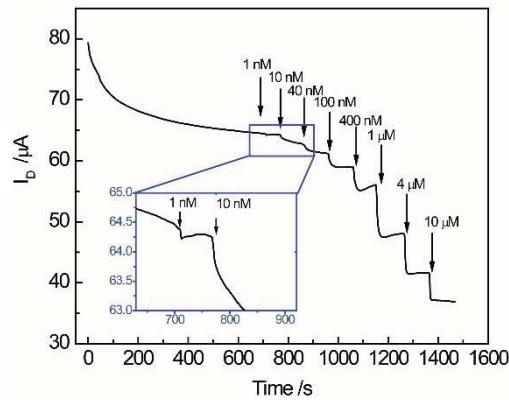


**Figure 3.10.** DC channel current response of the OEET during the addition of dopamine with different concentrations.  $V_D = 0.05$  V,  $V_G = 0.4$  V.

The conventional steady state measurement was also carried out for dopamine sensing with the same device as a control. As seen in Figure 3.10, The detection limit could only reach 10 nM, which is a little bit lower than the AC method. Another notable drawback for DC method is that the time needed for the device to be



stabilized is relatively longer (more than 600 s), which is much longer than the time needed for AC characterization, as can be seen from Figure 3.8. The rapid stable signal collected from AC methods should be ascribed to sensing mechanism. As the recorded signal is stimulated from the small AC voltage fluctuation (50 mV sinusoidal  $v_g$ ), it is much easier for the ionic exchange at PEDOT:PSS channel/electrolyte interface to reach equilibrium, while for conventional DC method, the ionic exchange equilibrium need to suffer from a sudden change of gate voltage bias from 0 V to 0.4 V, which leads to longer time for DC drain current to be stabilized. This feature could shed light on further improvement of OECT operation for rapid sensing requirements.

### 3.5 Cell Activity Monitoring

Besides acting as an electrochemical sensor as discussed above, organic electronic devices, especially the OECT, have also attracted significant attention in the past few years as a versatile, dynamic method for investigation of biological activities.<sup>148–152</sup> Lin *et al.* reported the monitoring of non-barrier tissue by OECTs in the DC measurement mode, which can be explained by the electrostatic interaction between the attached cells and the active layer of OECTs.<sup>95</sup> After recent improvements in miniaturization and high density integration of OECTs,<sup>77,153,154</sup> it is possible to raise the speed of the device response and then operate the OECT array over a broad range of frequencies. For example, the OECT has been employed to combine with the electrochemical impedance spectroscopy to investigate trans-epithelial resistance and cell layer capacitance information through broadband frequencies.<sup>56,145</sup> Recently, Ramuz reported the monitoring of various types of barrier and non-barrier tissue cells by combining measurement of transconductance with transepithelial resistance data.<sup>55</sup> However, these work mostly focus on the monitoring of cell or tissue layers,

not the activity of the specific single cell. Huerta demonstrated the possibility to modify the OECT structure with a capillary tube-micropipette tip system in order to record the activity of the 3D cyst cell cultures, which is rather dependent on the geometry of the device.<sup>58</sup>

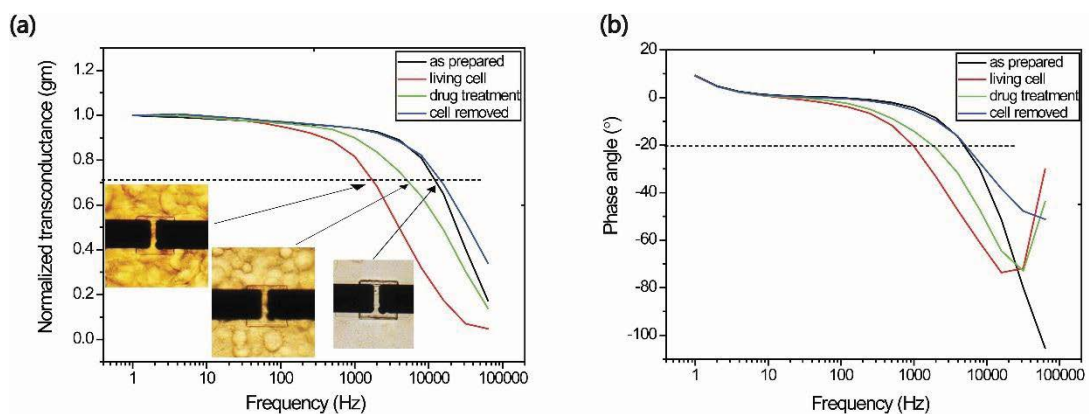


**Figure 3.11.** Monitoring the effect of living cells and drug treatment (5-FU) by (a) transconductance and (d) corresponding phase angle change. Inset, bright field images of cells seeded on the channel of device. Each image corresponds to one curve as indicated.

Here in this section we investigated the possibility to monitor the activity of single or few cells on the planar structure, due to the advantage of miniaturization of the OECT channel to cellular dimensions. Before seeding of the cells, the OECT device was first characterized in transconductance as a function of frequency, as a non-cell control. Then the human breast adenocarcinoma (MDA-MB-231) were seeded in the PDMS well of the device, and the cells were grown in the culture incubator before taken out for characterization.

As shown in Figure 3.11(a), the typical transconductance – frequency spectrum with a plateau region and an abrupt drop at high frequencies could be recorded for monitoring cell activities. To numerically compare the different conditions, we extracted the cut-off frequency, defined at -3 dB of the transconductance value at DC bias.<sup>58</sup> The Fluorouracil (5-FU), a medication which is used in the treatment of



cancer, was employed to investigate the effect of drug treatment on transconductance characterization. As seen in Figure 3.11(a) and (b), the characterization of non-cell control (black line), living cancer cell (red line), dead cell induced by 5-FU treatment (green line), and the final condition by removing all the cells from the device (blue line) were carried out.

As shown in Figure 3.11(a), first the cells were seeded and grown on the channel area of the device as discussed above, and the cut-off frequency decreased from 11905.2 Hz to 1765.9 Hz, indicating the transepithelial resistance effect due to the cell coverage on the channel area, which could inhibit the ion to electron conversion occurred at the interface between aqueous electrolyte and PEDOT:PSS active layer. After addition of proper amount Fluorouracil into the cell culture and incubated for one day, the cut-off frequency increased to 4937.5 Hz, pointing out the weaken of impermeable barrier effect for the ion exchange in channel. This could also be confirmed from the bright field optical images inserted in Figure 3.11(a), the seeded cells were well adhered to the surface of the substrate, containing some interaction with neighbored cells. After the treatment of Fluorouracil, it was clearly observed that the cells changed back to the spherical shape, and the attachment to the substrate was not tight as the untreated cells, which means that the PEDOT:PSS active layer could have more possibility to contact with the electrolyte and carry out ion exchange.

The associated phase angle characterization (Figure 3.11(b)) typically followed the same trends as discussed in the transconductance – frequency curves. It is worth noting that, in order to compare the transconductance curves under various conditions, the intensities needed to be normalized at the DC bias, as the absolute value could be affected by the seeding and grown of the cancer cells on the device. However, the characterization of associated phase angle showed a perfect overlap for



various treatments of cells at low frequency region. This could be explained as the change of phase angle only depends on the relative difference between the phase of input sinusoidal gate signal and the responding channel current signal, not the absolute value of transconductance of the device. Therefore, the discussion of cut-off frequency changes based on phase angle shift could be more reliable. In addition, this trend is also consistent with the characterization response to various KCl concentration in electrolytes, as indicate in Figure 3.7(a) and (b), where with the continuous reduction of ionic concentration, the transconductance shows a decrease in absolute value while the shift of cut-off frequency to lower region, however, the phase angle only shows a horizontal shift of cut off frequency when the ionic concentration varied from  $10^{-1}$  M to  $10^{-3}$  M. This phenomenon indicates the advantage to use the characterization of phase angle shift to monitor and assess the cell activities on OECT devices.

### 3.6 Summary

In conclusion, we have demonstrated a novel and convenient approach for fabrication and miniaturization of OECT arrays. With the raising speed of device response, the transconductance characterization could be introduced not only as an electrochemical sensor, for high sensitive and fast detection of dopamine, but also, to be adopted for monitoring cell coverage and activities on the channel of devices. The main advantage over conventional electrical methods is the capability to collect high quality data through a broad frequency range at a relative low gate voltage modulation. The miniaturized channel area could benefit enhancement of the device resolution to detect the activity of single or few cells. Therefore, the approach here could be regarded as a promising method for further applications in biological system, such as specific drug screening or toxicity testing.



# Chapter 4 High Mobility p-type Conjugated Polymers for Applications in Organic Electrochemical Transistors

## 4.1 Introduction

Conjugated polymers have been extensively investigated for applications in organic electronic devices during the last several decades, since the first report of conducting polymer by Shirakawa et al. in 1977.<sup>3</sup> Numerous types of electronic devices have been developed with excellent performance and promising commercialized application prospects. Recently, OTFTs which could present stable and superior performance when operated in aqueous electrolytes, are emerging in the field of bioelectronics, due to the intrinsic soft nature and excellent biointerfacing properties of the conjugated polymers.<sup>155–158</sup>

The two categories of OTFTs, which are OFETs and OECTs, have been well discussed in the introduction chapter previously presented. A comprehensive investigation has been carried out for understanding the structure-property relationship of conjugated polymers through the OFET platform over the past half century, and such kind of devices have been successfully employed in various fields of current electronic industry, including active matrix displays,<sup>61</sup> flexible and stretchable sensors<sup>159,160</sup> and multifunctional e-skins.<sup>161</sup> In contrast, the research into OECTs is less historical. It was only after Wrighton et al. demonstrated the first model of OECT with polypyrrole in 1984,<sup>29</sup> that many research laboratories set out to focus on the device design and active layer material selection aiming to acquire high performance OECTs. A remarkable advantage of OECTs, compared to its peer



OFETs, is that the channel area (normally conjugated polymers), is directly exposed to the aqueous electrolyte, and the device is modulated by the electrochemical doping/dedoping process (through ionic penetration into the film) between the channel and the electrolyte environment. Therefore, OECTs possess several key features in the field of biological sensing or signal transduction, such as low working voltage (less than 1 V), high amplification capability (high transconductance), highly sensitive to ionic movements or potential changes in the electrolytes, and most importantly, excellent stability for long-term operation in aqueous environments.

In the past few years, the majority of the OECTs reported relied on the commercialized highly doped semiconducting polymer, poly(3,4-ethyl-enedioxy thiophene):poly(styrene sulfonate) (PEDOT:PSS),<sup>77,95,162</sup> which presents intrinsically high conductivity and a stable depletion mode operation of OECTs. Considering for the fact that the PEDOT:PSS aqueous dispersion is very challenging to be chemically modified or functionalized for specific applications, and the high acidity liquid limits the available options of processing techniques, synthetic chemists turn to develop alternative strategies to apply novel conjugated polymers into OECTs. Conjugated polyelectrolytes, such as PEDOT or polythiophene backbone modified with an alkyl side chain terminated by either sulfonate or carboxylic acid groups, were employed in OECTs, benefiting from efficient intrinsic ionic exchange properties.<sup>43,44,163–166</sup> Besides, ion-free conjugated polymers with designed polar side chains (such as ethylene glycol) were successfully demonstrated to fabricate high transconductance accumulation mode OECTs, both with p-type<sup>45,167</sup> and n-type polymers.<sup>46,168,169</sup> Therefore, further efforts should be focused on better understanding of the structure-property relationship for synthesis of novel conjugated polymers integrated in high performance OECTs.

In this work, we systematically investigated the performance of several high mobility



p-type conjugated polymers (as shown in Figure 4.1) when operated in aqueous electrolytes, utilizing the OECT platform. These polymers have been reported to present high performance when fabricated into OFET structure, which were normally tested under inert gas environment. The OECT characterization was first carried out for all the polymers. Then for the selected PFT-100 based OECT which demonstrated superior electrical performance, further optimization with annealing temperature, electrochemical impedance spectroscopy characterization and device response to various ionic electrolyte concentration and species were investigated for a comprehensive understanding of the doping/dedoping process and ionic penetration into the conjugated polymer film. This would also contribute to clarify the mechanism of ion/hole transport and interaction inside these conjugated polymers based OECTs.

## 4.2 Experimental Section

### 4.2.1 Materials

Commercialized conjugated polymers: (chemical structures shown in Figure 4.1)

poly[4-(4,4-dihexadecyl-4H-cyclopenta[1,2-b:5,4-b']dithiophen-2-yl)-alt-4,7-(5-fluorobenzoc[1,2,5]thiadiazole)] (PFT-100, 75kDa, PDI: 2.5)

poly[4-(4,4-dihexadecyl-4H-cyclopenta[1,2-b:5,4-b']dithiophen-2-yl)-alt-[1,2,5]thiadiazolo[3,4-c]pyridine] (PCDTPT, 76 kDa, PDI: 2.5)

poly[[2,3,5,6-tetrahydro-2,5-bis(2-octyldodecyl)-3,6-dioxopyrrolo[3,4-c]pyrrole-1,4-diyl]-2,5-thiophenediylthieno[3,2-b]thiophene-2,5-diyl-2,5-thiophenediyl]

(two batches, DPP-DTT: 100 kDa, PDI: 3.0 and PDPP2T-TT-OD: 98 kDa, PDI: 2.5) were purchased from 1-Material Inc., Canada.

DPP-DTT copolymerized with DTT( $C_{10}H_{20}OH$ ) at the monomer ratio of 0.95:0.05 ( $(DPP-DTT)_{0.95}-(TT-TOH)_{0.05}$ ) was customized synthesized. Sodium chloride, sodium glycolate, 1,2-dichlorobenzene (DCB), 1-methylnaphthalene (1-MNT) and phosphate buffered saline (PBS) solution were purchased from Sigma Aldrich Co., USA. Sodium poly(styrene sulfonate) ( $M_w$  75000, 30% w/v aqueous solution) was purchased from Alfa Aesar. AZ5214 and SU-8 2002 photoresists were purchased from Microchemicals GmbH.

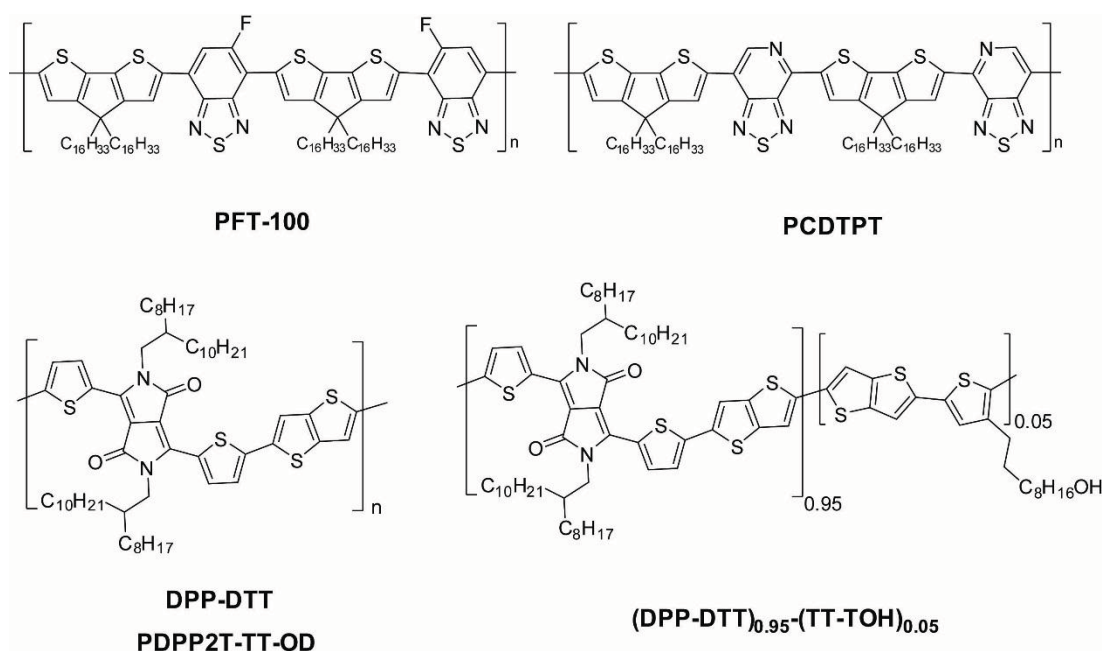


**Figure 4.1.** Chemical Structures and abbreviations of the semiconducting polymers tested in this work.

## 4.2.2 Device Fabrication

The OECTs were fabricated through a previously reported photolithography microfabrication process. First, the glass substrates were thoroughly cleaned by ultrasonication in acetone, deionized water and isopropanol in sequence. Then source drain electrodes (Cr/Au, 10 nm/100 nm) were deposited and patterned on glass substrates through magnetron sputtering and a lift-off process. Then the electrodes



were packaged by an insulating layer of SU-8 2002 photoresist, leaving only the channel area uncovered. The conjugated polymers were dissolved in organic solvents (DCB or 1-MNT) at 5 mg/mL and then spin coated on the channel area at 3000 rpm for 40 s. The devices were then baked under different temperatures for 60 min, resulting in the well-defined OECT with channel length (L) and width (W) 30  $\mu\text{m}$  and 60  $\mu\text{m}$  respectively.

### 4.2.3 Device Characterization

PBS solution or other aqueous electrolytes were dropped on the channel area of OECTs, and then a platinum wire was immersed into the electrolytes, acting as the gate electrode. The typical output and transfer characteristics of OECT were measured using two Keithley 2400 sourcemeters with common source configuration, controlled and data collected by a customized LabVIEW program. The pulsed voltage signal was applied from an Agilent 33220A waveform generator. The electrochemical impedance spectroscopy (EIS) measurements were carried out with Zahner electrochemical workstation and a three-electrode-system, including gold electrode with defined area (0.09  $\text{cm}^2$ ) coated with thin film of conjugated polymers (working electrode), and conventional silver/silver chloride reference electrode and platinum wire counter electrode, all immersed in aqueous electrolyte with defined ionic species and concentrations.

## 4.3 Electrical Measurements

The output and transfer characteristics of PFT-100 based OECTs in PBS solution were illustrated in Figure 4.2(a) and 4.2(b). The output curves were available through reversed sweeping source drain current  $I_D$  versus source drain voltage  $V_D$  (0

V to  $-0.6$  V), with a fixed gate voltage  $V_G$  applied, which was increasing by step from  $0$  V to  $-0.5$  V. The transfer characteristics were extracted by sweeping the  $I_D$  versus  $V_G$  ( $-0.8$  V $\sim$  $0.4$  V), under a constant  $V_D$  at  $-0.5$  V. It could be clearly observed in the logarithmic y-axis scale (Figure 4.2(b), black curve) that the  $I_D$  of OEET with PFT-100 as active layer material could be modulated over three orders of magnitude ( $10^{-8}$  A to  $10^{-5}$  A) by operating in the low and narrow  $V_G$  range. From the linear scale point of view (Figure 4.2(b), red curve), the threshold voltage  $V_{th}$  was a little bit high that a negative  $V_G < -0.6$  V needs to be applied to generate the  $I_D$  higher than  $10^{-5}$  A. This feature also implies a large transconductance ( $g_m$ , defined as  $\partial I_D / \partial V_G$ ) over  $0.4$  mS could be available under negative  $V_G$  biased, indicating the remarkable amplification capability of the OEET.

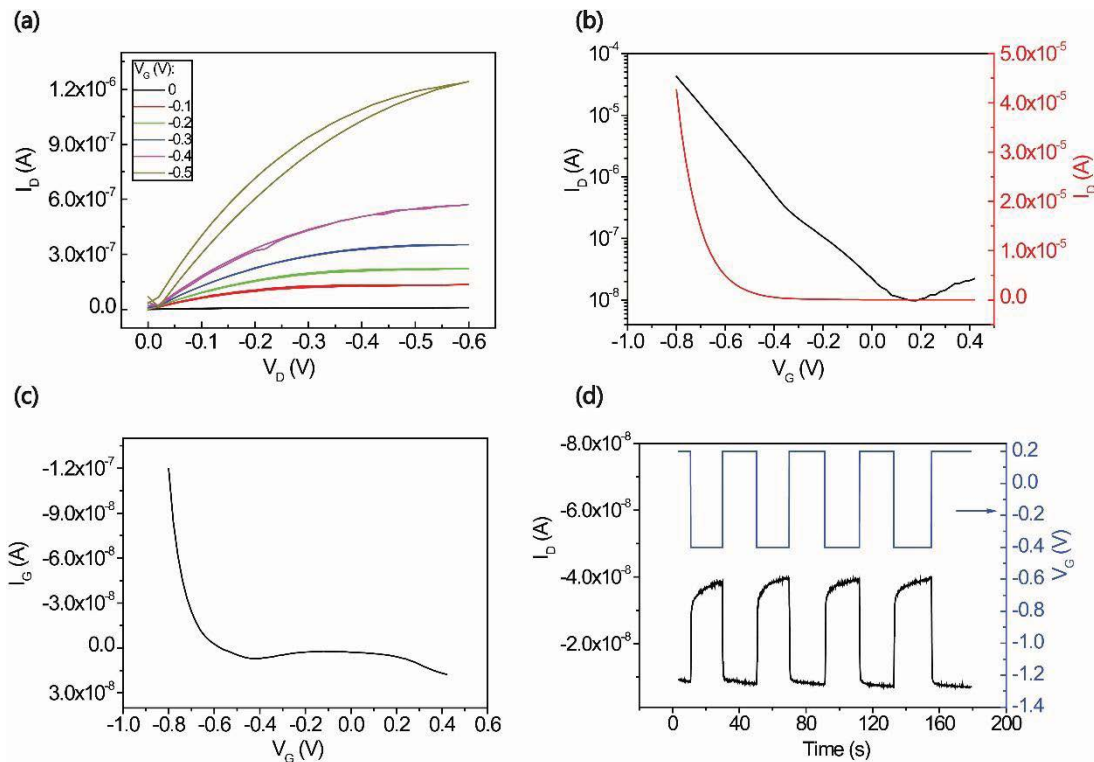


**Figure 4.2.** (a) Output characteristics of PFT-100 based OEET for  $-0.5$  V  $< V_G < 0$  V; (b) transfer characteristics at  $V_D = -0.5$  V, with  $I_D$  shown in linear (red) and logarithmic (black) scale; (c) the gate leakage  $I_G$  of the OEET during transfer measurement; (d) transient characteristics of  $I_D$  (black) in response to a pulsed  $V_G$  (blue) switched between  $0.2$  V and  $-0.4$  V.



As plotted in Figure 4.2(c), the gate leakage current ( $I_G$ ) was restricted under  $10^{-7}$  A over the whole operation range of  $V_G$ , indicating the device was well packaged from the aqueous electrolytes and the recorded  $I_D$  was mostly contributed by the electrochemical doping enhanced source-drain current, instead of the current flowed between source and gate electrode. The temporal response of OECT were measured under a pulsed  $V_G$  switched between 0.2 V and -0.4 V. (Figure 4.2(d)) According to the OECT model presented by Bernardis and Malliaras in 2007,<sup>75</sup> the  $I_D$  followed an exponential behavior as the ionic/electronic pathway could be simplified as a RC circuit. It is obvious that the transient time for switch off was much shorter than that needed for switch on (tens of seconds), which should be ascribed to ionic penetration behavior into the polymer film under  $V_G$  biases with opposite directions.

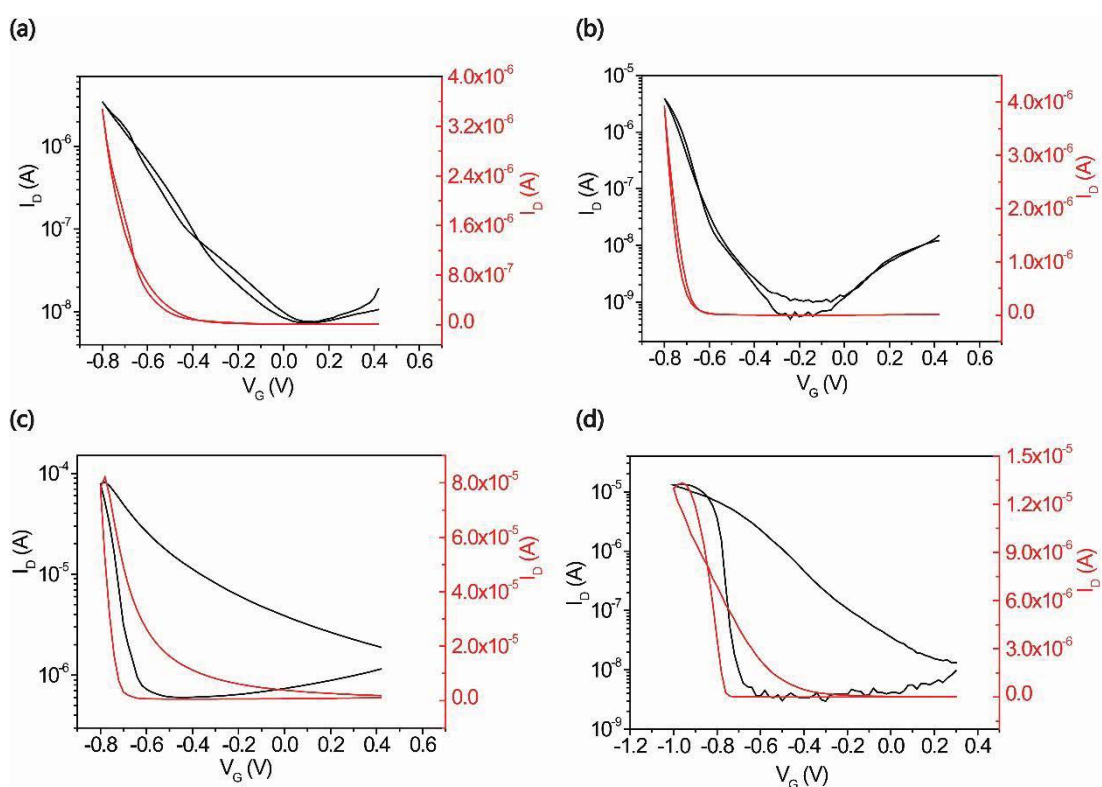


**Figure 4.3.** Transfer characterization of (a) PCDTPT, (b) DPP-DTT, (c) PDPP2T-TT-OD and (d) (DPP-DTT)<sub>0.95</sub>-(TT-TOH)<sub>0.05</sub> at  $V_D = -0.5$  V, with  $I_D$  shown in linear (red) and logarithmic (black) scale.

Owing to the high degree of similarity in backbone structure of the conjugated



polymers, transfer characteristics of PCDTPT were also similar to that of PFT-100, as shown in Figure 4.3(a). The only difference is that the maximum current and transconductance at  $V_G = -0.8$  V are almost one order of magnitude lower than that of PFT-100 based OECTs. This device performance variance could be ascribed to the minor structure difference between the fluorobenzo-thiadiazolo unit (PFT-100) and the thiadiazolo-pyridine unit (PCDTPT). The fluorine atom linked to the carbocyclic backbone (in PFT-100) was reasonable to perform stronger polarity than the nitrogen atom embedded in the pyridine ring (in PCDTPT), considering its higher electronegativity and less affected by steric hindrance of the backbone structure. Furthermore, this remarkable feature would facilitate the penetration and transport of negative charges (chloridion from the aqueous electrolyte) into the polymer film, which would then enhance the efficiency of electrochemical doping and the current modulation in OECTs. From another point of view, the films with stronger negative polarity tend to be more favorable for aqueous interaction, due to the dipole-dipole interaction between fluorine atom and water molecules. In other words, this film would perform better swelling capability, therefore increase the possibility for ions to penetrate into the bulk of the film under the negative  $V_G$  bias. Considering for the effects discussed above, it is reasonable that the PFT-100 based OECT showed better device performance compared to PCDTPT based ones.

Then three polymers based on the well-demonstrated diketopyrrolo-pyrrole-dithienylthieno-thiophene donor acceptor conjugated system were tested in PBS solution for OECT performance. As illustrated in Figure 4.3(b), the DPP-DTT based OECT also performed more than three orders of magnitude modulation of  $I_D$  and very small hysteresis. However, the  $V_{th}$  shifted to negative  $V_G$  direction which means that a larger  $V_G$  needs to be applied to generate a comparable  $I_D$  for operation during applications. The high  $V_{th}$  is a key drawback for OECTs based on this kind of



structured conjugated polymers, (similar high  $V_{th}$  observed in Figure 4.3(c) and 4.3(d), red curves) which might be explained by the ionization potential level (related to the HOMO level) of the polymers. The higher ionization potential for the DPP-DTT based polymers made these polymer backbones more difficult to be oxidized during ion penetration process, therefore not enough holes could be generated under low  $V_G$  bias, leading to the low channel current. Further improvements should be focused on tuning of the ionization potential of the conjugated system, thus the electrochemical doping process could be initiated at a lower negative  $V_G$  bias or even a positive  $V_G$  bias.

Besides the high  $V_{th}$ , another drawback of PDPP2T-TT-OD and (DPP-DTT)<sub>0.95</sub>-(TT-TOH)<sub>0.05</sub> based OECTs were the notable large hysteresis loop between forward and reverse scan of transfer curves. (Figure 4.3(d)) This might result in the signal delay for the need of rapid device response in sensing or stimulating applications. The major reason of such kind of phenomenon should be ascribed to highly organized crystallinity of the conjugated polymer backbone. The DPP core facilitated the planarization of the polymer backbone, subsequently performed a strong aggregating process in both the solution and film state, and at last relative high degree of crystallinity for charge transport.<sup>170,171</sup> However, this high crystallinity structure would hinder the penetration of negative ions into the film, as well as ionic migration back to the aqueous electrolytes. Therefore, when the  $V_G$  bias decreased (reverse scan), it took the ions embedded in the film longer time to permeate out, resulting in a delayed on current when the device is switched off.

As can be concluded from the discussion above, the conventional advantages of conjugated polymers which are suitable for high performance in OFETs, such as adjusted HOMO level, strong  $\pi$ - $\pi$  stacking, denser crystalline domain for efficient hole/electron transport, might be not applicable to OECTs which are characterized in

aqueous electrolytes. Consequently, further structure design and synthetic strategies of these conjugated polymers should be focused on facilitation of the ionic/electronic exchange between the polymer film and the aqueous electrolytes, which means, stronger polarity, more porous polymer microstructure and lower ionization potential to enhance the electrochemical doping process.

## 4.4 Effect of Thermal Annealing

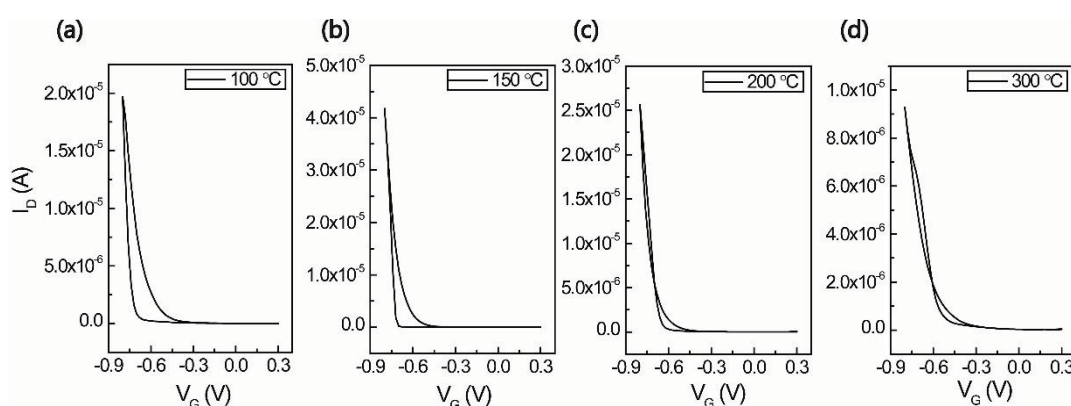


**Figure 4.4.** Comparison of transfer curves of PFT-100 based OECT prepared with different annealing temperature (a) 100 °C, (b) 150 °C, (c) 200 °C, and (d) 300 °C.

Through screening the OECT performance based on the conjugated polymers listed in Figure 4.1, PFT-100 was demonstrated to be promising for further investigation considering for its superior performance in OECT compared to other materials. Hence, we characterized the OECT performance with PFT-100 films under increasing annealing temperature from 100 °C to 300 °C, as shown in Figure 4.4. As can be observed from the transfer curves, the hysteresis loop tends to be reduced as the annealing temperature increased. The  $V_{th}$  value discussed here was defined to be extracted from the forward scan of the transfer curve ( $V_G$  sweep from 0.3 V to -0.8 V). As shown in Figure 4.4, a significant downward trend of  $V_{th}$ , from 0.683 V at 100 °C to 0.482 V at 300 °C, approximately. Besides, it could also be concluded that

the reduced hysteresis effect with increasing annealing temperature should be ascribed to the decrease of  $V_{th}$  in the forward scan of transfer curve. This phenomenon implies that thermal annealing of the films majorly affects the process that ion penetration into the film rather than ions migrated back to the solution. Another point worth to be noted is that, with annealing temperature reached up to 300 °C, the maximum  $I_D$  turned to slightly decrease (below  $10^{-5}$  A), which might due to the preferred adjustment in crystallinity of conjugated polymer aggregates under high temperature annealing. The denser packing of polymer chains would hence hinder the ion penetration and reduce the electrochemical doping, which directly leading to a lower channel current.

## 4.5 Impedance Analysis

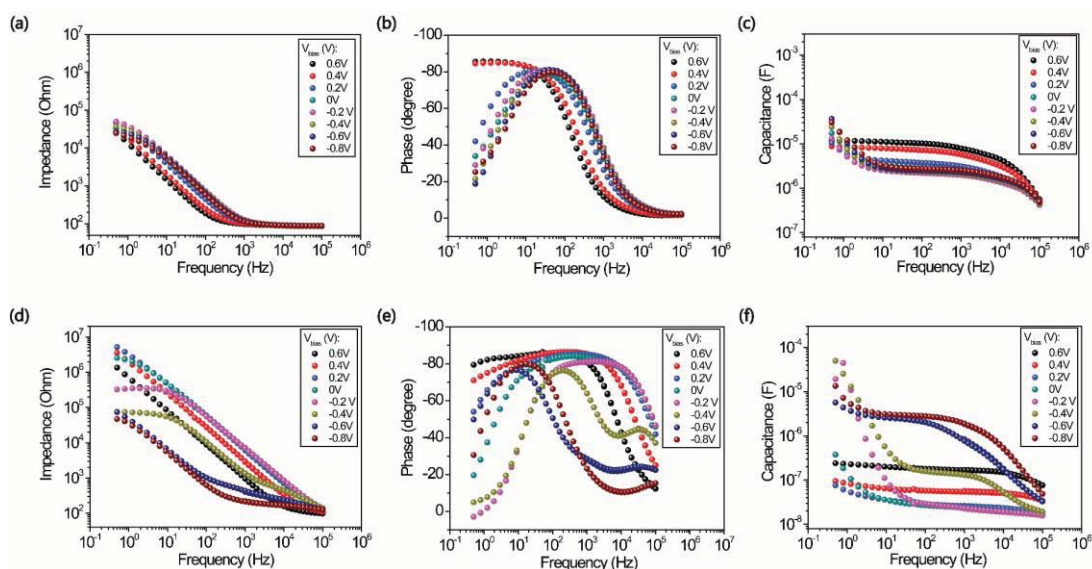


**Figure 4.5.** Impedance, phase and effective capacitance from EIS for (a-c) gold electrode and (d-f) PFT-100 film (coated on gold electrode) with the same area at a bias voltage ranging from 0.6 V to -0.8 V, applied from working electrodes.

The impedance characterization was then carried out to investigate the difference in capacitive behavior between impenetrable metal electrode surface and the polymer film. Herein, the impedance and phase graphs for planar gold electrode and PFT-100



film coated on gold electrodes were plotted in Figure 4.5. For the gold electrode, no significant change was observed in impedance spectrum with varying voltage bias applied from 0.6 V to -0.8 V. (Figure 4.5(a), (b)) The effective capacitance was then extracted from the relationship  $C = 1/(2\pi f \cdot Z_{im})$ , where  $f$  is the frequency and  $Z_{im}$  is the imaginary part of complex impedance. As can be seen from Figure 4.5(c), the extracted capacitance came to a plateau region at low frequency range, which could be taken to evaluate the capacitance change for steady state characterization of OECTs. This not significant changes in capacitance for the gold electrode might be ascribed to the electrical double layer capacitance formed on the impenetrable surface, which is not sensitive to the bias variation.

On the contrary, the impedance spectrum for PFT-100 film varied over two orders of magnitude when the voltage bias changed from 0.6 V to -0.8 V. (Figure 4.5(d)) More resistive ( $0^\circ > \varphi > -45^\circ$ ) character was also appeared for negative biased phase graphs. (Figure 4.5(e)) Evaluated based on the plateau region shown in Figure 4.5(f), the modulation of effective capacitance with corresponding bias voltage was much larger than that of the gold electrode. This phenomenon should be correlated with the amorphous and porous nature of the polymer chains deposited at the surface of metal electrode, which partially allow ion penetration into or out of the films depending on the direction of voltage bias applied. Under such circumstance, the electrical double layer capacitance should be replaced by the volumetric capacitance, the concept which was brought forward<sup>27</sup> and clarified in detail<sup>78</sup> recently. This should be a key feature dominating the performance of conjugated polymer based OECTs, which apparently needs more consideration for developing novel synthetic strategies for these conjugated polymers.

## 4.6 Effect of Electrolyte Size and Concentration

The effect of electrolyte concentration and species in aqueous environment for the operation of OECTs were then investigated. As illustrated in Figure 4.6(a), with decreasing concentration of sodium chloride from 1 M to  $10^{-4}$  M, the modulation by applied gate voltage was less effective, reduced to almost one order of magnitude. As the off-current is stable around  $10^{-9}$  A, the reduced modulation was majorly reflected on the decrease of the maximum current at  $V_G = -0.8$  V, which was extracted and plotted versus ionic concentration in Figure 4.6(b). This relationship implies that the channel current in OECT was dominated by the ions in the aqueous electrolytes, emphasizing the importance of the mechanism of electrochemical doping.

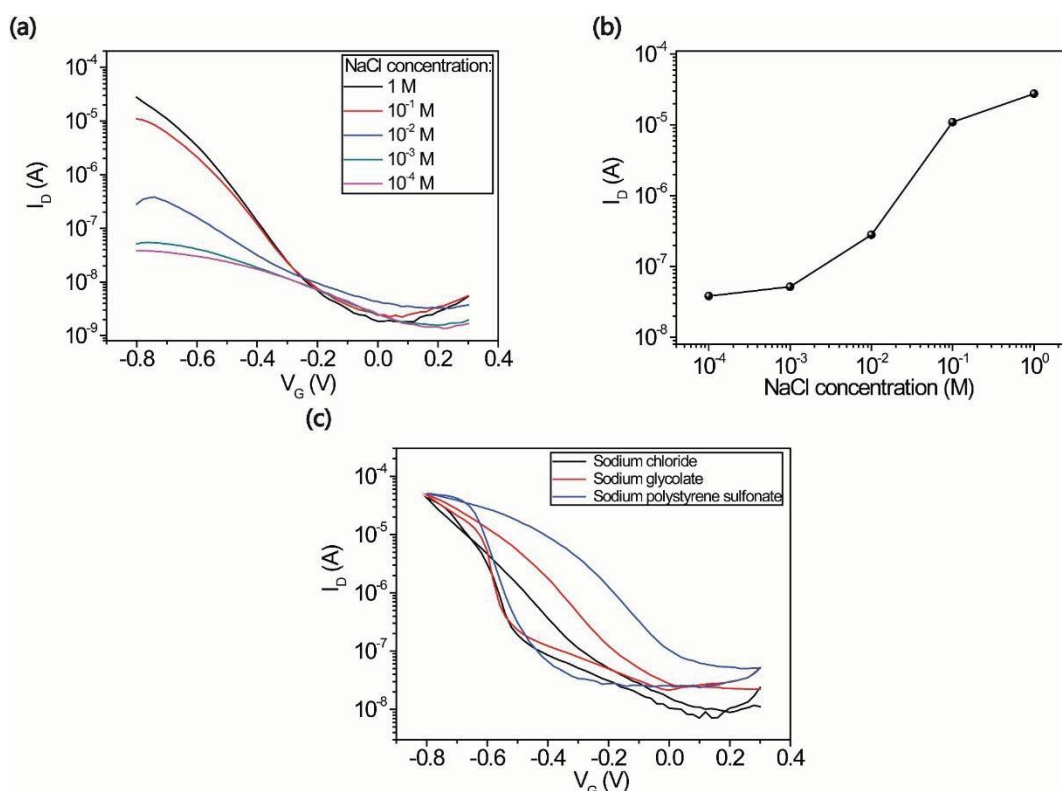


**Figure 4.6.** (a) Transfer characteristics of PFT-100 based OECT operated in sodium chloride aqueous electrolyte with various concentrations; (b) Drain current  $I_D$  value extracted at  $V_G = -0.8$  V versus the electrolyte concentration; (c) Transfer characteristics of PFT-100 based OECTs operated in aqueous solution with different



electrolytes.

The size (volume) effect of ionic species was then investigated by employing three different anions, chloridion, glycolate, and polystyrene sulfonate with the same counterion, sodium cation. From the literature reports, the radius of chloridion and polystyrene sulfonate were around 0.332 nm and 6.55 nm respectively.<sup>172,173</sup> This remarkable change in the volume of the anions would lead to an obvious change in the device performance. The transfer characteristics of PFT-100 based OECTs immersed in these electrolytes were then illustrated in Figure 4.6(c). A general trend could be observed that with the increasing size of negative ions, the hysteresis loop was notably enlarged. Considering that the forward scans of transfer curves were almost overlapped, the large hysteresis should originate from the horizontal shift (along x-axis) of reversed scan in transfer curves. This fact indicates that, the major barrier of ionic volume for electrochemical doping is in the drift out process, not the film penetration step. It is reasonable considering that the negative  $V_G$  was applied in an approximate steady state (with the slow scanning rate), under such an electrical field, all the negative charges were driven to penetrate into the PFT-100, leading to the indistinguishable forward transfer curves. In contrast, for the reverse scan, anions with larger volume (such as polystyrene sulfonate) were more difficult to drift out from the polymer film, as no driving force applied to attract them towards the gate electrode when  $V_G$  decreased from -0.8 V while still in negative range. Hence the ions were still embedded in the film and participated in the electrochemical doping process to contribute to the channel current flow.

The device characterization associated with varying ionic species implies the multi possibility to employ the OECT for the diverse needs of applications. This also threw light on the device optimization and conjugated polymer design strategies that the major efforts should be focused on enhancing the ionic/electronic exchange occurred



both at the polymer/aqueous electrolyte interface and inside the bulk film, which could lead to more efficient electrochemical doping and hence better device performance.

## 4.7 Summary

In conclusion, several high mobility p-type conjugated polymer were integrated in OECT platform and characterized in aqueous electrolytes. The device performance was analyzed with corresponding chemical structures, emphasizing the importance of facilitating the ionic penetration and transport in the polymer film. PFT-100 was demonstrated to perform superior performance and further systematically characterized with increasing thermal annealing temperature, electrochemical impedance spectroscopy, varying electrolyte concentrations and ionic species with different sizes. The structure-property relationship and the polymer/ion interaction were elucidated in detail, which would be beneficial for further design of high performance accumulation mode OECTs.



# Chapter 5 Label Free RNA Sensors Based on Capacitance Modulated Organic Electrochemical Transistors

In recent years, the interaction between semiconducting polymers and biomolecules attracts great attention from academic and industrial communities, which has a critical impact on integration of bioelectronic devices into biological environment. However, the nature of this interaction and its influence on device performance has been rarely investigated and is yet unclear. In this chapter, we developed a flexible, label-free RNA sensor based on a p-type accumulation mode organic electrochemical transistor (OECT) with single-strand DNA probe immobilized on the p(g2T-TT) channel material. The complementary RNA target was successfully detected at the concentration down to  $10^{-12}$  M in physiological environments, possibly ascribed to the capacitance change generated from the interaction between the RNA molecules with the semiconducting polymer chains. The mechanism was further investigated by characterization of transistor performance and film capacitance with increasing ionic volume from chloridion to polystyrene sulfonate in the electrolyte medium. The OECT platform opens a new way for further study of conjugated polymer-biomolecule interaction, which is also promising for flexible biosensing applications.

## 5.1 Introduction

Ribonucleic acid (RNA) is a negative charged polymeric molecule which plays an essential and indispensable role in various biological processes including gene expression, cell proliferation and development.<sup>174,175</sup> Recent progresses have



indicated that some categories of RNA molecules are closely tied to the generation and metastasis of cancer cells, which could be employed as a promising cancer biomarker for early diagnosis and therapy.<sup>176,177</sup> Therefore, various strategies have been developed for sensitive and rapid detection of RNA molecules in biological environment. The majority of conventional standard sensing techniques are developed based on quantitative polymerase chain reaction (PCR) and optical detection, which highly relies on time-consuming precision equipment or functionalization with fluorescence labels, such as quantum dots, metal nanoparticles or organic dyes.<sup>178,179</sup> Aiming to improve the simplicity, sensitivity, speed and lower the limit of detection, electrochemical methods are introduced to RNA molecule sensing.<sup>180</sup> Typically the detected signal and quantification are based on small changes in voltage or current in the presence of trace quantities of target RNA molecules, which could avoid the complex biomolecular labeling procedure and more direct information could be available conveniently.

Organic electrochemical transistor (OECT) has been widely employed in the development of highly sensitive biosensors, taking advantage of the intrinsic amplification function combined with superior biocompatibility raised from unique ion-to-electron conversion feature during device operation.<sup>17,47,49</sup> Our group has demonstrated a label-free DNA sensor by employing OECT integrated in flexible microfluidic system, based on the sensing mechanism of surface potential change on gate electrode through DNA hybridization.<sup>118</sup> A floating gate design was reported by White et al. for DNA sensing with electrolyte gated transistor, which physically separated the bio-recognition interface with electronic device and circuits.<sup>119,181</sup> Recently a layer-by-layer polyelectrolyte assembly strategy was introduced to PEDOT:PSS based OECT for RNA detection down to 0.1 ng/mL, based on a nonspecific electrostatic absorption mechanism.<sup>88</sup>



In this chapter, we report a novel method for label-free, in-situ detection of RNA biomarkers by employing the OECT platform integrated with a recently reported high performance semiconducting polymer p(g2T-TT).<sup>45</sup> The device is fabricated on flexible substrates, with demonstrated stable electrical performance under different bending states, indicating that it is capable for wearable healthcare applications. Then the single-stranded DNA probes are chemically immobilized on the surface of p(g2T-TT) channel area, which is used to specifically detect the complementary RNA molecule at concentration down to 1 pM. The sensing mechanism is related to the interaction between the captured RNA and the p(g2T-TT) channel. We found that under the negative voltage biased physiological electrolyte environment, the negative charged RNA strands were driven to penetrate inside the p(g2T-TT) film, which further hinder the electrochemical doping process of chloridion from electrolyte during the device operation, resulting in an obvious change in the volumetric capacitance of channel material and thus leading to a pronounced response in channel current. Furthermore, the OECT was successfully applied to detect a selected sequence of interleukin (IL)-8 mRNA, the biomarker for early detection of oral squamous cell carcinoma, which indicates the possibility for applications in noninvasive cancer diagnosis.

## 5.2 Experimental Section

### 5.2.1 Materials

Phosphate buffered saline (PBS) solution (pH 7.4), chloroform, sodium chloride and sodium glycolate were purchased from Sigma-Aldrich Co., USA. Sodium poly(styrene sulfonate) (Mw 75000, 30% w/v aqueous solution) was purchased from Alfa Aesar. AZ5214 and SU-8 2002 photoresists were purchased from Microchemicals



GmbH. (3-Glycidyloxypropyl)trimethoxysilane (GOPS) was purchased from International Laboratory, USA. Poly(2-(3,3'-bis(2-(2-(2-methoxyethoxy)ethoxy)ethoxy)-[2,2'-bithiophen]-5-yl)thieno [3,2-b]thiophene), p(g2T-TT), was synthesized by Iain McCulloch's Group. All the DNA and RNA sequences were ordered from Sangon Biotech Co., China.

## 5.2.2 Device Fabrication

The OECT devices were fabricated following a previously reported method.<sup>182</sup> Briefly, the polyethylene terephthalate (PET) substrate was thoroughly cleaned and then photo lithographically patterned with Cr/Au (10 nm / 100 nm) electrodes through magnetron sputtering deposition. The p(g2T-TT) polymer and SU-8 2002 insulating layer were then patterned in sequence, forming the active channel area with 60  $\mu\text{m}$  width and 30  $\mu\text{m}$  length. The p(g2T-TT) polymer was spin coated from chloroform at 2 mg/mL and annealed at 100 °C for 1 h before patterning.

To immobilize DNA probe on the surface of OECTs, the p(g2T-TT) channel area was exposed to O<sub>2</sub> plasma treatment (20 W/ 2 min) to generate hydroxyl functional groups, then the GOPS was deposited by vapor deposition method in a vacuumed desiccator at 95 °C for 1 h. Subsequently the amino modified DNA probe solution (adjusted to pH 9) was dropped on the channel for probe immobilization, through the ring-opening reaction of the epoxy from GOPS with the amino group from DNA.

## 5.2.3 Device Characterization

A small droplet (10  $\mu\text{L}$ ) of aqueous solutions (PBS or other ionic electrolytes) was dropped on the OECT to connect the channel area with gate electrode. The output and transfer characteristics of the OECTs were carried out using two Keithley 2400



sourcemeters with customized LabVIEW program. Electrochemical impedance spectroscopy (EIS) measurements were performed with Zahner Zennium pro electrochemical workstation and a three-electrode-system, including Indium tin oxide (ITO) electrodes ( $0.2 \text{ cm}^2$ ) coated with thin film of p(g2T-TT) polymer (working electrode), a platinum wire as counter electrode and Ag/AgCl reference electrode. Effective capacitance was derived from  $1/(2\pi f \cdot Z_{im})$  and used for calculation of areal and volumetric capacitance, where  $f$  is the frequency and  $Z_{im}$  is the imaginary part of impedance. Atomic Force microscopy (AFM) characterization was performed with a Bruker Nanoscope 8 microscope in tapping-in-air mode. The film thickness was recorded by Bruker Dektak XT surface profilometer. Fourier transform infrared spectroscopy (FT-IR) was introduced for direct characterization of the polymer film surface using the attenuated total reflectance (ATR) accessory of Bruker Vertex 70 spectrometer.

### 5.3 Electrical Measurements

As illustrated in Figure 5.1(a), the flexible OECT with gold electrodes and poly(2-(3,3'-bis(2-(2-(2-methoxyethoxy)ethoxy)ethoxy)-[2,2'-bithiophen]-5-yl)thio[3,2-b] thiophene), p(g2T-TT), the active layer, were integrated on thin polyethylene terephthalate (PET) substrates through photolithography microfabrication process. The PET substrate was thin enough ( $200 \mu\text{m}$ ) so that the device could be easily bent to various status. (Figure 5.1(b)) The typical output and transfer characteristics were performed in Figure 5.1(c) and 5.1(d), indicating the OECT with p(g2T-TT) as active layer was operated in p-type accumulation mode. For transfer characteristics, the drain voltage  $V_D$  was fixed at  $-0.5\text{V}$ , and the  $I_D$  vs.  $V_G$  sweeping was recorded under different bending radii, demonstrating the stable device performance under different bending status, indicating that it is promising for real applications in

wearable electronics (Figure 5.1(d)).

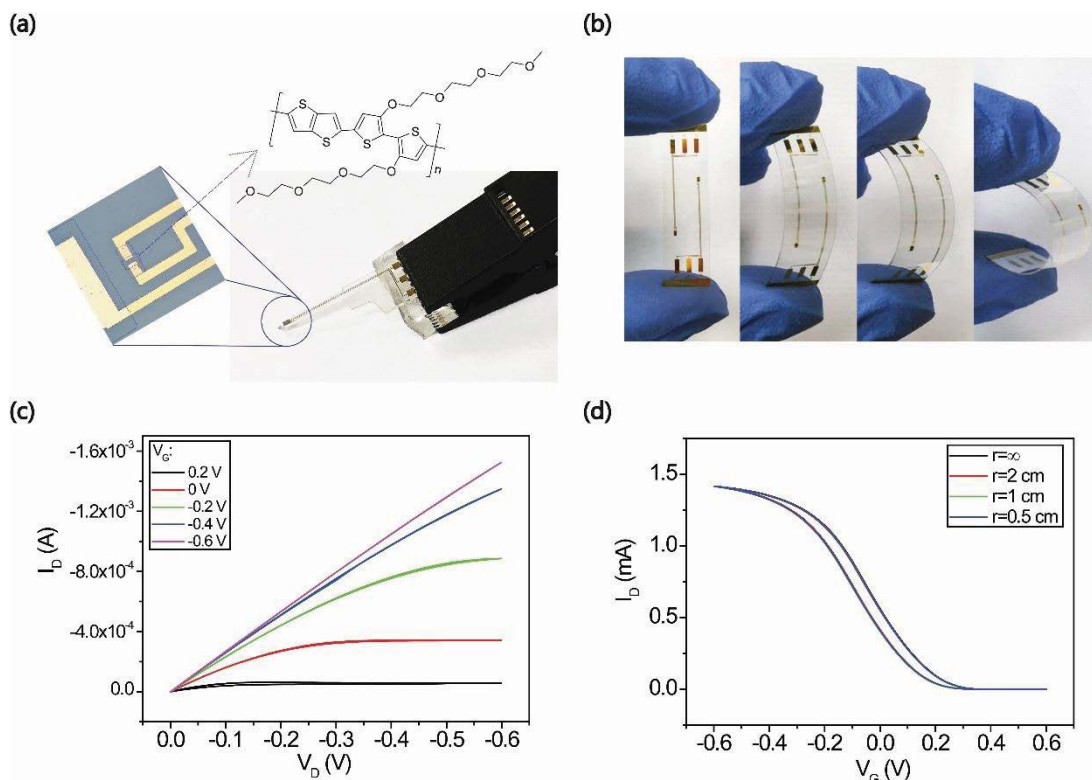


**Figure 5.1.** (a) Optical images of OECT pattern with the molecular structure of p(g2T-TT); (b) photographs of flexible OECT with different bending statuses; (c) output characteristics (drain current  $I_D$  versus drain voltage  $V_D$ ) under gate voltage  $V_G$  varying from 0.2 to -0.6 V; (d) transfer curves ( $I_D \sim V_G$ ) with different bending radii.

## 5.4 Label-free RNA Sensor Based on OECTs

### 5.4.1 Effect of Channel Thickness on RNA Sensitivity

The OECT was chemical functionalized (following the procedures in device fabrication section) to be employed for detection of RNA hybridization. As illustrated in Figure 5.2(a), the source drain electrodes were well protected by the coverage of an insulating layer of SU-8 photoresist, leaving only the channel area exposed to aqueous electrolyte. The single strand DNA sequences were then

immobilized on the surface of p(g2T-TT) film, acting as a probe for complementary RNA sequence capture. Under the condition of negative  $V_G$  bias, the negative charged RNA molecules captured at the device surface were forced to partially penetrate and interact with the p(g2T-TT) chains, affect the volumetric capacitance of the bulk channel film and then the electrical performance of the OEET. Therefore, the device is capable to be employed as a RNA sensor.

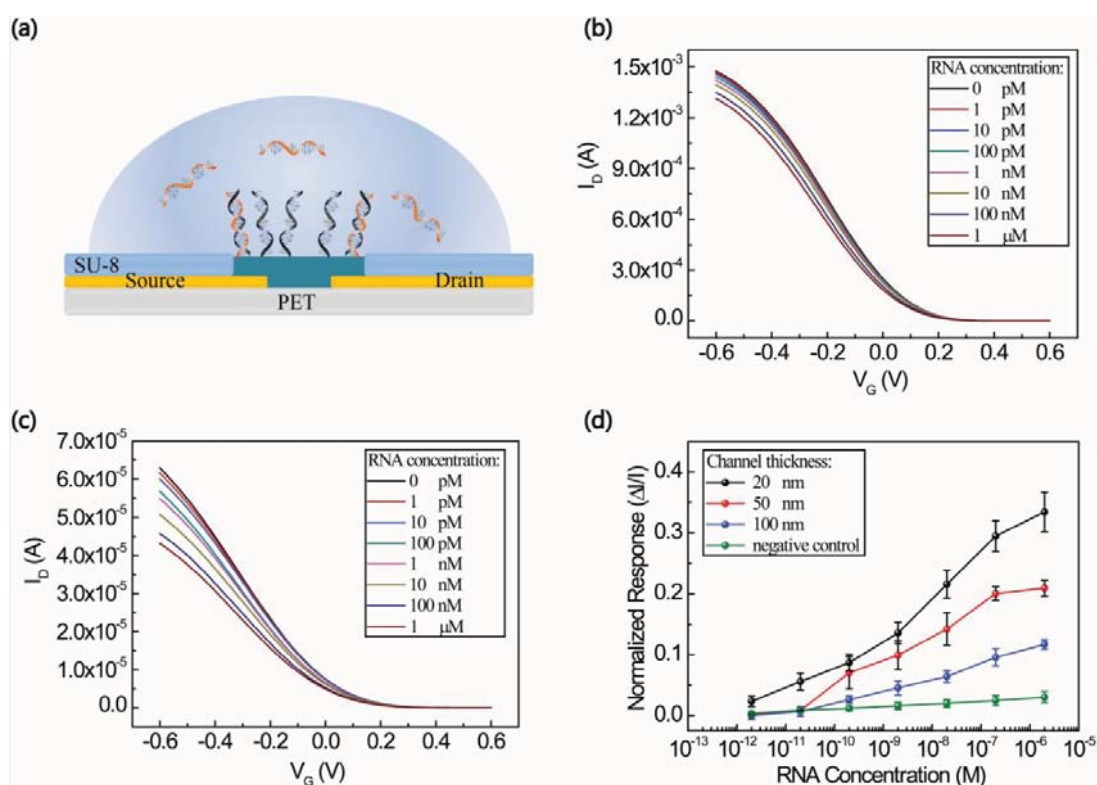


**Figure 5.2.** (a) Schematic of the OEET cross-section for RNA sensing; the change in transfer curves of the modified OEET with (b) thick p(g2T-TT) film and (c) thin p(g2T-TT) film upon addition of increasing concentration of mRNA; (d) Normalized current response of OEET with different channel thickness (thick,  $\sim 100$  nm; medium,  $\sim 50$  nm; thin,  $\sim 20$  nm) to varying RNA concentrations.

The sequence of the amino group modified DNA probe is 5'-NH<sub>2</sub>-C6-TCA ACA TCA GTC TGA TAA GCT A-3'. The complementary miRNA-21 single strand with the sequence 5'-U AGC UUA UCA GAC UGA UGU UGA-3' and a random sequenced RNA 5'-U UGU ACU ACA CAA AAG UAC UG-3', where G is guanine,



C is cytosine, A is adenine, T is thymine, were tested following the same procedure. The devices were characterized in PBS solution before and after the incubation period for RNA hybridization, to investigate only the influence of RNA molecules bonded to the surface of the device.

The OECT with thick p(g2T-TT) channel layer (~100 nm) was first taken for RNA sensing. As can be seen from the transfer curves in Figure 5.2(b), the maximum current of the device was still maintained at mA level (at  $V_G = -0.6$  V) after  $O_2$  plasma treatment and chemical functionalization step, indicating that most of the bulk film was not affected by the surface modification and could still carry out efficient doping/dedoping process to support hole transport throughout the channel. In such cases, the addition of complementary RNA molecules could only lead to small changes in channel current. (around 10 % decrease calculated from maximum current after 1  $\mu$ M RNA incubation) In order to enhance the device response and sensitivity to RNA detection, the p(g2T-TT) layer was spin coated at higher rotational speed to make the film thinner. When the channel thickness decreased to ~20 nm, the device showed a significant enhanced response to the addition of RNA molecules. As seen from Figure 5.2(c), the maximum current extracted from the transfer curves decreased in the percentage of ~31%, indicating that the existence of RNA strands at the surface performed a more significant impact on the thinner channel film, compared to the thicker ones. The statistic normalized response of the device exposed to RNA solution with increasing concentrations (1 pM to 1  $\mu$ M) was plotted in Figure 5.2(d), illustrating the effect of channel thickness on the change of current response.

## 5.4.2 Capacitance Modulated Sensing Mechanism

The sensing mechanism is sketched out in Figure 5.3(a). Under negative  $V_G$  bias, the

cations in the electrolyte were forced to drift to accumulate at the gate electrode, while the anions (mostly chloridion) were driven to penetrate into the p(g2T-TT) film and generate corresponding holes on the conjugated thiophene backbone of the polymer chain through the doping process. Therefore, the channel was turned on and the drain current was dependent on this reversible doping/dedoping process. The channel current in the saturation regime is given by<sup>28</sup>

$$I_D = \frac{W}{2L} \cdot \mu \cdot C^* \cdot (V_{th} - V_G)^2 = \frac{W}{2L} \cdot \mu \cdot d \cdot C_i \cdot (V_{th} - V_G)^2 \quad (5.1)$$

where  $W$  and  $L$  are the width and length of channel,  $\mu$  is the hole mobility,  $C^*$  is the volumetric capacitance,  $V_{th}$  is the threshold voltage,  $d$  is the thickness of channel layer, and  $C_i$  is the capacitance per unit area.

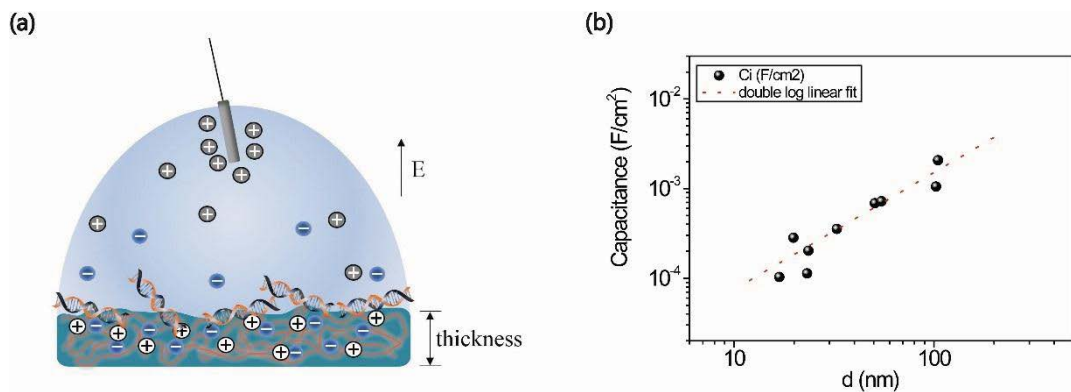


**Figure 5.3.** (a) Schematic of the sensing mechanism illustrating the interaction between RNA and polymer in the channel area of OEET; (b) Capacitance of p(g2T-TT) film corresponding to the film thickness  $d$ .

Considering that the RNA molecules possess a large amount of phosphate groups, which means a relatively low isoelectric point ( $\sim 2$ ),<sup>183</sup> they are expected to perform like polyanions in the neutral PBS solution environment ( $pH = 7.4$ ). Therefore, the RNA molecules captured at the surface of device were also driven to inject into the bulk of p(g2T-TT) film, which performs good swelling property due to the existence of glycolated side chain. The polyanionic RNA molecules covered on the p(g2T-TT)



chains reduces the effective surface area for electrochemical doping, which in turn decreases the volumetric capacitance  $C^*$  in equation 5.1, subsequently reduces the channel current  $I_D$ . Another possible explanation is that considering the electrostatic interaction of like charged ionic species, chloridion are largely repulsed from the region surrounding the RNA chains, which are negatively charged. In this situation, the electrochemical doping by the penetration of chloridion was greatly influenced. As shown in Figure 5.3(b), the areal capacitance of the p(g2T-TT) film extracted at  $V_{\text{bias}} = -0.6$  V was characterized under different film thickness, fitting linearly over two orders of magnitude, which indicates that the negative charged ions interact with the polymer backbones in p(g2T-TT) film uniformly and with the same possibility (without source drain voltage applied). This is also in consistent with the volumetric capacitance model previously reported for PEDOT:PSS.<sup>27</sup> Therefore, with the decrease of channel thickness, a lower channel current  $I_D$  was observed, as seen from Figure 5.2. Meanwhile, the reduction of channel volume enhanced the influence of RNA molecules at the channel/electrolyte interface, resulting in a larger device response for thinner film OECTs.

### 5.4.3 Impedance Analysis on RNA Sensing

The immobilization process of RNA on the surface of p(g2T-TT) film could be further characterized with EIS. Figure 5.4(a) and 5.4(b) shows the effective capacitance (per unit area) and the phase response of p(g2T-TT) film (processing the same chemical functionalization as for the OECT sensor) after incubation with increasing concentration of RNA solutions. The EIS was carried out under a constant voltage bias of -0.6 V, which was comparable to the situation for transfer characterization. From the phase response in the impedance spectrum, it was clearly observed that the p(g2T-TT) film performed more resistive character ( $0^\circ > \varphi > -45^\circ$ )

at high frequency range ( $10^2$  Hz to  $10^5$  Hz), while was dominated by more capacitive character ( $-45^\circ > \varphi > -90^\circ$ ) at low frequency range ( $< 10^2$  Hz). This could be explained by the fact that the reversible penetration behavior of anions between the p(g2T-TT) film and the aqueous electrolyte has a limited rate, which could not respond fast enough to high frequency voltage driven, in consistent with the typical AC characterization of PEDOT:PSS based OECT devices.<sup>182</sup> From another point of view, with the increasing RNA concentration, the peak of phase curves located between  $10^3$  to  $10^4$  Hz showed a slightly shift to lower frequency, which is closely related to the dielectric relaxation process during the characterization, also demonstrated the influence of surface captured RNA molecules on the ion penetration process into the p(g2T-TT) film.

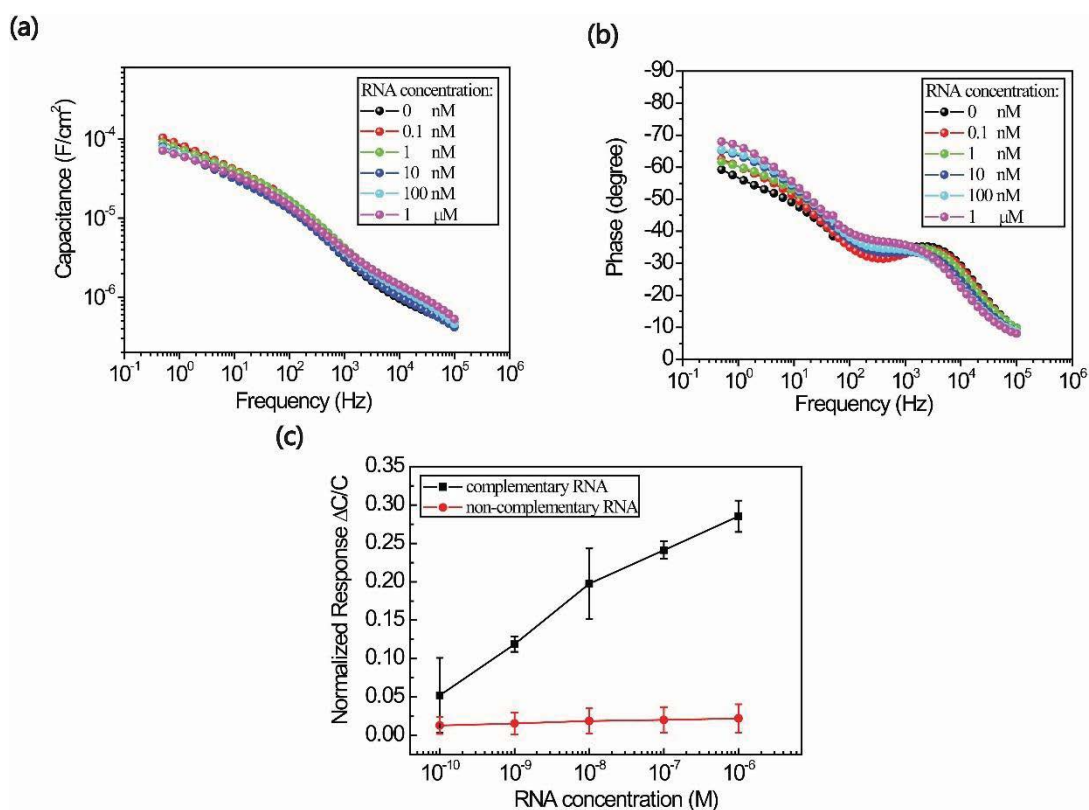


**Figure 5.4.** (a) Effective areal capacitance and (b) phase from EIS for p(g2T-TT) film coated on ITO substrate and modified with increasing RNA concentrations; (c) normalized capacitance response as a function of RNA concentration.

The change of capacitance to the addition of RNA at low frequency was extracted and plotted in Figure 5.4(c). A normalized capacitance response up to 30% was observed when the RNA concentration increased to  $\mu\text{M}$  range, which is consistent with the OECT sensor response. A controlled experiment was carried out for incubation of non-complementary RNA molecules on p(g2T-TT) film, in which there was only slight physical absorption and no hybridization process occurred. The less than 4 % capacitance change in control experiment demonstrated that the response was induced only by the capture of RNA molecules at the surface of p(g2T-TT) film.

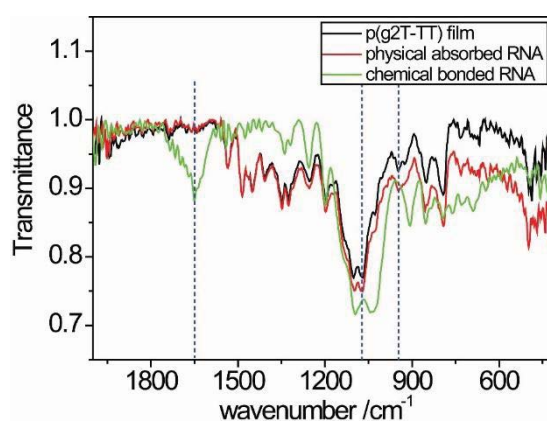


**Figure 5.5.** Attenuated total reflection (ATR) Fourier transform infrared spectra of pure p(g2T-TT) film (black) and films with physical absorbed (red) or chemical bonded (green) RNA molecules.

The FT-IR spectroscopy with ATR module was further introduced to investigate the surface modification of RNA molecules on p(g2T-TT) film, as illustrated in Figure 5.5. The ATR crystal was directly contacted to the surface of p(g2T-TT) film. Considering that the penetration depth of the infrared light into the sample is typically around several micrometers, the surface modifications could be effectively monitored by this technique. First, the dominant spectral band centered at 1070 to 1101  $\text{cm}^{-1}$  was assigned to the C-O-C stretching vibration from the glycolated side chain on p(g2T-TT). As can be seen from the spectrum, a shift from 1070  $\text{cm}^{-1}$  to

1043  $\text{cm}^{-1}$  and broaden of the absorption band was observed for p(g2T-TT) with chemical bonded RNA, which should be ascribed to the influence of electronegative nucleic acid functional groups on the polymer. Besides, the peak shift from 947  $\text{cm}^{-1}$  to 906  $\text{cm}^{-1}$  might be explained by the P-O stretching vibration from the phosphate group. A new generated peak within 1750 to 1570  $\text{cm}^{-1}$  spectral range was related to the C=C, C=O stretching vibration of conjugated ketone and C=O, N-H vibration in the amide structure from the bases of RNA. Other absorption peaks related to the intrinsic p(g2T-TT) structure were not changed after RNA modification, demonstrating the stable background control for spectrum analysis.

#### 5.4.4 Oral Cancer Biomarker Sensing

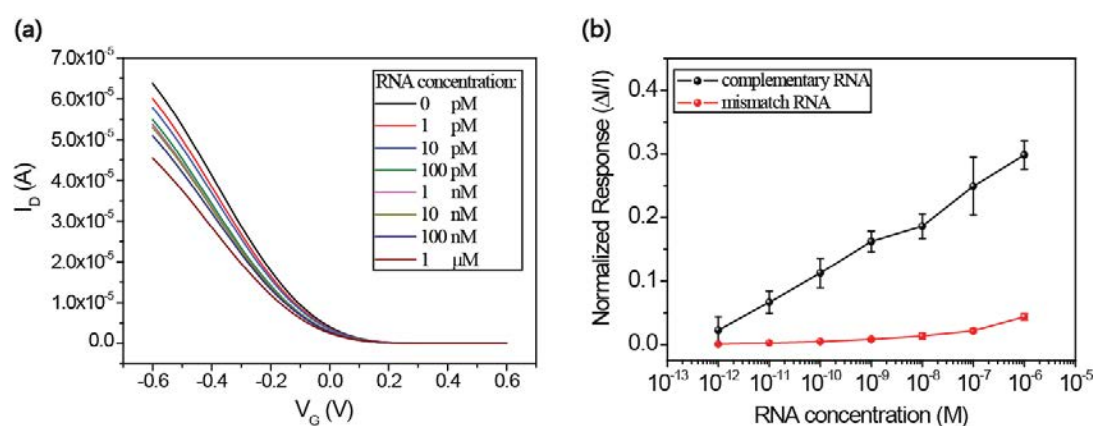


**Figure 5.6.** (a) The change of transfer curves of DNA probe modified OECT upon addition of increasing concentration of oral cancer biomarker IL-8 mRNA; (b) normalized current response of the device response to complementary RNA sequence and 4-base mismatched RNA sequence.

To meet the growing demand for rapid and non-invasive disease diagnosis, molecular analysis of body fluids, such as saliva,<sup>126,128</sup> sweat<sup>113</sup> or skin interstitial fluid,<sup>184</sup> has attracted more and more research interests.<sup>105</sup> Recent researches have demonstrated that certain cell-free RNA species could present in saliva sample at the level sufficient for oral cancer diagnosis.<sup>185</sup> Therefore, developing rapid, highly



sensitive and selective sensors for detecting salivary RNA biomarkers could bring new insight for early and efficient disease identification through non-invasive methods.

Here we tried to employ the p(g2T-TT) based OECT sensor platform for detection of interleukin (IL)-8 mRNA, which has been confirmed to present at a higher level in saliva sample for patients with oral squamous cell carcinoma.<sup>186</sup> The amino functional group modified complementary DNA probe, with the sequence of 5'-NH<sub>2</sub>-C6-GAG GGT TGT GGA GAA GTT TTT GAA GAG GGC TGA G-3', was first immobilized on the channel area of OECT sensor following the same procedure as previously described. Then the target IL-8 RNA characteristic sequence 5'-C UCA GCC CUC UUC AAA AAC UUC UCC ACA ACC CUC-3' and a 4-base mismatched RNA sequence 5'-C UCA ACC CUC GUC AAA GAC UUC UCC CCA ACC CUC-3' were measured under the same condition. The transfer response and the corresponding normalized response to RNA concentration were illustrated in Figure 5.6. The sensing of target RNA molecule by the functionalized OECT showed a limit of detection down to 1 pM, and the normalized current response was higher than 30 % when the RNA concentration raised up to  $\mu$ M level. Meanwhile, the 4-base mismatched RNA molecules lead to a device response below 5 %, demonstrating the high selectivity and specificity of the label-free OECT sensors.

## 5.5 Size Effect on Polymer/Ion Interaction

### 5.5.1 Effect on Operation of OECTs

To further investigate the effect of ionic doping for the p(g2T-TT) film and the OECT performance, three monovalent anions with the same counterion (sodium cation) and different hydration volume, chloridion, glycolate and polystyrene

sulfonate were chosen as the electrolyte in aqueous environment. The radius of these monovalent anions was estimated by the molecular weight and a simple spherical model,

$$V_{anion} = \frac{M_w}{N_A \cdot \rho_{solution}} = \frac{4}{3} \pi r^3 \quad (5.2)$$

where  $V_{anion}$  is the volume of the anion,  $M_w$  is the molecular weight,  $N_A$  is the Avogadro constant,  $\rho_{solution}$  is the density of the electrolyte solution, and  $r$  is the radius of the anion. Then the radius could be derived as,

$$r = \sqrt[3]{\frac{3M_w}{4\pi \cdot N_A \cdot \rho_{solution}}} \quad (5.3)$$

The molar mass and calculated radius of these anions were plotted in Figure 5.7(a), which indicates a monotonic increase relationship. The estimated radius was fitted quite well in the range reference value from literature,<sup>172,173</sup> which could be taken for further comparison and analysis.

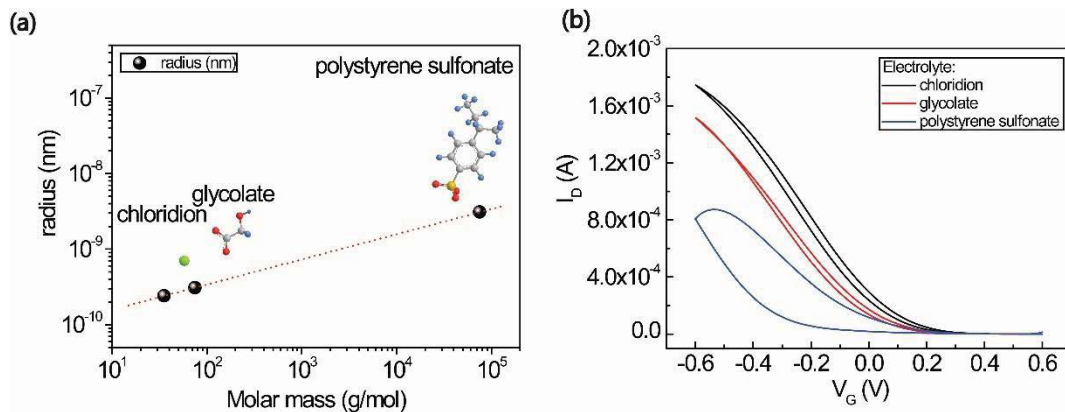


**Figure 5.7.** (a) The calculated radius of three monovalent anions versus the corresponding molar mass; (b) transfer characteristics of OECT with different electrolyte anions at the same concentrations of 1 M (with the same sodium counterion).

The p(g2T-TT) based OECT was then operated with these anions as electrolyte (at a



fixed concentration of 1 M) instead of PBS solution. The corresponding transfer curves were illustrated in Figure 5.7(b). It could be clearly observed that with the increasing of the anion radius, the maximum drain current significantly reduced to lower than one half of the original current as measured in chloridion. Besides, the hysteresis loop was clearly enlarged, especially when the device was characterized in polystyrene sulfonate electrolyte environment, indicating that anions with larger volume were more difficult to penetrate into the interspaces of p(g2T-TT) film under negative  $V_G$  biased, and to drift back into the aqueous solution when  $V_G$  turned into positive. According to equation 5.1, such remarkable drop in  $I_D$  should be correlated to the change in volumetric capacitance of the p(g2T-TT) film. Therefore, the EIS characterization was further carried out for investigation of the effect of different anions.

### 5.5.2 Impedance Analysis

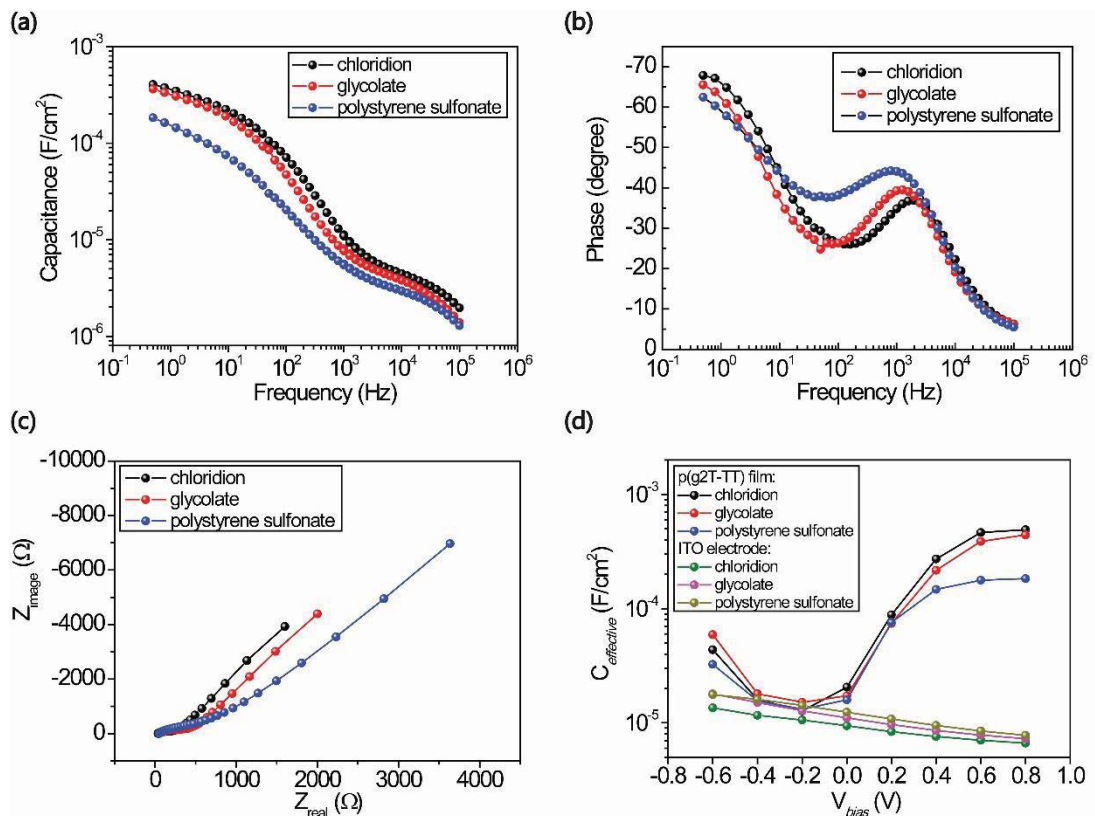




**Figure 5.8.** (a) Effective capacitance, (b) phase and (c) Nyquist plot from EIS for p(g2T-TT) film characterized in different electrolytes. (d) Comparison of the effective capacitance of p(g2T-TT) film and ITO electrode at varying bias voltage  $V_{\text{bias}}$  in different electrolytes.

The effective areal capacitance and the phase angle versus frequency were plotted in Figure 5.8(a) and 5.8(b). Generally, the impedance behavior of p(g2T-TT) film under different ionic solutions were similar compared to the spectrum collected in PBS solution previously. A decrease in the effective capacitance at low frequency range (1 Hz) was observed when polystyrene sulfonate was taken as the anion for doping of p(g2T-TT) backbone instead of chloridion, which is again in consistent with the downward percentage of the maximum drain current from transfer characterizations. The Nyquist plot, as shown in Figure 5.8(c), presented another way to compare the difference of these anion electrolytes. The Nyquist plot obtained in polystyrene sulfonate solution, are further away from the imaginary impedance axis, compared to the one obtained from chloridion solution, which suggests that the negative charged polystyrene sulfonate chains, are more likely to be hindered from injecting into the p(g2T-TT) film.<sup>187</sup> Furthermore, the effective capacitance for p(g2T-TT) film (coated on ITO substrate) and pure ITO electrode, immersed in these three kinds of electrolyte solutions, were characterized and extracted under different voltage bias (-0.6 V to 0.8 V), as illustrated in Figure 5.8(d). The sign of bias voltage here is defined by the three-electrode-system in the EIS (applied from the working electrode), which is opposite to the sign of the  $V_G$  applied during the operation of OECT. Therefore, when the bias increased in the positive direction, which means that more anions are attracted to the p(g2T-TT) film (or ITO), the capacitance of p(g2T-TT) came through an increase to almost two orders of magnitude, due to the electrochemical doping process. However, for ITO electrode, there was no upward trend when the bias voltage increased, which should be ascribed to the formation of double layer capacitance for such kind of impenetrable planar metal surface. The



effective capacitance of ITO at the negative biased range overlaps with those for the p(g2T-TT) film, indicating that when there is no electrochemical doping occurred, (anions are driven towards the counter electrode) the p(g2T-TT) film also performs like a double layer capacitor.

## 5.6 Summary

As a short conclusion, p-type accumulation mode OECT with p(g2T-TT) as active layer has demonstrated remarkable sensing capability for label free detection of RNA biomarkers in physiological environment with a limit of detection down to pM level. The OECT biosensor was fabricated on flexible substrates, with stable performance under different bending status, which is promising for wearable healthcare applications. The sensing mechanism is based on the capacitance change of p(g2T-TT) film modulated by the interaction with the RNA biomarkers hybridized at the surface of the channel film. The effect of anion volume in the aqueous electrolytes was systematically investigated on p(g2T-TT) film and OECT devices, throwing light on further understanding of volumetric capacitance and doping/dedoping process of p(g2T-TT) film with different negative charged species.



## Chapter 6 Conclusions and Perspectives

### 6.1 Conclusions

In this thesis, the OECT platform was systematically investigated from several aspects, such as device fabrication, operating mechanism and sensing applications. The strategies for functionalization of OECTs for chemical and biological sensing applications were overviewed, including channel material, electrolyte and gate modification, which indicates the promising future for integrating OECT platform into healthcare and wearable applications.

First, a novel, convenient and universal technique for miniaturization of OECT was developed through multilayer photolithography process. By miniaturizing the channel length and width of OECTs to micrometre range, the response time of device could be shorted to  $10^{-5}$  s, opening up the possibility to introduce AC measurements into electrochemical sensing applications. The ion strength sensing, dopamine sensing (with detection limit down to 1 nM) and cell activity monitoring were successfully demonstrated with PEDOT: PSS based OECTs, illustrating a promising analytical method for further bioelectronic applications.

Several high mobility p-type conjugated polymers (with thiadiazole or diketo pyrrolo-pyrrole backbone repeating units) were utilized as the active layer of OECT and characterized to screen the suitability of these polymers for OECT operation in aqueous electrolytes. Then for the selected polymer which demonstrated superior electrical performance, further process optimization, impedance characterization and ionic response were carried out for comprehensive understanding of the doping/dedoping process and ionic penetration behavior in the conjugated polymer



film. The analysis of structure-property relationship would further shed light on design strategies of semiconducting materials for high performance OECTs employed in bioelectronic applications.

Another p-type semiconducting polymer p(g2T-TT), with the glycolated side chain grafted on thiophene backbone, was integrated in OECT device and the electrical performance was thoroughly characterized. Based on its distinct characteristics in high transconductance and fast switching speed for OECT working in accumulation mode, p(g2T-TT) based OECT was utilized for label-free, high sensitive RNA sensing application. Single strand mRNA with a concentration down to  $10^{-12}$  M could be detected by the OECT previously immobilized with complementary single strand DNA probe on the channel area. The capacitance modulated sensing mechanism and polymer/electrolyte interaction was discussed in detail.

## 6.2 Perspectives

As discussed in this thesis, the fabrication process, operating mechanism, semiconducting materials and device functionalization all played important roles in the performance of OECT and its application as chemical and biological sensors. Although several models have been proposed to elaborate the device physics of OECTs, the ionic/electronic interaction inside the polymer backbone still needs further investigation for better understanding of the device operation. Several advanced techniques, such as electrochemical strain microscopy<sup>188</sup> and charge accumulation spectroscopy<sup>189</sup>, have been employed for characterization of local ionic transport at the organic semiconductor-liquid interface or inside the polymer film. However, the behavior of ion injection and its relationship with generated electronic charges (electrochemical doping/dedoping process) on a micro level is still not yet



clearly clarified, due to lack to suitable analytical methods. Therefore, this would be an opportunity for physicists and instrumentation engineers to collaborate on exploring the possibilities to employ more suitable instruments for in-situ analysis, which would better benefit the understanding of operating mechanism and device design of OECTs.

Design and synthesis of new p-type and n-type semiconductors, both polymers and small molecules, is another promising direction for development of high performance OECTs with specific functions. As emphasized in this thesis, the structure-property relationship reveals the critical guideline which needs to be comprehensively investigated to synthesize materials which could present stable and superior performance during operation in aqueous electrolytes. The synthetic freedom, the key feature for organic devices, could be well utilized for design and fabrication of OECT with specific applications.

Taking the advantage of efficient control of channel electrical state in OECT by ion motions, different categories of neuromorphic and memory devices can further be developed. The structure and function of certain nervous system could be mimicked by specific design and operation of OECT devices. The investigation in simulation of short-term and long-term memory would better contribute to the development of neuromorphic computation and memory industry.

Through improvements in fabrication processes and techniques, high-throughput, low-cost, flexible OECT sensors could be available for integration into large area display applications and other consumer markets. The unique features, such as superior stability for operation in aqueous electrolyte, high transconductance for signal amplification, and convenient functionalization with biomolecules, are promising to be integrated into smart and wearable electronic devices for healthcare



or diagnosis applications.

With the rapid development of fabrication techniques and functionalization strategies, OECTs have been successfully exploited in tremendous cutting-edge applications. It is no doubt that continuous progress would be reached in this emerging interdisciplinary field. From a greater point of view, both efforts in fundamental mechanism investigation and explorations in applications, would efficiently expedite the maturity of this technology and its commercialization in the not-too-distant future.



## References

- (1) Forrest, S. R.; Thompson, M. E. Introduction: Organic Electronics and Optoelectronics. *Chem. Rev.* **2007**, *107* (4), 923–925.
- (2) Melzer, C.; von Seggern, H. Enlightened Organic Transistors. *Nat. Mater.* **2010**, *9* (6), 470–472.
- (3) Shirakawa, H.; Louis, E. J.; MacDiarmid, A. G.; Chiang, C. K.; Heeger, A. J. Synthesis of Electrically Conducting Organic Polymers: Halogen Derivatives of Polyacetylene, (CH) X. *J. Chem. Soc. Chem. Commun.* **1977**, *16*, 578.
- (4) Heeger, A. J. Semiconducting and Metallic Polymers: The Fourth Generation of Polymeric Materials. *Curr. Appl. Phys.* **2001**, *1* (4–5), 247–267.
- (5) Koch, N. Organic Electronic Devices and Their Functional Interfaces. *ChemPhysChem* **2007**, *8* (10), 1438–1455.
- (6) Günes, S.; Neugebauer, H.; Sariciftci, N. S. Conjugated Polymer-Based Organic Solar Cells. *Chem. Rev.* **2007**, *107* (4), 1324–1338.
- (7) Cheng, Y.-J.; Yang, S.-H.; Hsu, C.-S. Synthesis of Conjugated Polymers for Organic Solar Cell Applications. *Chem. Rev.* **2009**, *109* (11), 5868–5923.
- (8) Friend, R. H.; Gymer, R. W.; Holmes, A. B.; Burroughes, J. H.; Marks, R. N.; Taliani, C.; Bradley, D. D. C.; Santos, D. A. Dos; Brédas, J. L.; Lögdlund, M.; et al. Electroluminescence in Conjugated Polymers. *Nature* **1999**, *397* (6715), 121–128.
- (9) Gross, M.; Müller, D. C.; Nothofer, H.-G.; Scherf, U.; Neher, D.; Bräuchle, C.; Meerholz, K. Improving the Performance of Doped  $\pi$ -Conjugated Polymers for Use in Organic Light-Emitting Diodes. *Nature* **2000**, *405* (6787), 661–665.
- (10) Liao, C.; Yan, F. Organic Semiconductors in Organic Thin-Film Transistor-Based Chemical and Biological Sensors. *Polym. Rev.* **2013**, *53* (3), 352–406.
- (11) Dimitrakopoulos, C. D.; Malenfant, P. R. L. Organic Thin Film Transistors for



- Large Area Electronics. *Adv. Mater.* **2002**, *14* (2), 99–117.
- (12) Klauk, H. Organic Thin-Film Transistors. *Chem. Soc. Rev.* **2010**, *39* (7), 2643.
- (13) Sirringhaus, H. Device Physics of Solution-Processed Organic Field-Effect Transistors. *Adv. Mater.* **2005**, *17* (20), 2411–2425.
- (14) Heilmeyer, G. H.; Zanoni, L. a. Surface Studies of  $\alpha$ -Copper Phthalocyanine Films. *J. Phys. Chem. Solids* **1964**, *25* (6), 603–611.
- (15) Tsumura, A.; Koezuka, H.; Ando, T. Macromolecular Electronic Device: Field-effect Transistor with a Polythiophene Thin Film. *Appl. Phys. Lett.* **1986**, *49* (18), 1210–1212.
- (16) Sirringhaus, H. 25th Anniversary Article: Organic Field-Effect Transistors: The Path Beyond Amorphous Silicon. *Adv. Mater.* **2014**, *26* (9), 1319–1335.
- (17) Rivnay, J.; Inal, S.; Salleo, A.; Owens, R. M.; Berggren, M.; Malliaras, G. G. Organic Electrochemical Transistors. *Nat. Rev. Mater.* **2018**, *3*, 17086.
- (18) Larsson, O.; Said, E.; Berggren, M.; Crispin, X. Insulator Polarization Mechanisms in Polyelectrolyte-Gated Organic Field-Effect Transistors. *Adv. Funct. Mater.* **2009**, *19* (20), 3334–3341.
- (19) Kergoat, L.; Herlogsson, L.; Braga, D.; Piro, B.; Pham, M. C.; Crispin, X.; Berggren, M.; Horowitz, G. A Water-Gate Organic Field-Effect Transistor. *Adv. Mater.* **2010**, *22* (23), 2565–2569.
- (20) Sayago, J.; Soavi, F.; Sivalingam, Y.; Cicoira, F.; Santato, C. Low Voltage Electrolyte-Gated Organic Transistors Making Use of High Surface Area Activated Carbon Gate Electrodes. *J. Mater. Chem. C* **2014**, *2* (28), 5690–5694.
- (21) Leonardi, F.; Casalini, S.; Zhang, Q.; Galindo, S.; Gutierrez, D.; Mas-Torrent, M. Electrolyte-Gated Organic Field-Effect Transistor Based on a Solution Sheared Organic Semiconductor Blend. *Adv. Mater.* **2016**, *28* (46), 10311–10316.
- (22) White, S. P.; Dorfman, K. D.; Frisbie, C. D. Operating and Sensing Mechanism of Electrolyte-Gated Transistors with Floating Gates: Building a Platform for



- Amplified Biodetection. *J. Phys. Chem. C* **2016**, *120* (1), 108–117.
- (23) Torsi, L.; Magliulo, M.; Manoli, K.; Palazzo, G. Organic Field-Effect Transistor Sensors: A Tutorial Review. *Chem. Soc. Rev.* **2013**, *42* (22), 8612.
- (24) Wang, D.; Noël, V.; Piro, B. Electrolytic Gated Organic Field-Effect Transistors for Application in Biosensors—A Review. *Electronics* **2016**, *5* (1), 9.
- (25) Magliulo, M.; Mallardi, A.; Mulla, M. Y.; Cotrone, S.; Pistillo, B. R.; Favia, P.; Vikholm-Lundin, I.; Palazzo, G.; Torsi, L. Electrolyte-Gated Organic Field-Effect Transistor Sensors Based on Supported Biotinylated Phospholipid Bilayer. *Adv. Mater.* **2013**, *25* (14), 2090–2094.
- (26) Schmoltner, K.; Kofler, J.; Klug, A.; List-Kratochvil, E. J. W. Electrolyte-Gated Organic Field-Effect Transistor for Selective Reversible Ion Detection. *Adv. Mater.* **2013**, *25* (47), 6895–6899.
- (27) Proctor, C. M.; Rivnay, J.; Malliaras, G. G. Understanding Volumetric Capacitance in Conducting Polymers. *J. Polym. Sci. Part B Polym. Phys.* **2016**, *54* (15), 1433–1436.
- (28) Rivnay, J.; Leleux, P.; Ferro, M.; Sessolo, M.; Williamson, A.; Koutsouras, D. A.; Khodagholy, D.; Ramuz, M.; Strakosas, X.; Owens, R. M.; et al. High-Performance Transistors for Bioelectronics through Tuning of Channel Thickness. *Sci. Adv.* **2015**, *1* (4), e1400251–e1400251.
- (29) White, H. S.; Kittlesen, G. P.; Wrighton, M. S. Chemical Derivatization of an Array of Three Gold Microelectrodes with Polypyrrole: Fabrication of a Molecule-Based Transistor. *J. Am. Chem. Soc.* **1984**, *106* (18), 5375–5377.
- (30) Gentile, F.; Delmonte, D.; Solzi, M.; Villani, M.; Iannotta, S.; Zappettini, A.; Coppedè, N. A Theoretical Model for the Time Varying Current in Organic Electrochemical Transistors in a Dynamic Regime. *Org. Electron.* **2016**, *35*, 59–64.
- (31) Friedlein, J. T.; Donahue, M. J.; Shaheen, S. E.; Malliaras, G. G.; McLeod, R. R. Microsecond Response in Organic Electrochemical Transistors: Exceeding the



- Ionic Speed Limit. *Adv. Mater.* **2016**, *28* (38), 8398–8404.
- (32) Doris, S. E.; Pierre, A.; Street, R. A. Dynamic and Tunable Threshold Voltage in Organic Electrochemical Transistors. *Adv. Mater.* **2018**, *30* (15), 1706757.
- (33) Demelas, M.; Scavetta, E.; Basiricò, L.; Rogani, R.; Bonfiglio, A. A Deeper Insight into the Operation Regime of All-Polymeric Electrochemical Transistors. *Appl. Phys. Lett.* **2013**, *102* (19), 193301.
- (34) Inal, S.; Malliaras, G. G.; Rivnay, J. Benchmarking Organic Mixed Conductors for Transistors. *Nat. Commun.* **2017**, *8* (1), 1767.
- (35) Larsson, O.; Laiho, A.; Schmickler, W.; Berggren, M.; Crispin, X. Controlling the Dimensionality of Charge Transport in an Organic Electrochemical Transistor by Capacitive Coupling. *Adv. Mater.* **2011**, *23* (41), 4764–4769.
- (36) Yaghmazadeh, O.; Cicoira, F.; Bernardis, D. A.; Yang, S. Y.; Bonnassieux, Y.; Malliaras, G. G. Optimization of Organic Electrochemical Transistors for Sensor Applications. *J. Polym. Sci. Part B-Polymer Phys.* **2011**, *49* (1), 34–39.
- (37) Tarabella, G.; Santato, C.; Yang, S. Y.; Iannotta, S.; Malliaras, G. G.; Cicoira, F. Effect of the Gate Electrode on the Response of Organic Electrochemical Transistors. *Appl. Phys. Lett.* **2010**, *97* (12), 123304.
- (38) Inal, S.; Rivnay, J.; Suiiu, A.-O.; Malliaras, G. G.; McCulloch, I. Conjugated Polymers in Bioelectronics. *Acc. Chem. Res.* **2018**, *51* (6), 1368–1376.
- (39) Ofer, D.; Crooks, R. M.; Wrighton, M. S. Potential Dependence of the Conductivity of Highly Oxidized Polythiophenes, Polypyrroles, and Polyaniline: Finite Windows of High Conductivity. *J. Am. Chem. Soc.* **1990**, *112* (22), 7869–7879.
- (40) Ofer, D.; Park, L. Y.; Schrock, R. R.; Wrighton, M. S. Potential Dependence of the Conductivity of Polyacetylene: Finite Potential Windows of High Conductivity. *Chem. Mater.* **1991**, *3* (4), 573–575.
- (41) Rivnay, J.; Inal, S.; Collins, B. A.; Sessolo, M.; Stavrinidou, E.; Strakosas, X.; Tassone, C.; Delongchamp, D. M.; Malliaras, G. G. Structural Control of



- Mixed Ionic and Electronic Transport in Conducting Polymers. *Nat. Commun.* **2016**, *7*, 11287.
- (42) Zhang, S.; Kumar, P.; Nouas, A. S.; Fontaine, L.; Tang, H.; Cicoira, F. Solvent-Induced Changes in PEDOT:PSS Films for Organic Electrochemical Transistors. *APL Mater.* **2015**, *3* (1), 14911.
- (43) Zeglio, E.; Eriksson, J.; Gabrielsson, R.; Solin, N.; Inganäs, O. Highly Stable Conjugated Polyelectrolytes for Water-Based Hybrid Mode Electrochemical Transistors. *Adv. Mater.* **2017**, *29* (19), 6–11.
- (44) Inal, S.; Rivnay, J.; Leleux, P.; Ferro, M.; Ramuz, M.; Brendel, J. C.; Schmidt, M. M.; Thelakkat, M.; Malliaras, G. G. A High Transconductance Accumulation Mode Electrochemical Transistor. *Adv. Mater.* **2014**, *26* (44), 7450–7455.
- (45) Giovannitti, A.; Sbircea, D.-T.; Inal, S.; Nielsen, C. B.; Bandiello, E.; Hanifi, D. A.; Sessolo, M.; Malliaras, G. G.; McCulloch, I.; Rivnay, J. Controlling the Mode of Operation of Organic Transistors through Side-Chain Engineering. *Proc. Natl. Acad. Sci.* **2016**, *113* (43), 12017–12022.
- (46) Giovannitti, A.; Nielsen, C. B.; Sbircea, D.-T.; Inal, S.; Donahue, M.; Niazi, M. R.; Hanifi, D. A.; Amassian, A.; Malliaras, G. G.; Rivnay, J.; et al. N-Type Organic Electrochemical Transistors with Stability in Water. *Nat. Commun.* **2016**, *7*, 13066.
- (47) Lin, P.; Yan, F. Organic Thin-Film Transistors for Chemical and Biological Sensing. *Adv. Mater.* **2012**, *24* (1), 34–51.
- (48) Sessolo, M.; Rivnay, J.; Bandiello, E.; Malliaras, G. G.; Bolink, H. J. Ion-Selective Organic Electrochemical Transistors. *Adv. Mater.* **2014**, *26* (28), 4803–4807.
- (49) Liao, C.; Zhang, M.; Yao, M. Y.; Hua, T.; Li, L.; Yan, F. Flexible Organic Electronics in Biology: Materials and Devices. *Adv. Mater.* **2015**, *27* (46), 7493–7527.



- (50) Yang, S. Y.; Defranco, J. a; Sylvester, Y. a; Gobert, T. J.; Macaya, D. J.; Owens, R. M.; Malliaras, G. G. Integration of a Surface-Directed Microfluidic System with an Organic Electrochemical Transistor Array for Multi-Analyte Biosensors. *Lab Chip* **2009**, *9* (5), 704–708.
- (51) Pappa, A. M.; Ohayon, D.; Giovannitti, A.; Maria, I. P.; Savva, A.; Uguz, I.; Rivnay, J.; McCulloch, I.; Owens, R. M.; Inal, S. Direct Metabolite Detection with an N-Type Accumulation Mode Organic Electrochemical Transistor. *Sci. Adv.* **2018**, *4* (6), eaat0911.
- (52) Braendlein, M.; Pappa, A.-M.; Ferro, M.; Lopresti, A.; Acquaviva, C.; Mameessier, E.; Malliaras, G. G.; Owens, R. M. Lactate Detection in Tumor Cell Cultures Using Organic Transistor Circuits. *Adv. Mater.* **2017**, *29* (13), 1605744.
- (53) Jimison, L. H.; Tria, S. A.; Khodagholy, D.; Gurfinkel, M.; Lanzarini, E.; Hama, A.; Malliaras, G. G.; Owens, R. M. Measurement of Barrier Tissue Integrity with an Organic Electrochemical Transistor. *Adv. Mater.* **2012**, *24* (44), 5919–5923.
- (54) Romeo, A.; Tarabella, G.; D’Angelo, P.; Caffarra, C.; Cretella, D.; Alfieri, R.; Petronini, P. G.; Iannotta, S. Drug-Induced Cellular Death Dynamics Monitored by a Highly Sensitive Organic Electrochemical System. *Biosens. Bioelectron.* **2015**, *68*, 791–797.
- (55) Ramuz, M.; Hama, A.; Rivnay, J.; Leleux, P.; Owens, R. M. Monitoring of Cell Layer Coverage and Differentiation with the Organic Electrochemical Transistor. *J. Mater. Chem. B* **2015**, *3* (29), 5971–5977.
- (56) Faria, G. C.; Duong, D. T.; Salleo, A.; Polyzoidis, C. A.; Logothetidis, S.; Rivnay, J.; Owens, R.; Malliaras, G. G. Organic Electrochemical Transistors as Impedance Biosensors. *Mrs Commun.* **2014**, *4* (4), 189–194.
- (57) Tria, S. A.; Ramuz, M.; Huerta, M.; Leleux, P.; Rivnay, J.; Jimison, L. H.; Hama, A.; Malliaras, G. G.; Owens, R. M. Dynamic Monitoring of Salmonella



- Typhimurium Infection of Polarized Epithelia Using Organic Transistors. *Adv. Healthc. Mater.* **2014**, *3* (7), 1053–1060.
- (58) Huerta, M.; Rivnay, J.; Ramuz, M.; Hama, A.; Owens, R. M. Research Update: Electrical Monitoring of Cysts Using Organic Electrochemical Transistors a. *APL Mater.* **2015**, *3* (3), 30701.
- (59) Bolin, M. H.; Svennersten, K.; Nilsson, D.; Sawatdee, A.; Jager, E. W. H.; Richter-Dahlfors, A.; Berggren, M. Active Control of Epithelial Cell-Density Gradients Grown along the Channel of an Organic Electrochemical Transistor. *Adv. Mater.* **2009**, *21* (43), 4379–4382.
- (60) Andersson, P.; Nilsson, D.; Svensson, P.-O.; Chen, M.; Malmström, A.; Remonen, T.; Kugler, T.; Berggren, M. Active Matrix Displays Based on All-Organic Electrochemical Smart Pixels Printed on Paper. *Adv. Mater.* **2002**, *14* (20), 1460–1464.
- (61) Andersson, P.; Forchheimer, R.; Tehrani, P.; Berggren, M. Printable All-Organic Electrochromic Active-Matrix Displays. *Adv. Funct. Mater.* **2007**, *17* (16), 3074–3082.
- (62) Nilsson, D.; Robinson, N.; Berggren, M.; Forchheimer, R. Electrochemical Logic Circuits. *Adv. Mater.* **2005**, *17* (3), 353–358.
- (63) Hamed, M.; Forchheimer, R.; Inganäs, O. Towards Woven Logic from Organic Electronic Fibres. *Nat. Mater.* **2007**, *6* (5), 357–362.
- (64) Tao, X.; Koncar, V.; Dufour, C. Geometry Pattern for the Wire Organic Electrochemical Textile Transistor. *J. Electrochem. Soc.* **2011**, *158* (5), H572.
- (65) Svensson, P.-O.; Nilsson, D.; Forchheimer, R.; Berggren, M. A Sensor Circuit Using Reference-Based Conductance Switching in Organic Electrochemical Transistors. *Appl. Phys. Lett.* **2008**, *93* (20), 203301.
- (66) Das, B. C.; Pillai, R. G.; Wu, Y.; McCreery, R. L. Redox-Gated Three-Terminal Organic Memory Devices: Effect of Composition and Environment on Performance. *ACS Appl. Mater. Interfaces* **2013**, *5* (21), 11052–11058.



- (67) Gkoupidenis, P.; Schaefer, N.; Strakosas, X.; Fairfield, J. A.; Malliaras, G. G. Synaptic Plasticity Functions in an Organic Electrochemical Transistor. *Appl. Phys. Lett.* **2015**, *107* (26), 263302.
- (68) Gkoupidenis, P.; Koutsouras, D. A.; Lonjaret, T.; Fairfield, J. A.; Malliaras, G. G. Orientation Selectivity in a Multi-Gated Organic Electrochemical Transistor. *Sci. Rep.* **2016**, *6* (1), 27007.
- (69) Gkoupidenis, P.; Schaefer, N.; Garlan, B.; Malliaras, G. G. Neuromorphic Functions in PEDOT:PSS Organic Electrochemical Transistors. *Adv. Mater.* **2015**, *27* (44), 7176–7180.
- (70) Simon, D. T.; Gabrielsson, E. O.; Tybrandt, K.; Berggren, M. Organic Bioelectronics: Bridging the Signaling Gap between Biology and Technology. *Chem. Rev.* **2016**, *116* (21), 13009–13041.
- (71) Moon, J.-M.; Thapliyal, N.; Hussain, K. K.; Goyal, R. N.; Shim, Y.-B. Conducting Polymer-Based Electrochemical Biosensors for Neurotransmitters: A Review. *Biosens. Bioelectron.* **2018**, *102* (11), 540–552.
- (72) Wu, X.; Zhou, J.; Huang, J. Integration of Biomaterials into Sensors Based on Organic Thin-Film Transistors. *Macromol. Rapid Commun.* **2018**, *39* (15), 1800084.
- (73) Pappa, A.-M.; Parlak, O.; Scheiblin, G.; Mailley, P.; Salleo, A.; Owens, R. M. Organic Electronics for Point-of-Care Metabolite Monitoring. *Trends Biotechnol.* **2018**, *36* (1), 45–59.
- (74) Shen, H.; Di, C. A.; Zhu, D. Organic Transistor for Bioelectronic Applications. *Sci. China Chem.* **2017**, *60* (4), 437–449.
- (75) Bernards, D. A.; Malliaras, G. G. Steady-State and Transient Behavior of Organic Electrochemical Transistors. *Adv. Funct. Mater.* **2007**, *17* (17), 3538–3544.
- (76) Cicoira, F.; Sessolo, M.; Yaghmazadeh, O.; DeFranco, J. A.; Yang, S. Y.; Malliaras, G. G. Influence of Device Geometry on Sensor Characteristics of



- Planar Organic Electrochemical Transistors. *Adv. Mater.* **2010**, *22* (9), 1012–1016.
- (77) Khodagholy, D.; Rivnay, J.; Sessolo, M.; Gurfinkel, M.; Leleux, P.; Jimison, L. H.; Stavriniidou, E.; Herve, T.; Sanaur, S.; Owens, R. M.; et al. High Transconductance Organic Electrochemical Transistors. *Nat. Commun.* **2013**, *4*, 2133.
- (78) Volkov, A. V.; Wijeratne, K.; Mitraka, E.; Ail, U.; Zhao, D.; Tybrandt, K.; Andreasen, J. W.; Berggren, M.; Crispin, X.; Zozoulenko, I. V. Understanding the Capacitance of PEDOT:PSS. *Adv. Funct. Mater.* **2017**, *27* (28), 1–10.
- (79) Robinson, N. D.; Svensson, P.-O.; Nilsson, D.; Berggren, M. On the Current Saturation Observed in Electrochemical Polymer Transistors. *J. Electrochem. Soc.* **2006**, *153* (3), H39.
- (80) Kaphle, V.; Liu, S.; Al-Shadeedi, A.; Keum, C.-M.; Lüssem, B. Contact Resistance Effects in Highly Doped Organic Electrochemical Transistors. *Adv. Mater.* **2016**, *28* (39), 8766–8770.
- (81) Friedlein, J. T.; Rivnay, J.; Dunlap, D. H.; McCulloch, I.; Shaheen, S. E.; McLeod, R. R.; Malliaras, G. G. Influence of Disorder on Transfer Characteristics of Organic Electrochemical Transistors. *Appl. Phys. Lett.* **2017**, *111* (2), 23301.
- (82) He, R.-X.; Zhang, M.; Tan, F.; Leung, P. H. M.; Zhao, X.-Z.; Chan, H. L. W.; Yang, M.; Yan, F. Detection of Bacteria with Organic Electrochemical Transistors. *J. Mater. Chem.* **2012**, *22* (41), 22072.
- (83) Seshadri, P.; Manoli, K.; Schneiderhan-Marra, N.; Anthes, U.; Wierchowicz, P.; Bonrad, K.; Di Franco, C.; Torsi, L. Low-Picomolar, Label-Free Procalcitonin Analytical Detection with an Electrolyte-Gated Organic Field-Effect Transistor Based Electronic Immunosensor. *Biosens. Bioelectron.* **2018**, *104*, 113–119.
- (84) Magliulo, M.; De Tullio, D.; Vikholm-Lundin, I.; Albers, W. M.; Munter, T.;



- Manoli, K.; Palazzo, G.; Torsi, L. Label-Free C-Reactive Protein Electronic Detection with an Electrolyte-Gated Organic Field-Effect Transistor-Based Immunosensor. *Anal. Bioanal. Chem.* **2016**, *408* (15), 3943–3952.
- (85) Kim, D. J.; Lee, N. E.; Park, J. S.; Park, I. J.; Kim, J. G.; Cho, H. J. Organic Electrochemical Transistor Based Immunosensor for Prostate Specific Antigen (PSA) Detection Using Gold Nanoparticles for Signal Amplification. *Biosens. Bioelectron.* **2010**, *25* (11), 2477–2482.
- (86) Buth, F.; Donner, A.; Sachsenhauser, M.; Stutzmann, M.; Garrido, J. A. Biofunctional Electrolyte-Gated Organic Field-Effect Transistors. *Adv. Mater.* **2012**, *24* (33), 4511–4517.
- (87) Shen, H.; Zou, Y.; Zang, Y.; Huang, D.; Jin, W.; Di, C.; Zhu, D. Molecular Antenna Tailored Organic Thin-Film Transistors for Sensing Application. *Mater. Horizons* **2018**, *5* (2), 240–247.
- (88) Pappa, A. M.; Inal, S.; Roy, K.; Zhang, Y.; Pitsalidis, C.; Hama, A.; Pas, J.; Malliaras, G. G.; Owens, R. M. Polyelectrolyte Layer-by-Layer Assembly on Organic Electrochemical Transistors. *ACS Appl. Mater. Interfaces* **2017**, *9* (12), 10427–10434.
- (89) Palazzo, G.; De Tullio, D.; Magliulo, M.; Mallardi, A.; Intranuovo, F.; Mulla, M. Y.; Favia, P.; Vikholm-Lundin, I.; Torsi, L. Detection beyond Debye's Length with an Electrolyte-Gated Organic Field-Effect Transistor. *Adv. Mater.* **2015**, *27* (5), 911–916.
- (90) Zhang, Y.; Inal, S.; Hsia, C. Y.; Ferro, M.; Ferro, M.; Daniel, S.; Owens, R. M. Supported Lipid Bilayer Assembly on PEDOT:PSS Films and Transistors. *Adv. Funct. Mater.* **2016**, *26* (40), 7304–7313.
- (91) Curto, V. F.; Marchiori, B.; Hama, A.; Pappa, A.-M.; Ferro, M. P.; Braendlein, M.; Rivnay, J.; Fiocchi, M.; Malliaras, G. G.; Ramuz, M.; et al. Organic Transistor Platform with Integrated Microfluidics for in-Line Multi-Parametric in Vitro Cell Monitoring. *Microsystems Nanoeng.* **2017**, *3* (2), 17028.



- (92) Zhang, Y.; Li, J.; Li, R.; Sbircea, D.-T.; Giovannitti, A.; Xu, J.; Xu, H.; Zhou, G.; Bian, L.; McCulloch, I.; et al. Liquid–Solid Dual-Gate Organic Transistors with Tunable Threshold Voltage for Cell Sensing. *ACS Appl. Mater. Interfaces* **2017**, *9* (44), 38687–38694.
- (93) D’Angelo, P.; Tarabella, G.; Romeo, A.; Giodice, A.; Marasso, S.; Cocuzza, M.; Ravanetti, F.; Cacchioli, A.; Petronini, P. G.; Iannotta, S. Monitoring the Adaptive Cell Response to Hyperosmotic Stress by Organic Devices. *MRS Commun.* **2017**, *7* (2), 229–235.
- (94) Yao, C.; Xie, C.; Lin, P.; Yan, F.; Huang, P.; Hsing, I. M. Organic Electrochemical Transistor Array for Recording Transepithelial Ion Transport of Human Airway Epithelial Cells. *Adv. Mater.* **2013**, *25* (45), 6575–6580.
- (95) Lin, P.; Yan, F.; Yu, J.; Chan, H. L. W.; Yang, M. The Application of Organic Electrochemical Transistors in Cell-Based Biosensors. *Adv. Mater.* **2010**, *22* (33), 3655–3660.
- (96) Lanzani, G. Organic Electronics Meets Biology. *Nat. Mater.* **2014**, *13* (8), 775–776.
- (97) Tarabella, G.; Mohammadi, F. M.; Coppede, N.; Barbero, F.; Iannotta, S.; Santato, C.; Cicoira, F. New Opportunities for Organic Electronics and Bioelectronics: Ions in Action. *Chem. Sci.* **2013**, *4* (4), 1395–1409.
- (98) Malliaras, G. G. Organic Bioelectronics: A New Era for Organic Electronics. *Biochim. Biophys. Acta - Gen. Subj.* **2013**, *1830* (9), 4286–4287.
- (99) Uguz, I.; Ganji, M.; Hama, A.; Tanaka, A.; Inal, S.; Youssef, A.; Owens, R. M.; Quilichini, P. P.; Ghestem, A.; Bernard, C.; et al. Autoclave Sterilization of PEDOT:PSS Electrophysiology Devices. *Adv. Healthc. Mater.* **2016**, *5* (24), 3094–3098.
- (100) Gu, X.; Yao, C.; Liu, Y.; Hsing, I.-M. 16-Channel Organic Electrochemical Transistor Array for In Vitro Conduction Mapping of Cardiac Action Potential. *Adv. Healthc. Mater.* **2016**, *5* (18), 2345–2351.



- (101) Strakosas, X.; Sessolo, M.; Hama, A.; Rivnay, J.; Stavrinidou, E.; Malliaras, G. G.; Owens, R. M. A Facile Biofunctionalisation Route for Solution Processable Conducting Polymer Devices. *J. Mater. Chem. B* **2014**, *2* (17), 2537.
- (102) Desbief, S.; di Lauro, M.; Casalini, S.; Guerin, D.; Tortorella, S.; Barbalinardo, M.; Kyndiah, A.; Murgia, M.; Cramer, T.; Biscarini, F.; et al. Electrolyte-Gated Organic Synapse Transistor Interfaced with Neurons. *Org. Electron. physics, Mater. Appl.* **2016**, *38*, 21–28.
- (103) Rivnay, J.; Wang, H.; Fenno, L.; Deisseroth, K.; Malliaras, G. G. Next-Generation Probes, Particles, and Proteins for Neural Interfacing. *Sci. Adv.* **2017**, *3* (6), e1601649.
- (104) Trung, T. Q.; Lee, N.-E. Flexible and Stretchable Physical Sensor Integrated Platforms for Wearable Human-Activity Monitoring and Personal Healthcare. *Adv. Mater.* **2016**, *28* (22), 4338–4372.
- (105) Kim, J.; Campbell, A. S.; Wang, J. Wearable Non-Invasive Epidermal Glucose Sensors: A Review. *Talanta* **2018**, *177*, 163–170.
- (106) Gao, W.; Emaminejad, S.; Nyein, H. Y. Y.; Challa, S.; Chen, K.; Peck, A.; Fahad, H. M.; Ota, H.; Shiraki, H.; Kiriya, D.; et al. Fully Integrated Wearable Sensor Arrays for Multiplexed in Situ Perspiration Analysis. *Nature* **2016**, *529* (7587), 509–514.
- (107) Fan, X.; Xu, B.; Wang, N.; Wang, J.; Liu, S.; Wang, H.; Yan, F. Highly Conductive Stretchable All-Plastic Electrodes Using a Novel Dipping-Embedded Transfer Method for High-Performance Wearable Sensors and Semitransparent Organic Solar Cells. *Adv. Electron. Mater.* **2017**, *3* (5), 1600471.
- (108) Khodagholy, D.; Curto, V. F.; Fraser, K. J.; Gurfinkel, M.; Byrne, R.; Diamond, D.; Malliaras, G. G.; Benito-Lopez, F.; Owens, R. M. Organic Electrochemical Transistor Incorporating an Ionogel as a Solid State Electrolyte for Lactate Sensing. *J. Mater. Chem.* **2012**, *22* (10), 4440.



- (109) Zhao, D.; Fabiano, S.; Berggren, M.; Crispin, X.; Huang, A. L.; Hammock, M. L.; Chortos, A.; Tee, B. C. K.; Tok, J. B. H.; Bao, Z.; et al. Ionic Thermoelectric Gating Organic Transistors. *Nat. Commun.* **2017**, *8*, 14214.
- (110) Thiburce, Q.; Campbell, A. J. Low-Voltage Polyelectrolyte-Gated Polymer Field-Effect Transistors Gravure Printed at High Speed on Flexible Plastic Substrates. *Adv. Electron. Mater.* **2017**, *3* (2), 1600421.
- (111) Yi, Z.; Natale, G.; Kumar, P.; Mauro, E. Di; Heuzey, M.-C.; Soavi, F.; Perepichka, I. I.; Varshney, S. K.; Santato, C.; Cicoira, F. Ionic Liquid–water Mixtures and Ion Gels as Electrolytes for Organic Electrochemical Transistors. *J. Mater. Chem. C* **2015**, *3* (25), 6549–6553.
- (112) Lee, J.; Kaake, L. G.; Cho, J. H.; Zhu, X.-Y.; Lodge, T. P.; Frisbie, C. D. Ion Gel-Gated Polymer Thin-Film Transistors: Operating Mechanism and Characterization of Gate Dielectric Capacitance, Switching Speed, and Stability. *J. Phys. Chem. C* **2009**, *113* (20), 8972–8981.
- (113) Scheiblin, G.; Aliane, A.; Strakosas, X.; Curto, V. F.; Coppard, R.; Marchand, G.; Owens, R. M.; Mailley, P.; Malliaras, G. G. Screen-Printed Organic Electrochemical Transistors for Metabolite Sensing. *Mrs Commun.* **2015**, *5* (3), 507–511.
- (114) Bihar, E.; Deng, Y.; Miyake, T.; Saadaoui, M.; Malliaras, G. G.; Rolandi, M. A Disposable Paper Breathalyzer with an Alcohol Sensing Organic Electrochemical Transistor. *Sci. Rep.* **2016**, *6* (1), 27582.
- (115) Khan, H. U.; Roberts, M. E.; Johnson, O.; Förch, R.; Knoll, W.; Bao, Z. In Situ, Label-Free DNA Detection Using Organic Transistor Sensors. *Adv. Mater.* **2010**, *22* (40), 4452–4456.
- (116) Gaylord, B. S.; Heeger, A. J.; Bazan, G. C. DNA Hybridization Detection with Water-Soluble Conjugated Polymers and Chromophore-Labeled Single-Stranded DNA. *J. Am. Chem. Soc.* **2003**, *125* (4), 896–900.
- (117) Dong, X.; Shi, Y.; Huang, W.; Chen, P.; Li, L. J. Electrical Detection of DNA



- Hybridization with Single-Base Specificity Using Transistors Based on CVD-Grown Graphene Sheets. *Adv. Mater.* **2010**, *22* (14), 1649–1653.
- (118) Lin, P.; Luo, X.; Hsing, I.-M.; Yan, F. Organic Electrochemical Transistors Integrated in Flexible Microfluidic Systems and Used for Label-Free DNA Sensing. *Adv. Mater.* **2011**, *23* (35), 4035–4040.
- (119) White, S. P.; Dorfman, K. D.; Frisbie, C. D. Label-Free DNA Sensing Platform with Low-Voltage Electrolyte-Gated Transistors. *Anal. Chem.* **2015**, *87* (3), 1861–1866.
- (120) Lai, S.; Barbaro, M.; Bonfiglio, A. The Role of Polarization-Induced Reorientation of DNA Strands on Organic Field-Effect Transistor-Based Biosensors Sensitivity at High Ionic Strength. *Appl. Phys. Lett.* **2015**, *107* (10), 103301.
- (121) Lai, S.; Demelas, M.; Casula, G.; Cosseddu, P.; Barbaro, M.; Bonfiglio, A. Ultralow Voltage, OTFT-Based Sensor for Label-Free DNA Detection. *Adv. Mater.* **2013**, *25* (1), 103–107.
- (122) Fu, Y.; Liu, K.; Sun, Q.; Lin, B.; Lu, D.; Xu, Z.; Hu, C.; Fan, G.; Zhang, S.; Wang, C.; et al. A Highly Sensitive Immunosensor for Calmodulin Assay Based on Enhanced Biocatalyzed Precipitation Adopting a Dual-Layered Enzyme Strategy. *Biosens. Bioelectron.* **2014**, *56*, 258–263.
- (123) Fu, Y.; Wang, N.; Yang, A.; Law, H. K.; Li, L.; Yan, F. Highly Sensitive Detection of Protein Biomarkers with Organic Electrochemical Transistors. *Adv. Mater.* **2017**, *29* (41), 1703787.
- (124) Liao, C.; Zhang, M.; Niu, L.; Zheng, Z.; Yan, F. Highly Selective and Sensitive Glucose Sensors Based on Organic Electrochemical Transistors with Graphene-Modified Gate Electrodes. *J. Mater. Chem. B* **2013**, *1* (31), 3820.
- (125) Zhang, L.; Wang, G.; Xiong, C.; Zheng, L.; He, J.; Ding, Y.; Lu, H.; Zhang, G.; Cho, K.; Qiu, L. Chirality Detection of Amino Acid Enantiomers by Organic Electrochemical Transistor. *Biosens. Bioelectron.* **2018**, *105*, 121–128.



- (126) Pappa, A.-M.; Curto, V. F.; Braendlein, M.; Strakosas, X.; Donahue, M. J.; Fiocchi, M.; Malliaras, G. G.; Owens, R. M. Organic Transistor Arrays Integrated with Finger-Powered Microfluidics for Multianalyte Saliva Testing. *Adv. Healthc. Mater.* **2016**, *5* (17), 2295–2302.
- (127) Minami, T.; Sasaki, Y.; Minamiki, T.; Wakida, S.; Kurita, R.; Niwa, O.; Tokito, S. Selective Nitrate Detection by an Enzymatic Sensor Based on an Extended-Gate Type Organic Field-Effect Transistor. *Biosens. Bioelectron.* **2016**, *81*, 87–91.
- (128) Liao, C. Z.; Mak, C. H.; Zhang, M.; Chan, H. L. W.; Yan, F. Flexible Organic Electrochemical Transistors for Highly Selective Enzyme Biosensors and Used for Saliva Testing. *Adv. Mater.* **2015**, *27* (4), 676–681.
- (129) Liao, C. Z.; Zhang, M.; Niu, L. Y.; Zheng, Z. J.; Yan, F. Organic Electrochemical Transistors with Graphene-Modified Gate Electrodes for Highly Sensitive and Selective Dopamine Sensors. *J. Mater. Chem. B* **2014**, *2* (2), 191–200.
- (130) Mak, C. H.; Liao, C.; Fu, Y.; Zhang, M.; Tang, C. Y.; Tsang, Y. H.; Chan, H. L. W.; Yan, F. Highly-Sensitive Epinephrine Sensors Based on Organic Electrochemical Transistors with Carbon Nanomaterial Modified Gate Electrodes. *J. Mater. Chem. C* **2015**, *3* (25), 6532–6538.
- (131) Xiong, C.; Wang, Y.; Qu, H.; Zhang, L.; Qiu, L.; Chen, W.; Yan, F.; Zheng, L. Highly Sensitive Detection of Gallic Acid Based on Organic Electrochemical Transistors with Poly(diallyldimethylammonium Chloride) and Carbon Nanomaterials Nanocomposites Functionalized Gate Electrodes. *Sensors Actuators, B Chem.* **2017**, *246*, 235–242.
- (132) Tang, H.; Yan, F.; Lin, P.; Xu, J. B.; Chan, H. L. W. Highly Sensitive Glucose Biosensors Based on Organic Electrochemical Transistors Using Platinum Gate Electrodes Modified with Enzyme and Nanomaterials. *Adv. Funct. Mater.* **2011**, *21* (12), 2264–2272.



- (133) Ji, X.; Lau, H. Y.; Ren, X.; Peng, B.; Zhai, P.; Feng, S.-P.; Chan, P. K. L. Highly Sensitive Metabolite Biosensor Based on Organic Electrochemical Transistor Integrated with Microfluidic Channel and Poly(N-Vinyl-2-Pyrrolidone)-Capped Platinum Nanoparticles. *Adv. Mater. Technol.* **2016**, *1* (5), 1600042.
- (134) Mulla, M. Y.; Tuccori, E.; Magliulo, M.; Lattanzi, G.; Palazzo, G.; Persaud, K.; Torsi, L. Capacitance-Modulated Transistor Detects Odorant Binding Protein Chiral Interactions. *Nat. Commun.* **2015**, *6* (1), 6010.
- (135) Guo, X.; Liu, J.; Liu, F.; She, F.; Zheng, Q.; Tang, H.; Ma, M.; Yao, S. Label-Free and Sensitive Sialic Acid Biosensor Based on Organic Electrochemical Transistors. *Sensors Actuators B Chem.* **2017**, *240*, 1075–1082.
- (136) Minamiki, T.; Minami, T.; Kurita, R.; Niwa, O.; Wakida, S.; Fukuda, K.; Kumaki, D.; Tokito, S. Accurate and Reproducible Detection of Proteins in Water Using an Extended-Gate Type Organic Transistor Biosensor. *Appl. Phys. Lett.* **2014**, *104* (24), 243703.
- (137) Bernardis, D. A.; Malliaras, G. G.; Toombes, G. E. S.; Gruner, S. M. Gating of an Organic Transistor through a Bilayer Lipid Membrane with Ion Channels. *Appl. Phys. Lett.* **2006**, *89* (5), 53505.
- (138) Owens, R. M.; Malliaras, G. G. Organic Electronics at the Interface with Biology. *MRS Bull.* **2010**, *35* (6), 449–456.
- (139) Lin, P.; Yan, F.; Chan, H. L. W. Ion-Sensitive Properties of Organic Electrochemical Transistors. *ACS Appl. Mater. Interfaces* **2010**, *2* (6), 1637–1641.
- (140) Nishizawa, M.; Matsue, T.; Uchida, I. Penicillin Sensor Based on a Microarray Electrode Coated with pH-Responsive Polypyrrole. *Anal. Chem.* **1992**, *64* (21), 2642–2644.
- (141) Zhang, M.; Liao, C.; Mak, C. H.; You, P.; Mak, C. L.; Yan, F. Highly Sensitive



- Glucose Sensors Based on Enzyme-Modified Whole-Graphene Solution-Gated Transistors. *Sci. Rep.* **2015**, *5*, 8311.
- (142) Tang, H.; Lin, P.; Chan, H. L. W.; Yan, F. Highly Sensitive Dopamine Biosensors Based on Organic Electrochemical Transistors. *Biosens. Bioelectron.* **2011**, *26* (11), 4559–4563.
- (143) Casalini, S.; Leonardi, F.; Cramer, T.; Biscarini, F. Organic Field-Effect Transistor for Label-Free Dopamine Sensing. *Org. Electron.* **2013**, *14* (1), 156–163.
- (144) Khodagholy, D.; Doublet, T.; Quilichini, P.; Gurfinkel, M.; Leleux, P.; Ghestem, A.; Ismailova, E.; Hervé, T.; Sanaur, S.; Bernard, C.; et al. In Vivo Recordings of Brain Activity Using Organic Transistors. *Nat. Commun.* **2013**, *4*, 1575.
- (145) Rivnay, J.; Ramuz, M.; Leleux, P.; Hama, A.; Huerta, M.; Owens, R. M. Organic Electrochemical Transistors for Cell-Based Impedance Sensing. *Appl. Phys. Lett.* **2015**, *106* (4), 43301.
- (146) Bernards, D. A.; Macaya, D. J.; Nikolou, M.; DeFranco, J. A.; Takamatsu, S.; Malliaras, G. G. Enzymatic Sensing with Organic Electrochemical Transistors. *J. Mater. Chem.* **2008**, *18* (1), 116–120.
- (147) Zhang, M.; Liao, C.; Yao, Y.; Liu, Z.; Gong, F.; Yan, F. High-Performance Dopamine Sensors Based on Whole-Graphene Solution-Gated Transistors. *Adv. Funct. Mater.* **2014**, *24* (7), 978–985.
- (148) Rivnay, J.; Owens, R. M.; Malliaras, G. G. The Rise of Organic Bioelectronics. *Chem. Mater.* **2014**, *26* (1), 679–685.
- (149) Strakosas, X.; Bongo, M.; Owens, R. M. The Organic Electrochemical Transistor for Biological Applications. *J. Appl. Polym. Sci.* **2015**, *132* (15), 41735.
- (150) Campana, A.; Cramer, T.; Simon, D. T.; Berggren, M.; Biscarini, F. Electrocardiographic Recording with Conformable Organic Electrochemical Transistor Fabricated on Resorbable Bioscaffold. *Adv. Mater.* **2014**, *26* (23),



- 3874–3878.
- (151) Leleux, P.; Rivnay, J.; Lonjaret, T.; Badier, J.; Bénar, C.; Hervé, T.; Chauvel, P.; Malliaras, G. G. Organic Electrochemical Transistors for Clinical Applications. *Adv. Healthc. Mater.* **2015**, *4* (1), 142–147.
- (152) Hempel, F.; Law, J. K.-Y.; Nguyen, T. C.; Munief, W.; Lu, X.; Pachauri, V.; Susloparova, A.; Vu, X. T.; Ingebrandt, S. PEDOT:PSS Organic Electrochemical Transistor Arrays for Extracellular Electrophysiological Sensing of Cardiac Cells. *Biosens. Bioelectron.* **2017**, *93*, 132–138.
- (153) Khodagholy, D.; Gurfinkel, M.; Stavriniidou, E.; Leleux, P.; Herve, T.; Sanaur, S.; Malliaras, G. G. High Speed and High Density Organic Electrochemical Transistor Arrays. *Appl. Phys. Lett.* **2011**, *99* (16), 163304.
- (154) Sessolo, M.; Khodagholy, D.; Rivnay, J.; Maddalena, F.; Gleyzes, M.; Steidl, E.; Buisson, B.; Malliaras, G. G. Easy-to-Fabricate Conducting Polymer Microelectrode Arrays. *Adv. Mater.* **2013**, *25* (15), 2135–2139.
- (155) Kergoat, L.; Piro, B.; Berggren, M.; Horowitz, G.; Pham, M.-C. Advances in Organic Transistor-Based Biosensors: From Organic Electrochemical Transistors to Electrolyte-Gated Organic Field-Effect Transistors. *Anal. Bioanal. Chem.* **2012**, *402* (5), 1813–1826.
- (156) Magliulo, M.; Manoli, K.; Macchia, E.; Palazzo, G.; Torsi, L. Tailoring Functional Interlayers in Organic Field-Effect Transistor Biosensors. *Adv. Mater.* **2015**, *27* (46), 7528–7551.
- (157) Rim, Y. S.; Bae, S.-H.; Chen, H.; De Marco, N.; Yang, Y. Recent Progress in Materials and Devices toward Printable and Flexible Sensors. *Adv. Mater.* **2016**, *28* (22), 4415–4440.
- (158) Zang, Y.; Huang, D.; Di, C.; Zhu, D. Device Engineered Organic Transistors for Flexible Sensing Applications. *Adv. Mater.* **2016**, *28* (22), 4549–4555.
- (159) Oh, J. Y.; Rondeau-Gagné, S.; Chiu, Y. C.; Chortos, A.; Lissel, F.; Wang, G. J. N.; Schroeder, B. C.; Kurosawa, T.; Lopez, J.; Katsumata, T.; et al. Intrinsically



- Stretchable and Healable Semiconducting Polymer for Organic Transistors. *Nature* **2016**, *539* (7629), 411–415.
- (160) Someya, T.; Bao, Z.; Malliaras, G. G. The Rise of Plastic Bioelectronics. *Nature* **2016**, *540* (7633), 379–385.
- (161) Sokolov, A. N.; Tee, B. C. K.; Bettinger, C. J.; Tok, J. B. H.; Bao, Z. Chemical and Engineering Approaches to Enable Organic Field-Effect Transistors for Electronic Skin Applications. *Acc. Chem. Res.* **2012**, *45* (3), 361–371.
- (162) Donahue, M. J.; Williamson, A.; Strakosas, X.; Friedlein, J. T.; McLeod, R. R.; Gleskova, H.; Malliaras, G. G. High-Performance Vertical Organic Electrochemical Transistors. *Adv. Mater.* **2018**, *30* (5), 1705031.
- (163) Persson, K. M.; Karlsson, R.; Svennersten, K.; Löffler, S.; Jager, E. W. H.; Richter-Dahlfors, A.; Konradsson, P.; Berggren, M. Electronic Control of Cell Detachment Using a Self-Doped Conducting Polymer. *Adv. Mater.* **2011**, *23* (38), 4403–4408.
- (164) Stavriniidou, E.; Gabrielsson, R.; Gomez, E.; Crispin, X.; Nilsson, O.; Simon, D. T.; Berggren, M. Electronic Plants. *Sci. Adv.* **2015**, *1* (10), e1501136–e1501136.
- (165) Toss, H.; Suspène, C.; Piro, B.; Yassar, A.; Crispin, X.; Kergoat, L.; Pham, M.-C.; Berggren, M. On the Mode of Operation in Electrolyte-Gated Thin Film Transistors Based on Different Substituted Polythiophenes. *Org. Electron.* **2014**, *15* (10), 2420–2427.
- (166) Schmidt, M. M.; ElMahmoudy, M.; Malliaras, G. G.; Inal, S.; Thelakkat, M. Smaller Counter Cation for Higher Transconductance in Anionic Conjugated Polyelectrolytes. *Macromol. Chem. Phys.* **2018**, *219* (2), 1700374.
- (167) Nielsen, C. B.; Giovannitti, A.; Sbircea, D.; Bandiello, E.; Niazi, M. R.; Hanifi, D. A.; Sessolo, M.; Amassian, A.; Malliaras, G. G.; Rivnay, J.; et al. Molecular Design of Semiconducting Polymers for High-Performance Organic Electrochemical Transistors. *J. Am. Chem. Soc.* **2016**, *138* (32), 10252–10259.
- (168) Sun, H.; Vagin, M.; Wang, S.; Crispin, X.; Forchheimer, R.; Berggren, M.;



- Fabiano, S. Complementary Logic Circuits Based on High-Performance N-Type Organic Electrochemical Transistors. *Adv. Mater.* **2018**, *30* (9), 1704916.
- (169) Giovannitti, A.; Maria, I. P.; Hanifi, D.; Donahue, M. J.; Bryant, D.; Barth, K. J.; Makdah, B. E.; Savva, A.; Moia, D.; Zetek, M.; et al. The Role of the Side Chain on the Performance of N-Type Conjugated Polymers in Aqueous Electrolytes. *Chem. Mater.* **2018**, *30* (9), 2945–2953.
- (170) Di Pietro, R.; Erdmann, T.; Carpenter, J. H.; Wang, N.; Shivhare, R. R.; Formanek, P.; Heintze, C.; Voit, B.; Neher, D.; Ade, H.; et al. Synthesis of High-Crystallinity DPP Polymers with Balanced Electron and Hole Mobility. *Chem. Mater.* **2017**, *29* (23), 10220–10232.
- (171) Di Pietro, R.; Erdmann, T.; Wang, N.; Liu, X.; Gräfe, D.; Lenz, J.; Brandt, J.; Kasemann, D.; Leo, K.; Al-Hussein, M.; et al. The Impact of Molecular Weight, Air Exposure and Molecular Doping on the Charge Transport Properties and Electronic Defects in Dithienyl-Diketopyrrolopyrrole-thieno[3,2-B]thiophene Copolymers. *J. Mater. Chem. C* **2016**, *4* (46), 10827–10838.
- (172) Tansel, B.; Sager, J.; Rector, T.; Garland, J.; Strayer, R. F.; Levine, L.; Roberts, M.; Hummerick, M.; Bauer, J. Significance of Hydrated Radius and Hydration Shells on Ionic Permeability during Nanofiltration in Dead End and Cross Flow Modes. *Sep. Purif. Technol.* **2006**, *51* (1), 40–47.
- (173) Nordmeier, E. Studies of Polyelectrolyte Solutions IV. Effects of Ionic Strength on the Effective Polyion Charge. *Polym. J.* **1993**, *25*, 19.
- (174) Ambros, V.; Petri, A.; Lindow, M.; Obad, S.; Kauppinen, S.; Ambros, V.; Kloosterman, W.; Plasterk, R.; Bushati, N.; Cohen, S.; et al. The Functions of Animal microRNAs. *Nature* **2004**, *431* (7006), 350–355.
- (175) McCaffrey, A. P.; Meuse, L.; Pham, T.-T. T.; Conklin, D. S.; Hannon, G. J.; Kay, M. A. Gene Expression: RNA Interference in Adult Mice. *Nature* **2002**, *418* (6893), 38–39.



- (176) Lu, J.; Getz, G.; Miska, E. A.; Alvarez-Saavedra, E.; Lamb, J.; Peck, D.; Sweet-Cordero, A.; Ebert, B. L.; Mak, R. H.; Ferrando, A. A.; et al. MicroRNA Expression Profiles Classify Human Cancers. *Nature* **2005**, *435* (7043), 834–838.
- (177) Cummins, J. M.; Velculescu, V. E. Implications of Micro-RNA Profiling for Cancer Diagnosis. *Oncogene* **2006**, *25* (46), 6220–6227.
- (178) Jamali, A. A.; Pourhassan-Moghaddam, M.; Dolatabadi, J. E. N.; Omid, Y. Nanomaterials on the Road to microRNA Detection with Optical and Electrochemical Nanobiosensors. *TrAC Trends Anal. Chem.* **2014**, *55*, 24–42.
- (179) Aslan, K.; Huang, J.; Wilson, G. M.; Geddes, C. D. Metal-Enhanced Fluorescence-Based RNA Sensing. *J. Am. Chem. Soc.* **2006**, *128* (13), 4206–4207.
- (180) Conde, J.; Edelman, E. R.; Artzi, N. Target-Responsive DNA/RNA Nanomaterials for microRNA Sensing and Inhibition: The Jack-of-All-Trades in Cancer Nanotheranostics? *Adv. Drug Deliv. Rev.* **2015**, *81*, 169–183.
- (181) Park, M. H.; Han, D.; Chand, R.; Lee, D. H.; Kim, Y. S. Mechanism of Label-Free DNA Detection Using the Floating Electrode on Pentacene Thin Film Transistor. *J. Phys. Chem. C* **2016**, *120* (9), 4854–4859.
- (182) Wang, N.; Liu, Y.; Fu, Y.; Yan, F. AC Measurements Using Organic Electrochemical Transistors for Accurate Sensing. *ACS Appl. Mater. Interfaces* **2018**, *10* (31), 25834–25840.
- (183) Dika, C.; Gantzer, C.; Perrin, A.; Duval, J. F. L. Impact of the Virus Purification Protocol on Aggregation and Electrokinetics of MS2 Phages and Corresponding Virus-like Particles. *Phys. Chem. Chem. Phys.* **2013**, *15* (15), 5691–5700.
- (184) Kim, J.; Salvatore, G. A.; Araki, H.; Chiarelli, A. M.; Xie, Z.; Banks, A.; Sheng, X.; Liu, Y.; Lee, J. W.; Jang, K.-I.; et al. Battery-Free, Stretchable Optoelectronic Systems for Wireless Optical Characterization of the Skin. *Sci.*



- Adv.* **2016**, 2 (8), e1600418–e1600418.
- (185) ZIMMERMANN, B. G.; PARK, N. J.; WONG, D. T. Genomic Targets in Saliva. *Ann. N. Y. Acad. Sci.* **2007**, 1098 (1), 184–191.
- (186) Wei, F.; Patel, P.; Liao, W.; Chaudhry, K.; Zhang, L.; Arellano-Garcia, M.; Hu, S.; Elashoff, D.; Zhou, H.; Shukla, S.; et al. Electrochemical Sensor for Multiplex Biomarkers Detection. *Clin. Cancer Res.* **2009**, 15 (13), 4446–4452.
- (187) Kumar, P.; Yi, Z.; Zhang, S.; Sekar, A.; Soavi, F.; Cicoira, F. Effect of Channel Thickness, Electrolyte Ions, and Dissolved Oxygen on the Performance of Organic Electrochemical Transistors. *Appl. Phys. Lett.* **2015**, 107 (5), 53303.
- (188) Giridharagopal, R.; Flagg, L. Q.; Harrison, J. S.; Ziffer, M. E.; Onorato, J.; Luscombe, C. K.; Ginger, D. S. Electrochemical Strain Microscopy Probes Morphology-Induced Variations in Ion Uptake and Performance in Organic Electrochemical Transistors. *Nat. Mater.* **2017**, 16 (7), 737–742.
- (189) Zhang, Y.; Han, G.; Qin, M.; Shen, Y.; Lu, X.; Yi, Y.; Zhao, N. Spectroscopic Study of Charge Transport at Organic Solid–Water Interface. *Chem. Mater.* **2018**, doi.org/10.1021/acs.chemmater.8b02260.